Università degli Studi di Bologna

Facoltà di Scienze Matematiche Fisiche e Naturali
Dipartimento di Chimica "G. Ciamician"

DOTTORATO DI RICERCA IN
SCIENZE CHIMICHE E CHIMICA INDUSTRIALE:
PROGETTO N.1
"SCIENZE CHIMICHE"
XIX Ciclo
CHIM/03

PHOTO- AND REDOX-ACTIVE SUPRAMOLECULAR SYSTEMS

Presentata dal Dott. **GIACOMO BERGAMINI**

Relatore: Chiar.mo Prof. **VINCENZO BALZANI**

Coordinatore: Chiar.mo Prof. **VINCENZO BALZANI**

Bologna 2007

Ph.D. in Chemical Sciences, Nineteenth Cycle
University of Bologna, Italy

Coordinator: Prof. Vincenzo Balzani

Secretary: Prof. Sergio Zappoli

This PhD has been supported by CIBA Specialty Chemicals

"... e più ragionevole arrivarci a poco per volta, montando prima due pezzi soli, poi il terzo e così via. Non abbiamo quelle pinzette che sovente ci capita di sognare di notte, come uno che ha sete sogna le sorgenti, e che ci permetterebbero di prendere un segmento, di tenerlo ben stretto e diritto, e di incollarlo nel verso giusto sul segmento che è già montato. Se quelle pinzette le avessimo (e non e detto che un giorno non le avremo) saremmo già riusciti a fare delle cose graziose che fin adesso le ha solo fatte il Padreterno, per esempio a montare non dico un ranocchio o una libellula, ma almeno un microbo o il semino di una muffa."
(Primo Levi, **La Chiave a Stella**, 1978)

"...it is reasonable to proceed a bit at a time, first attaching two pieces, then adding a third, and so on. We don't have those tweezers we often dream of at night, the way a thirsty man dreams of springs, that would allow us to pick up a segment, hold it firm and straight, and paste it in the right direction on the segment that has already been assembled. If we had those tweezers (and it's possible that, one day, we will), we would have managed to create some lovely things that so far only the Almighty has made, for example, to assemble - perhaps not a frog or a dragonfly - but at least a microbe or the spore of a mold"
(Primo Levi, **The Monkey's Wrench**)

CONTENTS

CHAPTER 1

Introduction

1.1 Supramolecular chemistry

Supramolecular chemistry is a highly interdisciplinary field that has developed astonishingly rapidly in the last four decades.[1] In the late 1980s, following the award of the 1987 Nobel Prize to Pedersen, Cram, and Lehn, there was a sudden increase of interest in supramolecular chemistry, a highly interdisciplinary field based on concepts such as molecular recognition, preorganization, and self-assembling.

The classical definition of supramolecular chemistry is that given by J.-M. Lehn, namely "*the chemistry beyond the molecule, bearing on organized entities of higher complexity that result from the association of two or more chemical species held together by intermolecular forces*".[2]

There is, however, a problem with this definition. With supramolecular chemistry there has been a change in focus from molecules to molecular assemblies or multicomponent systems. According to the original definition, however, when the components of a chemical system are linked by covalent bonds, the system should not be considered a supramolecular species, but a molecule.

Although the classical definition of supramolecular chemistry as “the chemistry beyond the molecule” is quite useful in general, from a functional viewpoint the distinction between what is molecular and what is supramolecular can be better based on the degree of intercomponent electronic interactions.[1a,3,4,5,6]

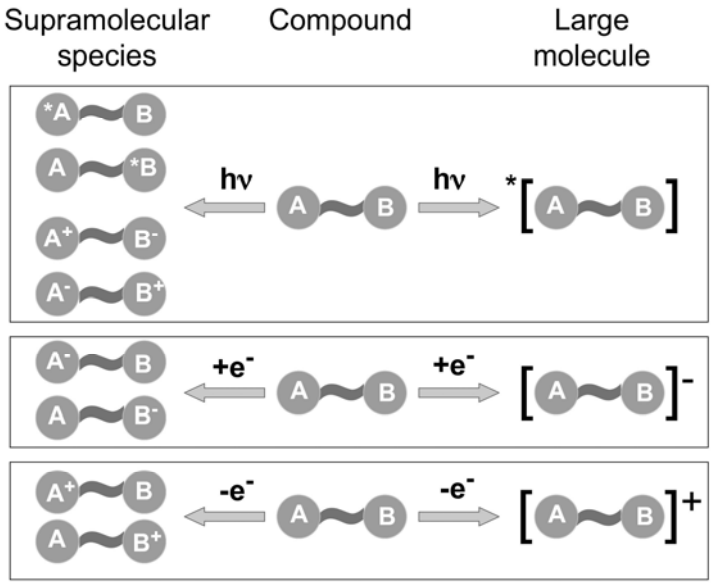

Figure 1.1. Schematic representation of the difference between a supramolecular system and a large molecule based on the effects caused by a photon or an electron input. For more details, see text.

This concept is illustrated, for example, in Figure 1.1.[7] In the case of a photochemical stimulation, a system A~B, consisting of two units (~ indicates any type of “bond” that keeps the units together), can be defined a supramolecular species if light absorption leads to excited states that are substantially localized on either A or B, or causes an electron transfer from A to B (or viceversa). By contrast, when the excited states are substantially delocalized on the entire system, the species can be better considered as a large molecule. Similarly (Figure 1.1),

oxidation and reduction of a supramolecular species can substantially be described as oxidation and reduction of specific units, whereas oxidation and reduction of a large molecule leads to species where the hole or the electron are delocalized on the entire system. In more general terms, when the interaction energy between units is small compared to the other relevant energy parameters, a system can be considered a supramolecular species, regardless of the nature of the bonds that link the units. It should be noted that the properties of each component of a supramolecular species, i.e. of an assembly of weakly interacting molecular components, can be known from the study of the isolated components or of suitable model molecules.

1.2 Bottom-up approach to Nanotechnology

Nanotechnology is an experimental field of applied science and technology that has as its goal the realization of systems and devices for transforming matter, energy, and information, based on nanometer-scale components with precisely defined molecular features. The term nanotechnology has also been used more broadly to refer to techniques that produce or measure features less than 100 nanometers in size. Two main approaches are used in nanotechnology: one is a "bottom-up" approach where materials and devices are built from smaller (molecular) components which assemble themselves chemically using principles such as molecular recognition; the other being a "top-down" approach where they

are synthesized or constructed from larger entities through an externally-controlled process.

The bottom-up approach to nanotechnology is relatively new. Until a few decades ago, in fact, nanotechnology was not considered an obtainable target by physicists.[8] The dominant idea, derived from quantum theory,[9] was that atoms are fuzzy entities that "must no longer be regarded as identifiable individuals",[10] and "form a world of potentialities or possibilities rather than one of things or facts".[11] From the point of view of quantum theory, molecular structure is not an intrinsic property, but a metaphor.[12] Such ideas, of course, were never shared by chemists who long before had established that atoms are material and reliable building blocks for constructing molecules and that molecules have well defined sizes and shapes.[13]

The idea that atoms could be used to construct nanoscale machines was first raised by R.P. Feynman "*There is plenty of room at the bottom*".[14] The key sentence of Feynman's talk was: "*The principles of physics do not speak against the possibility of maneuvering things atom by atom*". As we will see below, however, chemists do not believe in the possibility of realizing an atom-by-atom approach to nanostructures.

In the framework of research on supramolecular chemistry the idea began to arise in a few laboratories that molecules are much more convenient building blocks than atoms for construction of nanoscale devices and machines. The main foundations of this idea were: (a) molecules are stable species, whereas atoms are difficult to handle; (b) Nature starts from molecules, not from atoms, to construct the great

number and variety of nanodevices and nanomachines that sustain life (vide infra); (c) most laboratory chemical processes deal with molecules, not with atoms; (d) molecules are objects that already have distinct shapes and carry device-related properties (e.g. properties that can be manipulated by photochemical and electrochemical inputs); and (5) molecules can self-assemble or can be connected to make larger structures.

In the following years supramolecular chemistry grew very rapidly[1] and it became clear that the supramolecular "bottom-up" approach opens virtually unlimited possibilities concerning design and construction of artificial molecular- level devices and machines. It also became increasingly evident that such an approach can make an invaluable contribution to a better understanding of molecular-level aspects of the extremely complicated devices and machines that are responsible for biological processes.[15]

It should not be forgotten that the development of the supramolecular bottom-up approach towards the construction of nanodevices and nanomachines was made possible by the large amount of knowledge gained in other fields of chemistry. Particularly important in this regard have been the contributions made by organic synthesis, which supplied a variety of building blocks, and by photochemistry,[1a] which afforded a means of investigating the early examples of molecular-level devices and machines (e.g. light-controlled molecular-level tweezers,[16] triads for vectorial charge separation,[17] and light-harvesting antennae[18]).

It should also be recalled that in the last few years the concept of molecules as nanoscale objects with their own shape, size and properties has been confirmed by new, very powerful techniques, such as single-molecule fluorescence spectroscopy and the various types of probe microscopy, capable of "seeing"[19] or "manipulating"[20] single molecules. It has been possible, for example, to make ordered arrays of molecules (e.g. to write words[21] and numbers[22] by aligning single molecules in the desired pattern) and even to investigate bimolecular chemical reactions at the single molecule level.[23]

The supramolecular systems studied in this thesis are the *dendrimers*.

1.3 Dendrimers

Dendrimers[24] are globular size, monodisperse macromolecules in which all bonds emerge radially from a central focal point or core with a regular branching pattern and with repeating units constituting the branching points. The term *dendrimer* refers to its characteristic tree-like structure and it derives from the Greek word *dendron* (tree) and *meros* (part). From a topological viewpoint, dendrimers contain three different regions: core, branches and surface. Each repetition synthetic cycle leads to the addition of one more layer of monomers in the branches, called *generation*. Therefore, the generation number of the dendrimer is equal to the number of repetition cycles performed and to the number of branching points present from the core towards the periphery.

The first example of an iterative synthetic approach toward dendrimers has been reported in 1978 by Vögtle,[25] who called it "cascade synthesis". In the mid-1980s, Tomalia[26] and Newkome[27] independently reported the divergent synthesis of two new families of dendrimers: poly(amidoamine) and the so-called "arborols", respectively. A growing interest on these macromolecules lead in 1990 to the convergent synthesis of aromatic polyether dendrimers by Fréchet.[28] The two different synthetic approaches can be explained as follows:

- in the divergent method, dendrimers are built from the core out to the periphery and in each step a new layer of branching units is added;
- the convergent method follows the opposite path: the skeleton of a dendron, defined as an entire branch, is built up step by step and finally reacted with the core moiety.

Dendrimer chemistry is nowadays a rapidly expanding field, as testified by the exponentially increasing number of papers published on this topic per year. Dendrimers keep attracting the attention of the scientific community because of their fascinating structure and unique properties: indeed the field of dendrimer chemistry has evolved from the initial pursue of synthesizing new large and aesthetically pleasant molecules, to their characterization and finally it has now moved towards functionality. Today dendrimers are used or are planned to be exploited in a variety of applications, taking advantage of the great number of functional units that can be incorporated inside them, their tree-like structure containing internal dynamic cavities, their well-defined dimensions close to that of

important biological molecules (Figure 1.2), like proteins and bioassemblies, the presence of an internal microenvironment different from the bulk of the solution, and their endo- and exo-receptor properties. As a result, applications ranging from the biological and medical field (artificial enzymes, drug-delivery and diagnostics systems) to nanoengeneering (molecular wires, light-emitting diodes), optical data transport (fiber optics), catalysis, energy-harvesting devices and mimics of natural photosynthesis are foreseen.[29]

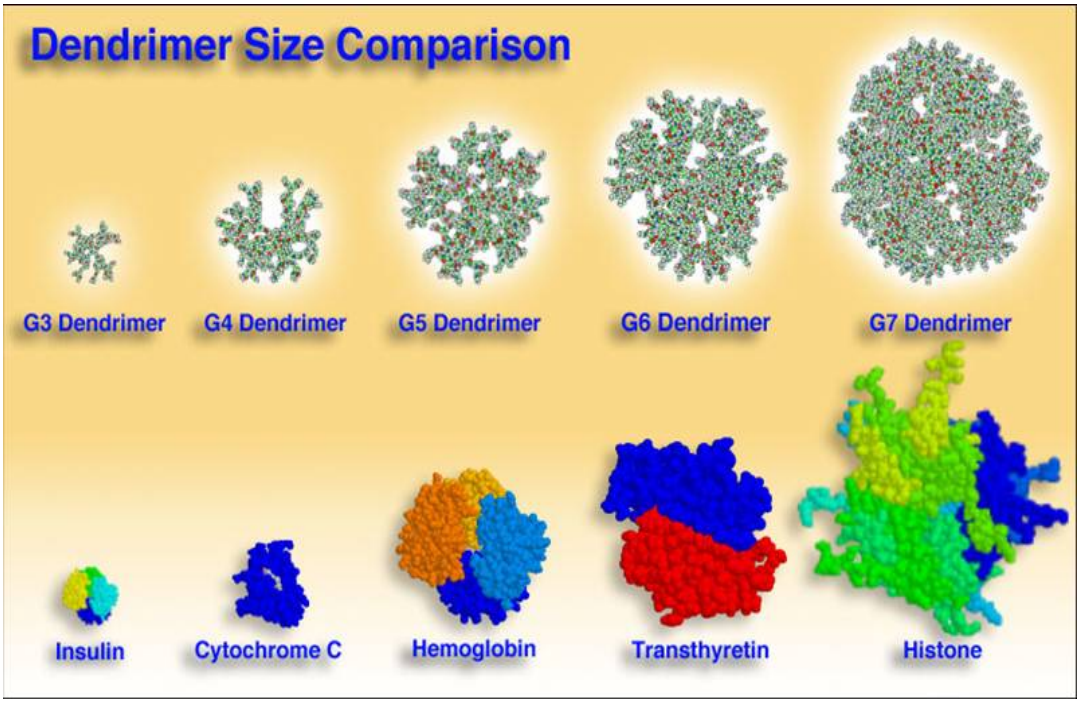

Figure 1.2. Dendrimer size in comparison with important biological molecules

1.4 Dendrimers and light

Currently, dendrimer research is developing swiftly in the direction of highly functional materials. Also in the field of photoactive dendrimers the complexity of

the systems has increased enormously. The investigation of dendritic structures functionalized with luminescent groups,[30] photoswitchable units,[31] energy and/or electron donor-acceptor components and the implementation of such functionalized dendrimers in devices,[32] provide insight in the fundamental processes occurring in such complex systems and in their future applications.

Since dendrimers can be functionalized with multiple chromophoric groups, that are in very close proximity, novel properties can arise compared to the single chromophoric system. Due to the stepwise synthesis, either divergent or convergent, chromophores can be implemented in the dendritic structure with high precision. The number of chromophores and the size of the dendrimer are very well controlled, which is of very great importance for some biological and biomedical applications. The presence of multiple chromophores in the same molecule enables the detection of single dendrimer *via* single molecule spectroscopy (SMS), which is particulary interesting for nanotechnology. Furthermore, an increased sensitivity with respect to specific classes of molecules can be established, enabling the detection of very low concentrations of these molecules. This is of great interest for the field of molecular recognition, e.g. for the development of biosensors (immuno-diagnostic).

A specific advantage of the dendritic framework is that a microenvironment can be crated around a single chromophore. By placing such protective environment around a chromophore its luminescence can be dramatically improved. Dendritic

substituents can also promote supramolecular organization of chromophores, e.g. inducing the formation of fibers or doughnut-like structures.

The possibility to functionalize chromophores with large dendritic substituents is particularly interesting for the development of light emitting diodes (LEDs). The dendritic wedges do not only prevent the aggregation of chromophores, thereby reducing the amount of self quenching, but they also provide a way to improve the solubility of the chromophores in polymers, rendering a more homogeneous blend.

The introduction of photoisomerizable groups, such as azobenzene derivatives, in dendrimers enables the controlled induction of a structural change, especially when those units are attached to the core or implemented in the branches. If attached at the periphery, these photisomerizable groups, can be used to “close” the surface of a dendrimer by means of a photoinduced increase of steric hindrance at the periphery. This type of dendrimers can be used as carriers of small molecules, while a controlled release of those guest molecules is possible using light, which induced the isomerization from *cis* to *trans*. In addition, azobenzene-functionalized materials are widely used in the field of datastorage.

The implementation of chromophores in dendritic structures can also provide more insight in the structural features of dendrimers. Dyes can be used as internal probes to investigate the microenvironment created by dendritic branches. At the same time the influence of external factor, e.g. the solvent or ions, on the microenvironment can be studied. This may concern a change in the conformation of the dendritic structure, but also the accessibility of the dendritic structure by

other molecules. The implementation of multiple chromophores within one dendrimers allows the investigation of internal interactions between the chromophores, such as the formation of excimers and energy and electron transfer processes. To what extend these interactions take place will depend on the flexibility of the dendritic framework and the position of the chromophores within the dendritic structure.

References

[1] (a) V. Balzani, F. Scandola, *Supramolecular Photochemistry*, Horwood, Chichester, **1991**. (b) F. Vögtle, *Supramolecular Chemistry. An introduction*, Wiley, Chichester, **1991**. (c) G. M. Whitesides, J. P. Mathias, C. T. Seto, *Science* **1991**, *254*, 1312.

[2] J.-M. Lehn, *Supramolecular Chemistry: Concepts and Perspectives*, VCH, Weinheim, **1995**.

[3] H. J. Schneider, A. Yatsimirsky, *Principles and Methods un Supramolecular Chemistry*, Wiley, Chichester, **2000**.

[4] J. W. Steed, J. L. Atwood, *Supramolecular Chemistry*, Wiley, Chichester, **2000**.

[5] J.-M. Lehn, In: M. V. Kisakürek (ed), *Organic Chemistry: Its Language and Its State of the Art*, VCH, Weinheim, **1993**, 77.

[6] A. M. Kaifer, M. Gómez-Kaifer, *Supramolecular Electrochemistry*, Wiley-VCH, Weinheim, **1999**.

[7] V. Balzani, F. Scandola, In: J. L. Atwood, J. E. D. Davies, D. D. Macnicol, F. Vögtle (eds*), Comprehensive Supramolecular Chemistry*, Pergamon Press, Oxford, **1996**, *10*, 687.

[8] D. Rouvrai, *Chem. Brit.* **2000**, *36*, 46.

[9] P. A. M. Dirac, *Proc. R. Soc. London, Ser. A* **1929**, *123*, 714.

[10] E. Schrödinger, *Science and Humanism: Physics in Our Time*, Cambridge University Press, Cambridge, **1951**, 27.

[11] W. Heisenberg, *Physics and Philosophy*, Harper and Row, New York, **1958**, 186.

[12] R.G. Woolley, *J. Chem. Ed*. **198**5, *62*, 1082.

[13] P.W. Atkins, *Physical Chemistry*, Second Edition, Oxford University Press, Oxford, **1982**, Ch. 1.

[14] (a) R.P. Feynman, *Eng. Sci.* **1960**, *23*, 22. (b) R.P. Feynman, *Saturday Rev.* **196**0, *43*, 45. See also: http://www.its.caltech.edu/~feynman.

[15] F. Cramer, *Chaos and Order. The Complex Structure of Living System*, VCH, Weinheim, **1993**.

[16] S. Shinkai, T. Nakaji, T. Ogawa, K. Shigematsu, O. Manabe, *J. Am. Chem. Soc.* **1981**, *103*, 111.

[17] P. Seta, E. Bienvenue, A. L. Moore, P. Mathis, R. V. Bensasson, P. Liddel, P. J. Pessiky, A. Joy, T. A. Moore, D. Gust, *Nature* **1985**, *316*, 653.

[18] B. Alpha, V. Balzani, J.-M. Lehn, S. Perathoner, N. Sabbatici, *Angew. Chem. Int. Ed. Engl.* **1987**, *26*, 1266.

[19] *Single Molecule Detection in Solution*, C. Zander, J. Enderlein, R. A. Keller, Wiley-VCH, Weinheim, **2002**.

[20] M. F. Crommie, *Science* **2005**, *309*, 1501.

[21] W. Schulz, *Chem. Eng. News* **2000**, *78*, 41.

[22] S.-W. Hla, G. Meyer, K.-H. Rieder, *ChemPhysChem* **2001**, *2*, 361.

[23] T. Christ, F. Kulzer, P. Bordat, T. Basché, *Angew. Chem. Int. Ed.* **2001**, *40*, 4192.

[24] (a) *Dendrimers and other Dendritic Polymers*, J. M. J. Fréchet, D. A. Tomalia, eds., Wiley, Sussex, **2001**. (b) G. R. Newkome, C. Moorefield, F. Vögtle, *Dendrimers and Dendrons: Concepts, Syntheses, Perspectives*, VCH, Weinheim, **2001**.

[25] E. W. Buhleier, W. Wehner, F. Vögtle, *Synthesis* **1978**, 155.

[26] D. A. Tomalia, H. Baker, J. R. Dewald, M. Hall, G. Kallos, S. Martin, J. Roeck, J. Ryder, P. Smith, *Polym. J.* **1985**, *17*, 117.

[27] G. R. Newkome, Z.-Q. Yao, G. R. Baker, K. Gupta, *J. Org. Chem.* **1985**, *50*, 2003.

[28] C. J. Hawker, J. M. J. Fréchet, *J. Am. Chem. Soc.* **1990**, *112*, 7638.

[29] For some recent reviews, see: (a) Mery, D.; Astruc, D *Coord. Chem. Rev.* **2006**, *250* 1965. (b) Tomalia, D. A.; Fréchet, J. M. J. Eds. Special Issue: Dendrimers and Dendritic Polymers. In: *Prog. Polym. Sci.* **2005**, *30 (3-4)*. (c) Scott, R. W. J.; Wilson, O. M.; Crooks, R. M.; *J. Phys. Chem. B* **2005**, *109*, 692. (d) Chase, P. A.; Klein Gebbink, R. J. M.; van Koten, G. *J. Organomet. Chem.* **2004**, *689*, 4016. (e) Ong, W.; Gomez-Kaifer, M.; Kaifer, A. E. *Chem. Commun.* **2004**, 1677. (f) Ballauff, M.; Likos, C. N. *Angew. Chem. Int. Ed.* **2004**, *43*, 2998. (g) Caminade, A.-M.; Majoral, J.-P. *Acc. Chem. Res.* **2004**, *37*, 341.

[30] P. Ceroni, G. Bergamini, F. Marchioni, V. Balzani, *Prog. Polym. Sci.* **2005**, *30*, 453, and reference therein.

[31] L.-X. Liao, F. Stellacci, D. V. McGrath, *J. Am. Chem. Soc.* **2004**, *126*, 2181.

[32] K. R. J. Thomas, A. L. Thompson, A. V. Sivakumar, C. J. Bardeen, S. Thayumanavan, *J. Am. Chem. Soc.* **2005**, *127*, 373.

CHAPTER 2

Photochemistry and Related Processes

2.1 Introduction

In a supermolecule most of the intrinsic properties of each units are expected to be maintained with relative minor changes that can be ascribed to the mutual perturbations between the units contained in system. For this reason the investigation of the photophysical, photochemical and electrochemical properties of model compounds is absolutely necessary to understand the properties of supramolecular systems. These properties, however, are usually not the simple superposition of those of the component units. In fact, it is possible that processes involving two or more components take place in a supermolecule, such as *(i)* intercomponent energy or electron transfer and/or *(ii)* cooperative effects (for example complexation of guest molecules or modification of the physical or chemical properties of the units).

The study of the new distinctive photochemical, photophysical and electrochemical properties of the supermolecule constitutes the object of supramolecular photochemistry and electrochemistry.

Dendrimers can be functionalised, in their different topological regions, with luminescent moieties: photoactive units can also be non-covalently hosted in the

cavities or associated on the dendrimer surface. Coupling luminescence with dendrimers is of particular interest since: (i) luminescence signals offer a handle to better understand the dendritic structure and superstructure; moreover, it is possible to monitor the interactions of the macromolecule with other chemical species and with the environment. (ii) Cooperation among the photoactive components can allow the dendrimer to perform useful functions such as light harvesting and signal amplification for sensing purposes.

2.2 Supramolecular photochemistry

Photochemistry is a science focused on the description of physical and chemical process, induced by the absorption of photons. It is a very broad discipline, embracing an extensive range of energetic, structural and dynamic processes.

While further investigations on the excited state properties of simple molecules are certainly required to arrive at complete understanding of the photochemical processes, there is an emerging need to study the photochemical behavior of supramolecular species in order to extend our knowledge of basic phenomena, make progress towards the understanding of complex photobiological processes via examination of simpler models, and find systems that might be useful for practical applications.[1]

Relatively new but very interesting applications of photochemistry are in the field of molecular devices. For instance, the possibility of using light energy as input to induce molecular movements is very important because it offers the possibility to

mache molecular machine work without accumulation of waste products. Other advantages of using photochemical energy input are: *(i)* light can be switched on and off very easily and rapidly *(ii)* lasers provide the opportunity of working in a very small space and very short time domains *(iii)* photons, besides supplying the energy needed to make the machine work, can also be useful to "read" the state of the system and thus to control and monitor the operations of the machine.

2.2.1 Basic aspects of photochemistry

A historic and very useful diagram used in photochemistry to represent the deactivation process of the electronic excited states is the Jablonski diagram, (Figure 2.1).

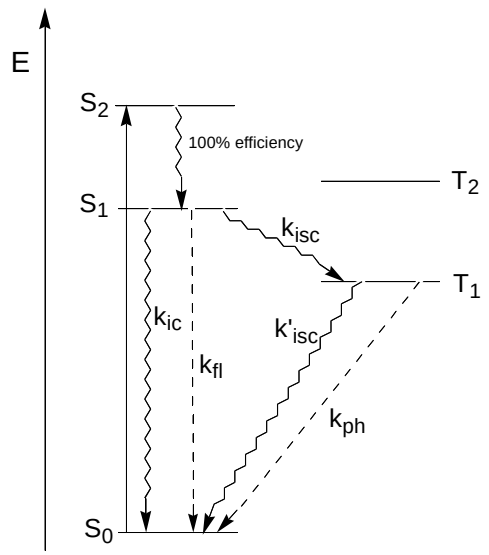

Figure 2.1. Jablonski diagram for an organic molecules. S_n Singlet state, T_n Triplet state, K_{isc} intersistem crossing rate constant, K_{ic} internal conversion rate constant, K_{fl} fluorescence rate constant, K_{ph} phosphorescence rate constant.

As reported on the diagram, in most cases the ground state of organic molecules is a singlet state (S_0), and the excited states are either singlets (S_1, S_2, etc) or triplets (T_1, T_2, etc). In principle, transitions between states having the same spin value are allowed, whereas those between states of different spin are forbidden. Therefore, the electronic absorption bands observed in the UV-visible spectrum of molecules usually correspond to $S_0 \rightarrow S_n$ transitions. Excited states are unstable species that undergo fast deactivation by intrinsic (first order kinetics) processes. When a molecule is excited to upper singlet excited states, it usually undergoes a fast and 100% efficient radiationless deactivation (internal conversion, ic) to the lowest excited singlet state, S_1. Such an excited state undergoes deactivation via three competing processes: nonradiative decay to the ground state (internal conversion, rate constant k_{ic}); radiative decay to the ground state (fluorescence, k_{fl}); conversion to the lowest triplet state T_1 (intersystem crossing, k_{isc}). In its turn, T_1 can undergo deactivation via nonradiative (intersystem crossing, k'_{isc}) or radiative (phosphorescence, k_{ph}) decay to the ground state S_0. When the molecule contains heavy atoms, the formally forbidden intersystem crossing and phosphorescence processes become faster.

The kinetic constants of the deactivation processes usually cannot be measured directly. What can be easily measured is the lifetime (τ) of an excited state, i.e. the time needed to reduce the excited state concentration by 2.718, which is given by the reciprocal of the summation of the first order deactivation rate constants:

$$\tau\,(S_1) = 1 / (k_{ic} + k_{fl} + k_{isc}) \qquad (1)$$

$$\tau\,(T_1) = 1 / (k'_{isc} + k_{ph}) \qquad (2)$$

The orders of magnitude of $\tau\,(S_1)$ and $\tau\,(T_1)$ are approximately 10^{-9}-10^{-7} s and 10^{-3}-10^{0} s, respectively.

Another quantity that can be measured is the quantum yield of fluorescence (ratio between the number of photons emitted by S_1 and the number of absorbed photons) and phosphorescence (ratio between the number of photons emitted by T_1 and the number of absorbed photons). These quantities, that can obviously range between 0 and 1, are given by the following expressions:

$$\Phi_{fl} = k_{fl} / (k_{ic} + k_{fl} + k_{isc}) \qquad (3)$$

$$\Phi_{ph} = k_{ph}\, k_{isc} / [(k'_{isc} + k_{ph})\,(k_{ic} + k_{fl} + k_{isc})] \qquad (4)$$

Deactivation of an excited state in fluid solution can occur not only by the above mentioned intrinsic (first order) decay channels, but also by interaction with other species (called “quenchers”) following second order kinetics. The two most important types of interactions are those leading to energy (eq. 6) or electron (eqs. 7 and 8) transfer (*A and *B stand for excited molecules).[2]

$$* A + h\nu \rightarrow *A \quad (5)$$

$$*A + B \rightarrow A + *B \quad (6)$$

$$*A + B \rightarrow A^{+} + B^{-} \quad (7)$$

$$*A + B \rightarrow A^{-} + B^{+} \quad (8)$$

In both cases, the luminescence of the species A is quenched, and in the case of energy transfer the luminescence of species A can be replaced by the luminescence of species B (sensitization process).

2.2.2 Energy and electron transfer

Energy and electron transfer processes can occur not only between distinct molecules in an encounter, but also between nearby molecular components in a supramolecular (multicomponent) species. For example, in a system consisting of A and B component units, excitation of A (eq. 9) may be followed by energy (eq. 10) or electron (eqs. 11 and 12) transfer to B:[2]

$$A—B + h\nu \rightarrow *A—B \quad (9)$$

$$*A—B \rightarrow A—*B \quad (10)$$

$$*A—B \rightarrow A^{+}—B^{-} \quad (11)$$

$$*A—B \rightarrow A^{-}—B^{+} \quad (12)$$

Energy and electron transfer processes between components of a supramolecular species take place following first order kinetics. They must compete, of course, with the intrinsic excited state decay, $1/\tau$ (eqs. 1 and 2, Figure 2.2).

Energy transfer requires electronic interactions and therefore its rate decreases with increasing distance, r. Depending on the electronic interaction mechanism, the distance dependence may follow a $1/r^6$ (resonance, also called Förster-type, mechanism) or e^{-r} (exchange, also called Dexter-type, mechanism).[2] In both cases, energy transfer is favoured when the emission spectrum of the donor overlaps the absorption spectrum of the acceptor.

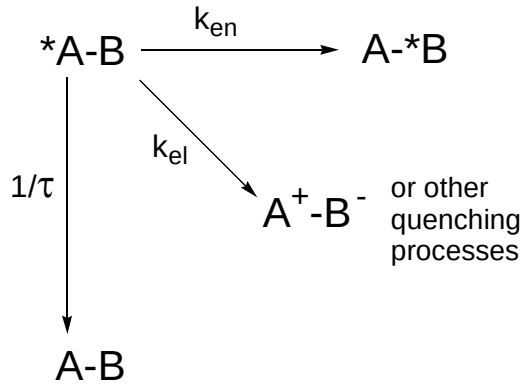

Figure 2.2. Diagram of deactivation processes that can occur between components of a supramolecular species. k_{en} energy transfer rate constant, k_{el} electron transfer rate constant, $1/\tau$ luminescence rate constant.

Quenching of an excited state by electron transfer needs electronic interaction between the two partners and obeys the same rules as electron transfer between ground state molecules (Marcus equation and related quantum mechanical elaborations)[3], taking into account that the excited state energy can be used, to a first approximation, as an extra free energy contribution for the occurrence of both oxidation and reduction processes.

2.2.3 Excimers and exciplex

In most cases, quenching of an excited state (for example, by energy transfer) takes place by a weak electronic interaction. When the excited state and the quencher undergo a relatively strong electronic interaction, new chemical species, which are called excimers (from excited dimers) or exciplexes (from excited complexes), depending on whether the two interacting units have the same or different chemical

nature (chapter 6, 7 and 8). It is important to notice that excimer and exciplex formation is a reversible process and that both excimers and exciplexes sometimes (but not always!) can give luminescence. Compared with the “monomer“ emission, the emission of an excimer or exciplex is always displaced to lower energy (longer wavelengths) and usually corresponds to a broad and rather weak band.

Excimers are usually obtained when an excited state of an aromatic molecule interacts with the ground state of a molecule of the same type. For example, between excited and ground state of anthracene units. Exciplexes are obtained when an electron donor (acceptor) excited state interacts with an electron acceptor (donor) ground state molecule. For example, between excited states of aromatic molecules (electron acceptors) and amines (electron donors). In dendrimers containing a variety of components both exciplex and excimer formation can take place[4, 5]. In such a case, as many as three different types of luminescence can be observed, namely “monomer“ emission, exciplex emission, and excimer emission (chapter 6).

It may also happen that in a supramolecular structure like a dendrimer there is a non negligible electronic interaction between adjacent chromophoric units already in the ground state. In such a case, the absorption spectrum of the species may substantially differ from the sum of the absorption spectra of the component units. When the units have the same chemical nature, the interaction leads to formation of dimers. When the two units are different, the interaction is usually charge-transfer in nature with formation of charge-transfer complexes. Excitation of such dimers

leads to an excited state that is substantially the same as the corresponding excimers, and excitation of the charge-transfer ground state complexes leads to an excited state that is substantially the same as that of the corresponding exciplexes.

References

[1] V. Balzani, L. Moggi, F. Scandola, *Supramolecular Photochemistry*, (Eds. V. Balzani), NATO ASI Series, D. Reidel, Dordrecht, **1987**.

[2] (a) V. Balzani, F. Scandola, *Supramolecular Photochemistry*, Chichester, UK:Horwood, **1991**. (b) N. J. Turro, *Modern Molecular Photochemistry*, Benjamin, **1978**. (c) A. Gilbert, J. Baggott, *Essentials of Molecular Photochemistry*, Backwell, Oxford, **1991**. (d) J. R. Lakowicz, *Principles of Fluorescence Spectroscopy*, *Plenum*, New York, **1999**.

[3] P. Piotrowiak, *Relationship between Electron and Electronic Exitation Transfer*, (Ed. V. Balzani), Electron Transfer in Chemistry, Wiley-VCH, Weinheim, **2001**, Vol. 1, p. 215.

[4] S. C. J. Meskers, M. Bender, J. Hübner, Y. V. Romanovskii, M. Oestreich, A. P. H. J. Schenning, E. W. Meijer, H. Baessler, *J Phys Chem A* **2001**, *105*, 10220.

[5] (a) J. Hofkens, L. Latterini, G. De Belder, T. Gensch, M. Maus, T. Vosch, Y. Karni, G. Schweitzer, F. C. De Schryver, A. Hermann, K. Müllen, *Chem Phys Lett* **1999**, *304*, 1. (b) Y. Karni, S. Jordens, G. De Belder, G. Schweitzer, J. Hofkens, T. Gensch, M. Maus, F. C. De Schryver, A. Hermann, K. Müllen, *Chem Phys Lett* **1999**, *310*, 73.

CHAPTER 3

Materials and methods

3.1 Materials

The synthesis of the investigated compounds and their structural characterization was performed by research groups that collaborate with our group since a long time.

In particular, the synthesis of the dendrimers described in the chapters 4, 5, 6, 7, 8, 9 and and their characterization have been performed by the research group of Prof. Fritz Vögtle of the Kekulé-Institut für Organische Chemie und Biochemie of the University of Bonn**.** The molecule studied and described in the chapter 10 was synthetized and characterized by the group of Prof. Marc Gingras of the Nice Institute of Chemistry, Université de Nice-Sophia Antipolis, France. The metal complex $[Ru(bpy)(CN)_4]^{2-}$ was provided by Prof. Maria Teresa Indelli of University of Ferrara, Italy.

In the chapter 11 is reported the work that I have done in the group of Prof. Frans De Schryver, Katholieke Universiteit of Leuven, Belgium. The molecule used in this work was synthetized by the group of Prof. Klaus Mullen of the Max Planck Institute in Mainz, Germany.

All the organic solvents were Merck Uvasol and were used without further purification. The salts, acids and bases solutions were prepared from commercial Fluka and Aldrich; products were used as received. Any other reagent or model compound occasionally used was of the best purity commercially available.

For weighting the samples for solution preparation a Mettler AT261 balance (sensitivity 0.01 mg, experimental error estimated <10%) was used.

3.2 Photophysical techniques

3.2.1 Electronic absorption spectra

All the absorption spectra in the 190–1100 nm range were recorded at room temperature on solutions contained in quartz cuvettes (optical pathlength 1 cm and 5 cm, Hellma®) by using a Perkin Elmer λ 40 spectrophotometer. The precision on the wavelength values was ± 2 nm. Molar absorption coefficient values were determined using the Lambert–Beer law; the experimental error, mostly due to weighting error, can be estimated to be around ± 5%.

3.2.2 Luminescence spectra

Fluorescence and phosphorescence emission and excitation spectra in the 250-900 nm range were recorded with Perkin Elmer LS 50 spectrofluorimeters equipped with Hamamatsu R928 or R955 photomultiplier. In case of weak luminescence signals the more sensitive Fluorolog 3 from ISA (Jobin Yvon-Spex) was used.

Room temperature spectra were recorded in the same spectrofluorimetric suprasil quartz cuvettes described for the electronic absorption spectra. In order to have comparable luminescence intensity measurements some correction had to be applied to the experimental data. These corrections were introduced to take into account instrumental geometrical effects and the distribution of the exciting light among the species effectively present in the solution.[1, 2]

Spectra in frozen matrix at 77 K were taken using quartz (or glass) tubes with an internal diameter of about 2 mm and a 20 cm length immersed in liquid nitrogen. A transparent dewar (glass or quartz) with a cylindrical terminal part with a 1 cm external diameter was employed. Such a device easily fit into the sample holder of the spectrofluorimeters above indicated. Luminescence spectra recorded in the 650-900 nm region were corrected for the non-linear response of the photomultiplier towards photons of different wavelength making reference to a previously experimentally determined calibration curve obtained. The precision on the wavelength values was ±2 nm.

Luminescence spectra in the near infrared (NIR) region were recorded by a home-made apparatus based on an Edinburgh CD900 spectrofluorimeter, which uses a Xenon lamp as the excitation source and a liquid nitrogen cooled hyperpure germanium crystal as a detector.

3.2.3 Luminescence quantum yield

Luminescence quantum yields were determined on solution samples at room temperature referring to the relative method optimized by Demas and Crosby. The quantum yield is expressed as:

$\Phi_S=\Phi_R(A_S/A_R)(n_S/n_R)^2$

where Φ, A and n indicate the luminescence quantum yield, the area subtended by the emission band (in the intensity versus frequency spectrum) and the refractive index of the solvent used for the preparation of the solution, respectively; the subscripts S and R stand for sample and reference, respectively. A_S and A_R must be relative to the same instrumental conditions ant to the same solution absorption at the excitation wavelength.

Different standards were selected depending on the spectral region of interests: naphthalene in degassed cyclohexane (Φ=0.23)[3], Fluorescein in NaOH 0.01 M (Φ=0.90)[4] or quinine sulphate in 1 M aqueous solution (Φ=0.546).[5] The experimental error was ± 15%.

3.2.4 Luminescence lifetime measurements

Excited state lifetimes in the range 0.5 ns-30 μs were measured with an Edinburgh Instrument time correlated single-photon counting technique.[6] A schematic view of this instrument is reported in figure 3.1. The excitation impulse is obtained by a gas discharge lamp (model nF900, filled with nitrogen or deuterium, depending on

excitation requirements) delivering pulses of 0.5 ns width at a frequency comprised between 1 and 100 kHz or by a pulsed diode laser (406 nm Picoquant). A photomultiplier tube (Hamamatsu R928P) cooled at –20°C and suitably amplified is used as stop detector.

Lifetimes in the range between 10 μs and 5 s were measured with the same Perkin Elmer LS 50 spectrofluorimeter employed for the luminescence spectra acquisition. In this case the excitation pulse is generated by a Xe lamp (5-50 Hz) and the emission decay directly recorded. The experimental error on the lifetime measurements is ± 10%.

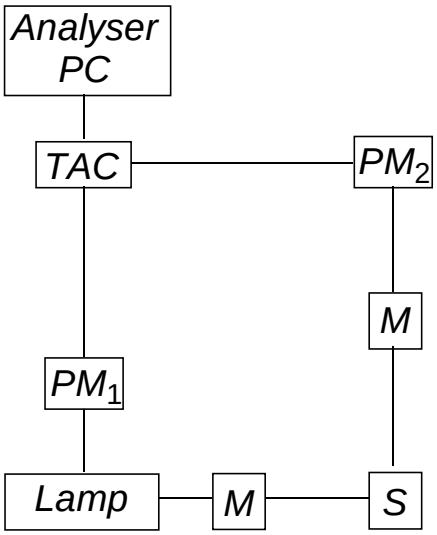

Figure 3.1. Experimental set-up of the single photon counting.

3.2.5 Titration experiments

Titration experiments have been performed directly in the spectrofluorimetric cuvettes previously described. 2.5 ml of dendrimer solution was introduced in the

cell with conventional pipettes and increasing amounts of a solution of the ion under examination added. Small volumes (of the order of 1-20 μl) were added in order to minimize the dilution effect which anyway was taken into account during data elaboration. Host concentrations were typically in the 10^{-5} 10^{-6} M range while guest solutions, before dilution, were between 10^{-3} - 10^{-4} M. During titration, usually both absorption and luminescence spectra were recorded. When possible, the fluorophores were excited at wavelength where absorption changes during the titration were small in order to simplify the luminescence spectra corrections. For the additions Hamilton microlitre syringes were used.

3.2.6 Laser flash photolysis

Laser flash photolysis experiments were carried out with a home made apparatus that is schematised in figure 3.2. In our set-up a Surelite Nd:YAG laser (pulse width ≤ 10 ns) was used as excitation source and a hight-pressure Xenon arc-lamp was used as analysing light. The signal after the sample was captured by a monochromator / photomultiplier detection system, recorded by a Tektronix TDS640A digitizer oscilloscope and transferred to a PC computer.

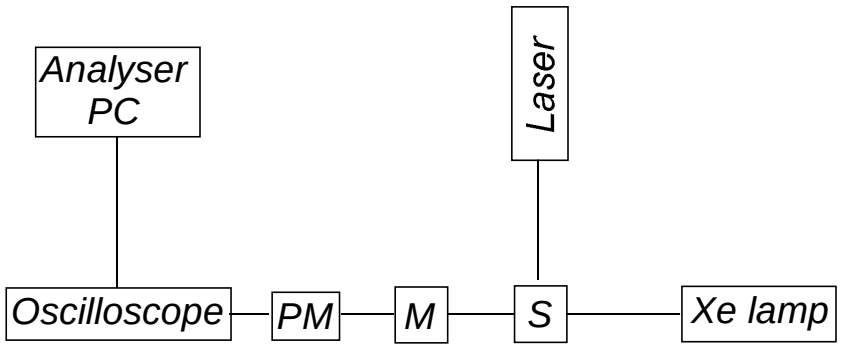

Figure 3.2. Laser flash photolysis experimental set-up.

3.2.7 Photochemical experiments

The experiments were carried out at room temperature on 3 ml solution (concentration in the range 10^{-5} to 10^{-4} M) contained in a quartz cell with optical pathlength of 1 cm. When necessary, the solution was degassed using the freeze–pump–thaw method (at least 3 cycles). The solution was continuously stirred during the irradiation with a Hellma Microver apparatus. Irradiation in the UV region was performed with a medium pressure Q400 Hanau mercury lamp (150 W); the wavelength of 287, 313, 365 and 436 nm were isolated by means of interference filters. The incident light intensity was measured using the ferric oxalate actinometer;[7] and was of the order of 10^{-7} Nhν/min. Irradiation in the visible region was performed with a tungsten halogen lamp (150 W, 24 V).

Photoreaction quantum yield were determined by monitoring the changes in absorbance associated with the disappearance of the reactants or the formation of the products, at a wavelength where the absorbance could be related to the concentration of these species.

3.3 Electrochemical experiments

3.3.1 Electrochemical setup

Electrochemical experiments were carried out with with an EcoChemie Autolab 30 multipurpose instrument interfaced to a personal computer.

The working electrode for the voltammetric experiments was a glassy carbon electrode (0.14 cm^2, Amel) or a Pt ultramicroelectrode (r = 5 μm); their surface was routinely polished with a 0.3 μm alumina–water slurry on a felt surface immediately prior to use.

The counter electrode was a Pt wire separated from the solution by means of a fine glass frit. This electrode was cleaned by burning on a Bunsen flame.

A silver wire were used in voltammetric studies as a reference and quasi–reference electrodes, respectively. In all cases a reference compound was added to the solution as a standard for potential values. The criteria for the choice of such a standard were (i) its chemical inertness towards the species under examination, and (ii) the ability to give reversible, well defined oxidation and/or reduction processes not overlapping with those of the sample. The most used standard was ferrocene, which is known to give a reversible monoelectronic oxidation process[8] and to be a relatively innocent species.

The solvent used was CH_3CN Romil of high–dry quality and taken under argon stream; the solution was continuously purged with argon during the experiments. The concentration of the examined compounds was around 5×10^{-4} M; 0.05 M

tetraethylammonium hexa-fluorophosphate (Fluka puriss.) were added as supporting electrolyte. These salts were dried at 110 °C for three days prior to use. All the potential values reported in the following Chapters are *reduction* potentials and referred to the SCE electrode, unless otherwise noted.

3.3.2 Cyclic voltammetric experiments

Cyclic voltammograms were obtained at sweep rates of 1-10 V s^{-1}. The criteria of (i) separation of less than 80 mV between cathodic and anodic peaks, (ii) close to unity ratio of the intensities of the cathodic and anodic currents, and (iii) constancy of the peak potential on changing sweep rate in the cyclic voltammograms were used to establish the reversibility of a process. For reversible processes, the halfwave potential value was calculated from the average of the potential values for anodic and cathodic peaks.

The number of electrons exchanged in a redox process has been evaluated by comparison of the current intensity of the corresponding voltammetric wave with that obtained for species undergoing redox processes which involve a known number of electrons. The following expression was used: [9]

$$n_S/n_R = (I_S C_R/I_R C_S)\,(M_S/M_R)^{0.275}$$

where n, I, C and M indicate the number of electrons exchanged in the process, the current intensity of the corresponding voltammetric wave, the concentration and

the molecular mass, respectively; the subscripts S and R refer to sample and reference, respectively. The term containing the molecular masses apply the correction for differences in the diffusion coefficient of the electroactive species.

The experimental error on the potential values for reversible processes was estimated to be within ± 5 mV.

The diffusion coefficients were determined by chronoamperometric experiments using either a glassy carbon (0.14 cm^2, Amel) or a Pt ultramicroelectrode (r = 5 μm) as working electrode.

3.4 Wide-field defocused imaging

Defocused imaging of a single molecule was performed using a wide-field fluorescent microscope (Figure 3.3c) consisting of an inverted optical microscope (IX71, Olympus) equipped with 1.3-N.A., 100x oil immersion objective (Plan Fluorite, Olympus) and a highly sensitive cooled CCD camera with 512 x 512 pixels (cascade 512B, Princeton Instruments Inc.) with a pixel size of 16 x 16 μm^2. For excitation, the 532 nm light from a diode-pumped solid state laser (CDPS532M-50, JDS Uniphase Co.) was used. The wide-field illumination for excitation was achieved by focusing the expanded and collimated laser beam onto the back-focal plane of the objective (Köhler illumination mode). The polarization of excitation light in the sample plane was carefully tuned to be circular using zero-order λ/4 and λ/2 waveplates in order to compensate for polarization shift of the dichroic mirror. The power density in the plane was usually adjusted to 1 - 10 kW/

cm^2. Emission is collected by the same objective and imaged by the CCD after passing through a dichroic mirror (z532rdc, Chroma Technology Co.) and an additional spectral filter (HQ542LP, Chroma Technology Co.) removing the excitation light. The image was further magnified 3.3 times with a camera lens before the CCD camera, resulting in a maximum field of view of 24.6 x 24.6 μm^2 (48 x 48 nm^2 per pixel). The imaging was performed under N_2 atmosphere to reduce the effect of photobleaching. All measurements were done at 295 ± 2 K.

By taking defocused images, the angular distribution of the emitted fluorescence of a single molecule is mapped as a spatial distribution of intensity, which reflects 3-D molecular orientation. To obtain the images, the sample was positioned by ~1 μm toward the microscope objective from the focus using a piezoelectric transducer (PI5173Cl, Physik Instrumente). Integration times per frame vary between 200 ms and 1 s, depending on the excitation power used. The obtained defocused images were analyzed using a routine written in MatLab software, in order to determine molecular orientation in each image frame. The images were first analyzed using a pattern matching routine to determine roughly the molecular orientation in each image frame, and then fitted precisely by a non-linear least-square algorithm, which determines the molecular dipole orientation and its position coordinate with an accuracy limited by the finite signal-to-noise ratio of experimentally measured images. The images were filtered for high frequent noise by a low pass filter to improve accuracy of the fitting.

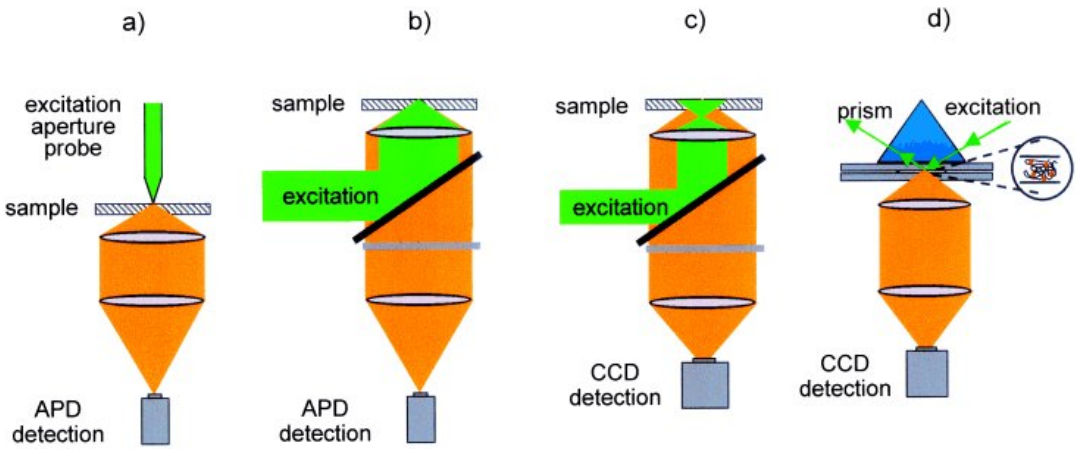

Figure 3.3. Four experimental approaches to detect single molecules: a) near-field microscopy, b) confocal microscopy, c) wide-field microscopy and d) total internal reflection (dark-field) microscopy .

References

[1] A. Credi, L. Prodi, *EPA Newsletter* **1996**, *58*, 50.

[2] A. Credi, L. Prodi, *Spectrochimica Acta A* **1998**, *54*, 159.

[3] I. B. Berlman, *Handbook of Fluorescence Spectra of Aromatic Molecules Academic*, London, **1965**.

[4] G. R. Fleming, A. W. E. Knight, J. M. Morris, R. J. S. Morrison, G. W. Robinson, *J. Am. Chem. Soc.* **1977**, *99*, 4306.

[5] S. R. Meech, D. Phillips, *J. Photochem.* **1983**, *54*, 159.

[6] J. R. Lakowicz, *Principles of Fluorescence Spectroscopy*, second editions, Kluwer Academic / Plenum Publishers, New York, **1999**.

[7] (a) C. G. Hatchard, C. A. Parker, *Proc. R. Soc. London A* **1956**, *235*, 518; (b) E. Fisher, *EPA Newsletter* **1984**, No. 21, p. 33.

[8] D. Dubois, G. Monitot, W. Kutner, M. T. Jones, K. M. Kadish, *J. Phys. Chem.* **1992**, *96*, 7137.

[9] J. B. Flanagan, S. Margel, A. J. Bard, F. C. Anson, *J. Am. Chem. Soc.* **1978**, *100*, 4248.

CHAPTER 4

Designing systems for a multiple use of light signals

4.1 Introduction

The photochemical and photophysical behavior of two dendrimers consisting of a benzophenone core and branches that contain dimethoxybenzene units has been investigated.

Benzophenone is one of the most extensively studied molecules from a photochemical and photophysical viewpoint.[1] Upon light excitation in deaerated solutions of inert solvents, benzophenone exhibits a weak (delayed) fluorescence and a strong phosphorescence, originating from the lowest n,π* S_1 and T_1 excited states, respectively. The T_1 excited state is long lived and can easily be involved in hydrogen abstraction reactions[2] and a variety of energy transfer processes.[3] For these reasons, benzophenone is an interesting unit to be used as a dendrimer component,[4] particularly when the dendrimer contains other photoactive groups. We have therefore synthesized two dendrimers (**BBG1** and **BBG2**, Scheme 4) consisting of benzophenone as a core, and branches that contain 1,3-dimethoxybenzene units (Frechét-type branches) that exhibit fluorescence and phosphorescence in the near UV spectral region. For comparison purposes, we have also investigated the behavior of dendron **DB2**, which is a branch of

dendrimer **BBG2**, and 4,4'-dimethoxybenzophenone (**DMBP**), a well known[5] derivative of benzophenone (**BP**).

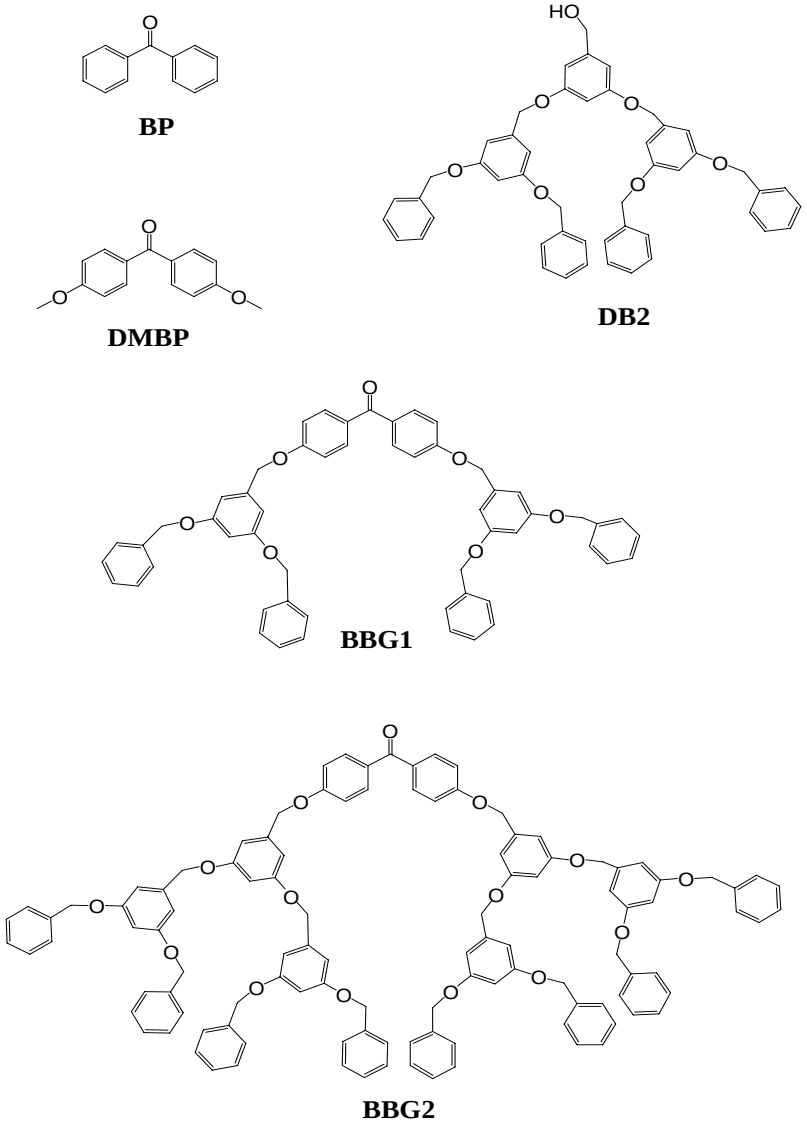

Scheme 4. Structure formulae of benzophenone (**BP**), 4,4'-dimethoxybenzophenone (**DMBP**), dendron **DB2**, and dendrimers **BBG1** and **BBG2**.

4.2 Results and discussion

As discussed elsewhere, dendrimers containing photoactive units can be considered as supramolecular species made of more or less distinct components. The subdivision of a supramolecular structure into components, however, is not always clear-cut because of electronic interactions.[6] From a purely structural viewpoint, dendrimers **BBG1** and **BBG2** can be considered as made of a benzophenone core with appended two dendrons (**DB2** in the case of **BBG2**). The absorption and emission properties discussed below, however, show that benzophenone is not fully satisfactory as a model for the dendritic core. This result is not unexpected since it is well known[5] that the properties of benzophenone are modified by the presence of substituents. We have therefore examined the properties of 4,4'-dimethoxybenzophenone (**DMBP**) and we have found that it is an excellent model compound for the dendritic core.

4.2.1 Absorption and emission spectra

The absorption and emission spectra of the investigated compounds (Figure 4.1) have been recorded in deaerated acetonitrile solution at 298 K and butyronitrile rigid matrix at 77 K.

Dendron **DB2** shows a relatively weak absorption band with λ_{max}= 280 nm (ε= 7100 M^{-1} cm^{-1}) and a fluorescence band (λ_{max}= 310 nm, $\Phi = 6 \times 10^{-3}$, $\tau < 1$ ns). Phosphorescence can only be observed in rigid matrix at 77 K (λ_{max}= 395 nm, τ = 1.31 s).

The **DMBP** model compound of the dendritic core shows an absorption band with λ_{max}= 290 nm (ε= 24700 M^{-1} cm^{-1}), a very weak, delayed[7] fluorescence band at 385 nm, almost hidden by the onset of the much stronger phosphorescence band (λ_{max}= 444 nm, τ = 90 μs [8]). At 77 K, the phosphorescence band (not shown) has λ_{max}= 433 nm and τ = 10.4 ms.

For dendrimers **BBG1** and **BBG2**, the absorption spectra are those expected from the presence of a **DMBP** unit and two or six dimethoxybenzene units, respectively (**BBG1**: λ_{max}= 284 nm, ε= 30600 M^{-1} cm^{-1}; **BBG2**: λ_{max}= 284 nm, ε= 40400 M^{-1} cm^{-1}). At 298 K, **BBG1** exhibits an emission spectrum identical to that of **DMBP**, but substantially less intense (λ_{max}= 444 nm, τ = 38 μs), and **BBG2** does not show any appreciable emission. At 77 K, however, **BBG2** shows a strong phosphorescence band (Figure 4.1d; λ_{max}= 436 nm, τ = 8.8 ms) which is almost identical (including lifetime) to those exhibited by **DMBP** and **BBG1** under the same conditions.

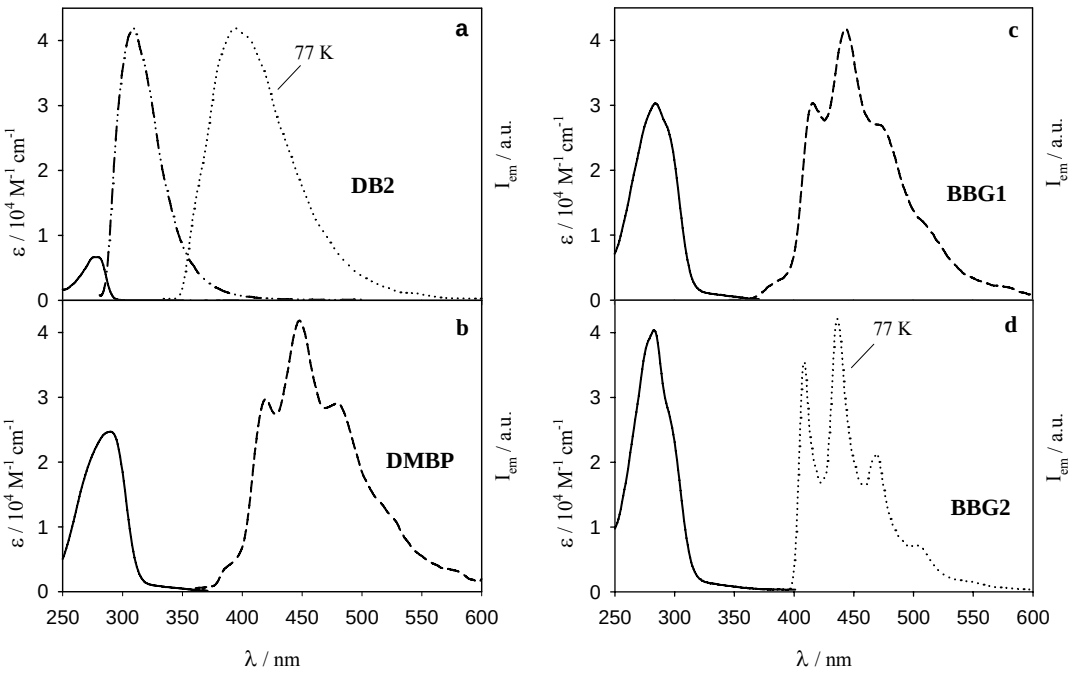

Figure 4.1. Absorption (solid line) and emission spectra of dendron **DB2** (a), 4,4'-dimethoxybenzophenone **DMBP** (b), and dendrimers **BBG1** (c) and **BBG2** (d) in deaerated acetonitrile solution at 298 K. The phosphorescence bands of **DB2** and **BBG2** in butyronitrile rigid matrix at 77 K are also shown. The emission intensities are in arbitrary units to facilitate the comparison of the forms of the spectra. Excitation at 280 nm. Emission lifetimes and more details are given in the text.

In aerated solution at 298 K, the phosphorescence bands of **DMBP** and **BBG1** are completely quenched.

The results obtained show that: (i) the fluorescence at 298 K and the phosphorescence at 77 K of the dimethoxybenzene units of the branches are completely quenched in the dendrimers; (ii) at 298 K, the strong phosphorescence band of **DMBP** is partially quenched in **BBG1** and totally quenched in **BBG2**, but at 77 K the three compounds exhibit the same phosphorescence band with quite

similar lifetime; (iii) the phosphorescence bands exhibited by **DMBP** and **BBG1** at 298 K are quenched by dioxygen.

4.2.2 Photochemical reactions

It is well known[1] that the $T_1(n,\pi*)$ excited state of benzophenone and its derivatives abstracts hydrogen from donor molecules efficiently. The reaction mechanism and the nature of the products formed in such hydrogen abstraction reactions have been studied in great detail.[1a] From the experimental viewpoint, the occurrence of hydrogen abstraction can be easily monitored by the disappearance of the absorption band related to the presence of the carbonyl group. As shown in Figure 4.1a, the dendrimer branches do not absorb at $\lambda > 290$ nm, so that the photoreaction of the benzophenone core of **BBG1** and **BBG2** can be studied by exciting with 313 nm light and monitoring the change in absorbance above 290 nm. It is also well known that the photochemical hydrogen abstraction is quite efficient from solvents like aliphatic alcohols, whereas it is negligible in the case of acetonitrile.[9] The photochemical reaction of **DMBP**, **BBG1**, and **BBG2** has been investigated under the same irradiation conditions in deaerated 1:2 v/v propan-2-ol/acetonitrile mixture and neat acetonitrile. In the mixed solvent (Figure 4.2a), the photoreaction occurs quite efficiently for each compound with a small increase in rate constant on passing from **DMBP** to **BBG1** and **BBG2**. In neat acetonitrile (Figure 4.2b), however, the photoreaction is negligible for **DMBP**, appreciable for **BBG1** and

very efficient for **BBG2**. In aerated solutions, the reaction rate was quenched in all cases.

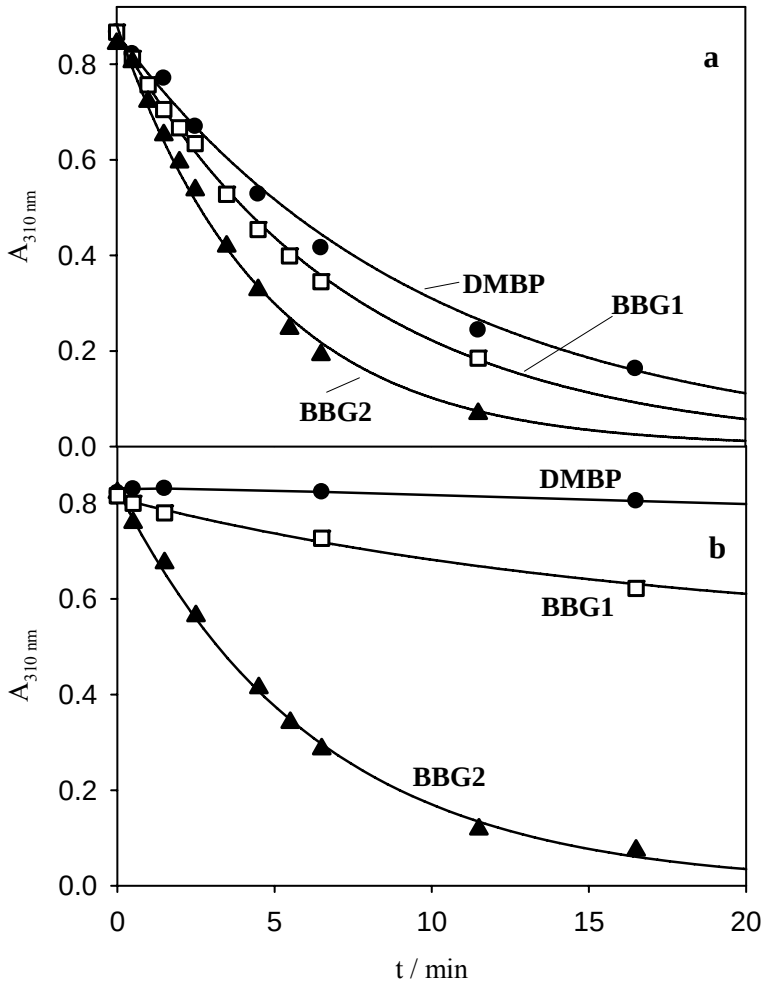

Figure 4.2. Changes in absorbance at 310 nm upon irradiation with 313 nm light for **DMBP** (circles), **BBG1** (squares) and **BBG2** (triangles) in 1:2 v/v propan-2-ol/acetonitrile (a) and neat acetonitrile (b) deaerated solutions. The intensity of the exciting light and the initial absorbance of the solution were the same in all cases.

The results obtained suggest that in the dendrimers, particularly in **BBG2**, the T_1 excited state of the core is involved in *intramolecular* hydrogen abstraction, a

reaction that has already been observed for compounds in which the molecular structure allows a close approach between the excited carbonyl group and hydrogen attached to an sp^3 hybridized carbon atom of the same molecule.[10] In the present case, the benzylic $–CH_2–$ hydrogens linked to a dimethoxybenzene unit are easy to abstract because of the great stabilization of the radical cation formed. The intramolecular nature of the photoreaction is confirmed by the fact that no absorbance decrease was observed upon irradiation of an isoabsorbing solution containing separated core and branches, i.e. a mixture of **DMBP** and **DB2**. The results obtained (Figure 4.2b) show that the opportunity for intramolecular hydrogen abstraction is larger for **BBG2** than for **BBG1**, as it can easily be understood from inspection of CPK models of the two dendrimers. Comparison of the data displayed in Figure 4.2a and 4.2b shows that in the hydrogen donating solvent mixture the intramolecular reaction competes with the intermolecular one for dendrimer **BBG1** and, even more, for **BBG2**. Finally, it should be noted that, after the hydrogen abstraction reaction, the fluorescence and, at 77 K, the phosphorescence of the dimethoxybenzene units of the dendrimer branches can be observed.

4.2.3 Intermolecular energy transfer processes

As mentioned above, both the phosphorescence intensity of **BBG1** and the hydrogen abstraction reactions of **BBG1** and **BBG2** are quenched by dioxygen. Quenching of the T_1 excited state of benzophenone-type compounds by dioxygen is

well known and takes place, in part, by energy transfer with formation of singlet oxygen, $^1\Delta$.[11] We have found that in aerated acetonitrile solutions irradiation of **BBG1** and **BBG2** causes the appearance of the singlet oxygen emission band with λ_{max}= 1260 nm. Since such an emission is very weak, it was not possible to check with sufficient accuracy whether the emission intensity is independent of the excitation wavelength.

In the presence of Tb^{3+} as an energy acceptor (1.5×10^{-4} M $Tb(CF_3SO_3)_3$), irradiation of **DMBP**, **BBG1** and **BBG2** (5.9×10^{-6} M) leads to the characteristic Tb^{3+} emission with λ_{max} = 547 nm,[12] due to a bimolecular energy transfer process.[13] A corrected excitation spectrum (emission wavelength 547 nm) of the solution containing **BBG2** matches the absorption spectrum, showing that the light absorbed by the dendrimer branches is as effective as that absorbed by the dendritic core in sensitizing the Tb^{3+} emission. No sensitized Tb^{3+} emission was obtained when dendron **DB2** was used in the place of dendrimer **BBG2**. These results shows that the above discussed quenching of the fluorescent excited state of the dimethoxybenzene units by the benzophenone core takes place by energy transfer.

4.2.4 Overview of the photochemical and photophysical behaviour of BBG2

Dendrimer **BBG2** can be viewed as a supramolecular species made of a benzophenone-like core and two branches containing altogether six dimethoxybenzene units. Its photochemical and photophysical behavior can be

schematically summarized by the scheme and the energy level diagram shown in Figures 4.3 and 4.4.

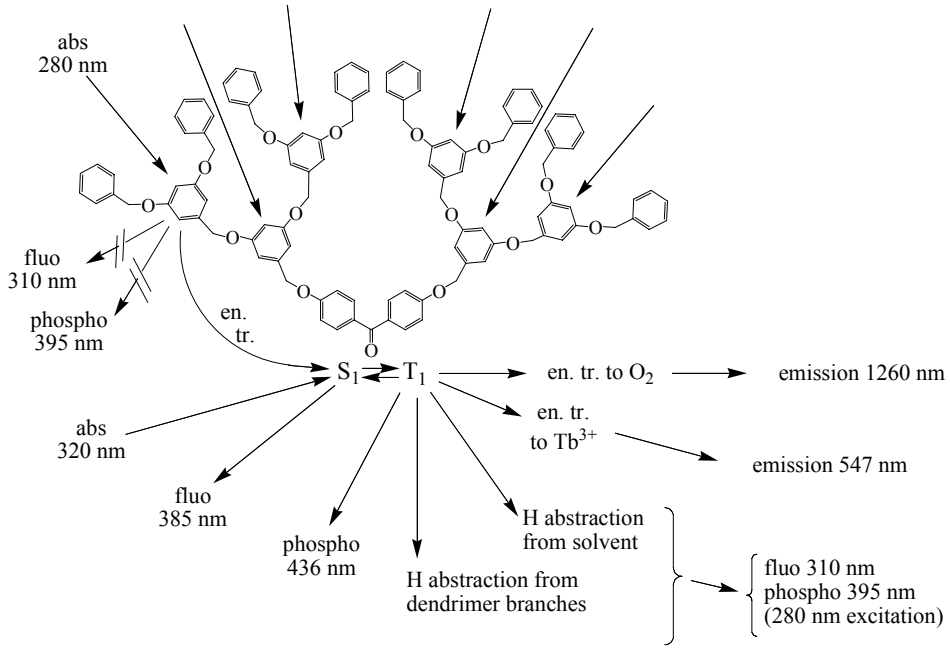

Figure 4.3. Schematic representation of the processes that can occur upon light excitation of **BBG2**.

Light excitation (λ_{ex} = 280 nm) of **DB2**, which is a model compound of the dendrimer branches, causes fluorescence (λ_{max} = 310 nm, Figure 4.1a) and, after inter system crossing, phosphorescence (at 77 K λ_{max} = 395 nm) of the dimethoxybenzene units. In dendrimer **BBG2** (Figures 4.3 and 4.4) the fluorescent S_1 excited state of the dimethoxybenzene units is completely quenched via energy transfer (presumably by a resonance mechanism[1]) to yield the S_1 excited state of the benzophenone-type core, that can also be directly populated by light absorption (λ_{ex}= 320 nm). The S_1 excited state of the core lies slightly above the correspondent T_1 excited state. The two states, in fact, are in thermal equilibrium.[7] Therefore, a

weak fluorescence and a stronger phosphorescence band would be expected, as it happens for **DMBP** (Figure 4.1b) and, to a smaller extent, for **BBG1** (Figure 4.1c). However in the case of **BBG2**, the T_1 excited state of the core is rapidly deactivated via intramolecular hydrogen abstraction (Figure 4.2b), a process that cannot occur for **DMBP** and that has low efficiency for **BBG1**. In a rigid matrix at 77 K, where hydrogen abstraction is prevented, the phosphorescence band exhibited by **DMBP** and **BBG1** is also observed for **BBG2** (Figure 4.1d). Since the rate of the photoreaction in 1:2 v/v propan-2-ol/acetonitrile is not much higher than that in neat acetonitrile for **BBG2** (Figure 4.2), the intramolecular hydrogen abstraction in the larger dendrimer competes with the intermolecular one. It should also be noted that the occurrence of the hydrogen abstraction reaction causes the disappearance of the benzophenone core, and therefore the revival of the dimethoxybenzene fluorescence and phosphorescence upon 280 nm excitation.

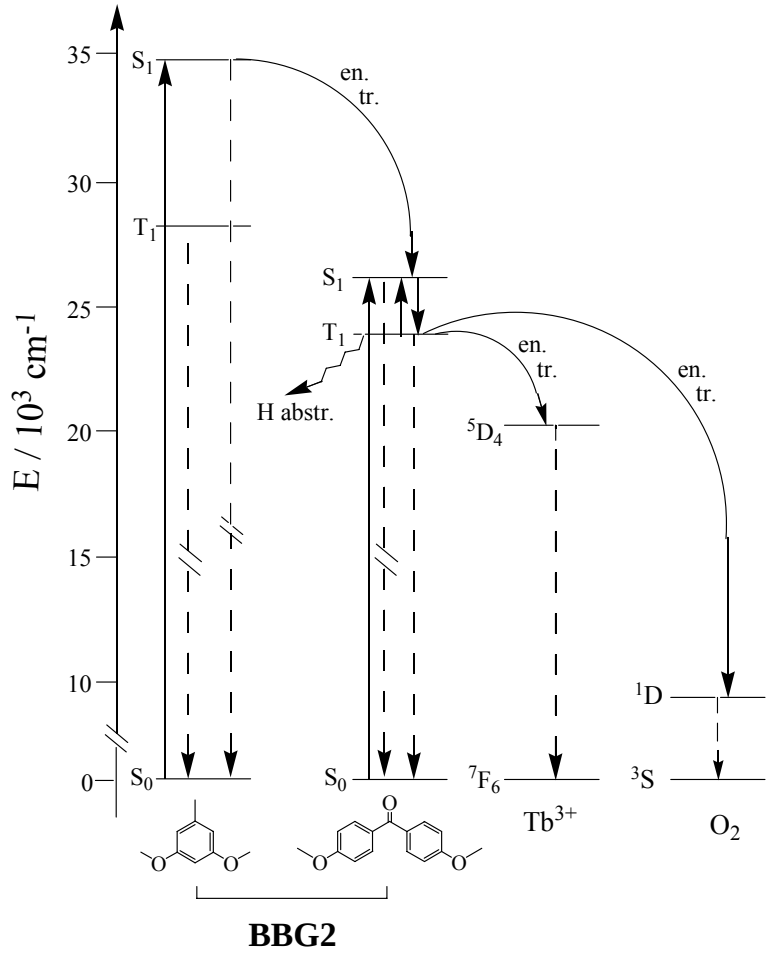

Figure 4.4. Energy level diagram showing the excited states involved in the photochemical and photophysical processes of dendrimer **BBG2**.

In aerated solution, the photoreaction rate of **BBG2** is substantially smaller, showing that there is a competition on the T_1 excited state between hydrogen abstraction and dioxygen quenching. The sensitized dioxygen emission observed for aerated acetonitrile solutions of **BBG2** shows that the quenching is due, at least in part, to energy transfer.

The sensitized Tb^{3+} emission observed upon excitation at 320 nm of solutions containing **BBG2** and $Tb(CF_3SO_3)_3$ shows that the T_1 excited state of the core can transfer energy to the metal ion. Finally, the lack of sensitized Tb^{3+} emission when **BBG2** is replaced by **DB2** and the fact that the intensity of the sensitized Tb^{3+} emission does not depend on the excitation wavelength across the dendrimer absorption spectrum shows that excitation of the dimethoxybenzene units of the dendrimer branches is followed by an efficient energy transfer to the Tb^{3+} ion via the T_1 excited state of the dendrimer core.

4.3 Conclusions

Dendrimer **BBG2** exhibits a quite complex photochemical and photophysical behavior that results from the competition among a variety of processes involving the dimethoxybenzene and benzophenone units: fluorescence, phosphorescence, intra- and inter-molecular quenching and sensitization, intra- and inter-molecular photoreactions.

It is indeed remarkable how **BBG2** makes a different use of light excitation depending on the experimental conditions, as shown by the following examples. Upon irradiation in deaerated acetonitrile solution at 77 K with 280 nm light, **BBG2** shows a stable phosphorescence with maximum at 436 nm originating from the benzophenone core. On heating the solution at room temperature, such an emission can no longer be observed, but, on continued irradiation, a fluorescent band with λ_{max} = 310 nm (typical of the dimethoxybenzene units) begins to appear

and its intensity progressively increases since the benzophenone core, which quenches the dimethoxybenzene fluorescence of the branches, undergoes hydrogen abstraction. On freezing again at 77 K the irradiated solution, the original 436 nm band does not reappear, and the 310 nm band, which is still present, is accompanied by an intense band with λ_{max} = 395 nm (phosphorescence of the dimethoxybenzene units). Such a permanent memory of the room temperature irradiation is not present, however, if the initial solution contains a sufficient concentration of Tb^{3+} ions. In such a case, excitation at 77 K with 280 nm light causes again a 436 nm emission that on thawing the solution is replaced by the Tb^{3+} emission at 547 nm. If the Tb^{3+} concentration is sufficiently high, the abstraction reaction is completely quenched and the interchange between the 436 and 547 nm bands takes place upon successive freeze/thaw cycles.

Finally, we would like to note that **BBG2** is indeed an outstanding example of a chemical compound that can be used to illustrate most of the processes that are discussed in an entire photochemical course.

References

[1] (a) A. Gilbert, J. Baggot, *Essential of molecular photochemistry*, Balckwell scientific publications, Oxford, **1991**. (b) N. J. Turro, *Modern Molecular Photochemistry*, The Benjamin/Cummings Publishing Co., Menlo Park, **1978**.

[2] (a) P. J. Wagner, R. J. Truman, A. E. Puchalski, R. Wake, *J. Am. Chem. Soc.* **1986**, *108*, 7727. (b) P. J. Wagner, R. J. Truman, J. C. Scaiano, *J. Am. Chem. Soc.* **1985**, *107*, 7093. (c) U. Pischel, S. Abad, L. R. Domingo, F. Boscá, M. A. Miranda, *Angew. Chem. Int. Ed.* **2003**, *42*, 2531.

[3] (a) A. Beeby, L. M. Bushby, D. Maffeo, J. A. G. Williams, *J. Chem. Soc, Perkin Trans 2* **2000**, 1281. (b) M. H. V. Werts, M. A. Duin, J. W. Hofstraat, J. W. Verhoeven, *Chem. Commun.* **1999**, 799. (c) A. P. Darmanyan, C. S. Foote, *J. Phys. Chem.* **1993**, *97*, 5032. (d) A. A. Lamola, P. A. Leermakers, G. W. Byers, G. S. Hammond, *J. Am. Chem Soc.* **1965**, *87*, 2322.

[4] S. Hecht, J. M. J. Fréchet, *J. Am. Chem. Soc.* **2001**, *123*, 6959.

[5] D. R. Kearns, W. A. Case, *J. Am. Chem. Soc.* **1966**, *88*, 5087.

[6] V. Balzani, A. Credi, M. Venturi, *Chem. Eur. J.* **2002**, *8*, 5525.

[7] J. Saltiel, H. C. Curtis, L. Metts, J. W. Miley, J. Winterle, M. Wrighton, *J. Am. Chem. Soc.* **1970**, *92*, 410.

[8] In deaerated acetonitrile solution benzophenone shows a phosphorescence band very similar to that of **DMBP** with $\tau = 70$ μs.

[9] J. Chilton, L. Giering, C. Steel, *J. Am. Chem. Soc.* **1976**, *98*, 1865.

[10] (a) P. J. Wagner, M. A. Meador, J. C. Scaiano, *J. Am. Chem. Soc.* **1984**, *106*, 7988. (b) E. F. Zwicker, L. I. Grossweiner, N. C. Yang, *J. Am. Chem. Soc.* **1963**, *85*, 2671.

[11] C. Schweitzer, Z. Mehrdad, A. Noll, E. –W. Grabner, R. Schmidt, *Helv. Chim. Acta* **2001**, *84*, 2493.

[12] In the case of **DMBP** and **BBG1** the sensitization of Tb^{3+} emission is accompanied by the complete quenching of the benzophenone phosphorescence.

[13] The quenching constant is 6×10^{-8} M^{-1} s^{-1} in the case of **DMBP**, as calculated by the decrease of the benzophenone T_1 lifetime upon addition of Tb^{3+}. In the case of **BBG2** the quenching constant was not calculated since the benzophenone phosphorescence is completely quenched also in the absence of Tb^{3+} by the competing intramolecular photoreaction.

CHAPTER 5

Forward (singlet-singlet) and backward (triplet-triplet) energy transfer in a dendrimer with peripheral naphthalene units and a benzophenone core

5.1 Introduction

Continuing our studies on energy-transfer processes,[1] we have investigated the photochemical and photophysical behaviour of two dendrimers consisting of a benzophenone core and branches that contain four (**BNG1**) and eight (**BNG2**) naphthalene units at the periphery (Scheme 5). Such dendrimers have been designed by purpose to investigate the occurrence of both forward (singlet-singlet naphthalene-to-benzophenone) and back (triplet-triplet benzophenone-to-naphthalene) energy transfer. In the presence of Tb^{3+} ions, the latter process is in competition with intermolecular energy transfer from triplet benzophenone to the lanthanide ion. Preorganization of the chromophoric groups in the dendritic structure has been exploited to obtain triplet-triplet annihilation and energy up-conversion in rigid matrix at 77 K, processes that are not feasible for mixtures of separated chromophoric groups.

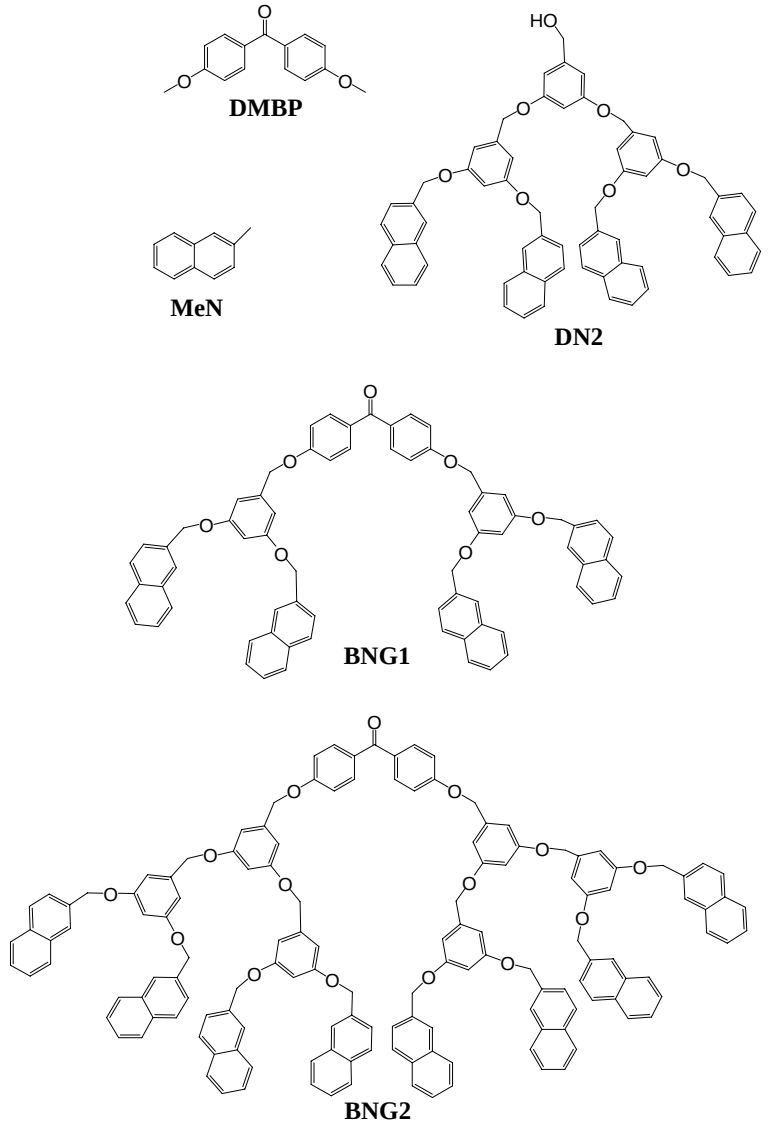

Scheme 5. Structure formulae of 4,4'-dimethoxybenzophenone **DMBP**, 2-methylnaphthalene **MeN**, dendron **DN2**, and dendrimers **BNG1** and **BNG2**.

5.2 Results and discussion

Benzophenone is one of the most extensively studied molecules from a photochemical and photophysical viewpoint.[2] Upon light excitation in deaerated

solutions of inert solvents, benzophenone exhibits a weak (delayed) fluorescence and a strong phosphorescence, originating from the lowest n,π* S_1 and T_1 excited states, respectively. The T_1 excited state is long lived and can easily be involved in hydrogen abstraction reactions[3] and a variety of energy transfer processes.[4] In compounds **BNG1** and **BNG2**, benzophenone is linked to two 1,3-dimethyleneoxybenzene-type (also called Fréchet-type) branches that carry naphthalene units in the periphery. Such units are known to exhibit a strong fluorescence and, in rigid matrix at 77 K, a very long-lived phosphorescence. The dimethyleneoxybenzene units contained in the dendrimers are potentially luminescent, but it has already been shown that their luminescent excited state is completely quenched by nearby naphthalene and dimethoxybenzophenone units.[1]

In order to better understand the photochemical and photophysical properties of dendrimers **BNG1** and **BNG2**, we have also investigated the behaviour of 4,4'-dimethoxybenzophenone (**DMBP**),[5] 2-methylnaphthalene (**MeN**), and dendron **DN2** as reference compounds (Scheme 5).

5.2.1 Absorption spectra

The absorption spectra (Figure 5.1) have been recorded in CH_2Cl_2 solution at 298 K. The model compound **DMBP** of the dendritic core shows an absorption band with λ_{max}= 290 nm (ε= 24700 M^{-1} cm^{-1}) and the model compound **DN2** of the dendritic branches shows a band with λ_{max}= 277 nm (ε= 31000 M^{-1} cm^{-1}). The

absorption spectra of the two dendrimers (**BNG1**: λ_{max}= 277 nm, ε=49000 $M^{-1}cm^{-1}$; **BNG2**: λ_{max}= 277 nm, ε= 89000 $M^{-1}cm^{-1}$) are those expected from the presence of the component units.

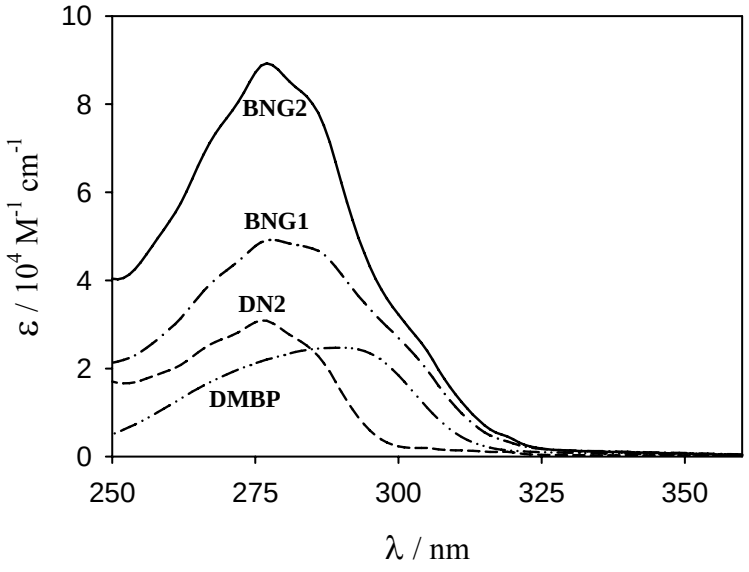

Figure 5.1. Absorption spectra of 4,4'-dimethoxybenzophenone **DMBP** (dashed-dotted-dotted line), dendron **DN2** (dashed line), and dendrimers **BNG1** (dashed-dotted line) and **BNG2** (solid line) in CH_2Cl_2 solution at 298 K.

5.2.2 Emission spectra

The emission spectra of the investigated compounds have been recorded in CH_2Cl_2 solution (298 K) and in $CH_2Cl_2/CHCl_3$ 1:1 v/v rigid matrix (77 K). The results obtained are summarized in Table 1.

At 298 K in deaerated solutions, excitation at 300 nm of model compound **DMBP** causes a very weak delayed[6] fluorescence band at 375 nm, almost hidden by the onset of the much stronger phosphorescence band (λ= 415 nm). On excitation at

270 nm, dendron **DN2** and dendrimers **BNG1** and **BNG2** (Figure 5.2) show a fluorescence band with λ_{max}=335 nm very similar to that of 2-methylnaphthalene **MeN**, except for a weak tail at lower energy (Figure 5.2, inset) that can be assigned to an excimer emission. The presence of two emitting species, namely naphthalene monomer and excimer, is proved by the double-exponential decay of the emission intensity: the longer lifetime component can be assigned to the excimer emission (weak tail in the 380-460 nm region). Corrected (see experimental section) emission spectra (Figure 5.2) and lifetimes (Table 5) showed that the fluorescence of the naphthalene units is strongly quenched in dendrimers **BNG1** and **BNG2** compared to the model compound **DN2**. No benzophenone fluorescence or phosphorescence can be observed in deaerated CH_2Cl_2 solutions of the dendrimers even when excitation is performed in the benzophenone band at 300 nm.

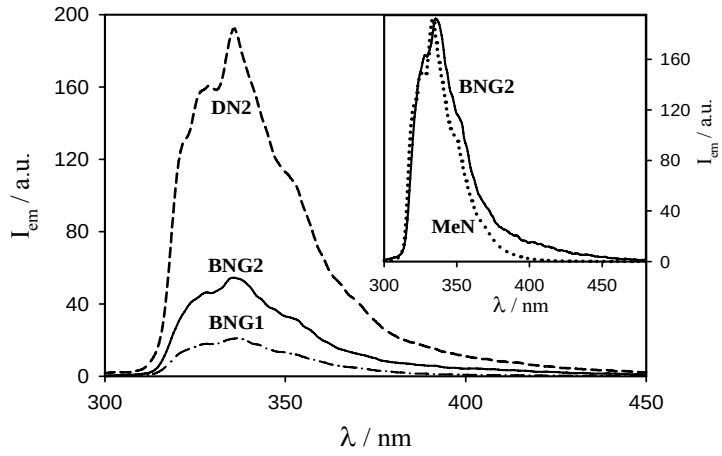

Figure 5.2. Fluorescence spectra of dendron **DN2** (dashed line), and dendrimers **BNG1** (dashed-dotted line) and **BNG2** (solid line) in CH_2Cl_2 solution at 298 K. Inset shows the normalized fluorescence spectra of dendrimer **BNG2** and 2-methylnaphthalene **MeN** in CH_2Cl_2, evidencing the excimer emission in **BNG2** (see text). λ_{exc}=270 nm.

In $CH_2Cl_2/CHCl_3$ 1:1 v/v rigid matrix at 77 K, upon excitation at 300 nm reference compound **DMBP** shows a strong, structured phosphorescence band with its highest energy feature at 406 nm (Figure 5.3a) and a double exponential decay (Table 5). As expected,[2,6] no fluorescence band can be observed. 2-methylnaphthalene **MeN** and reference compound **DN2** show a fluorescence band with its highest energy feature at 321 nm, and a phosphorescence band with its highest energy feature at 478 nm (Figure 5.3a). Upon excitation at 270 nm, dendrimers **BNG1** and **BNG2** show a fluorescence band similar to that exhibited by 2-methylnaphthalene, but lower in intensity and corresponding to a shorter lifetime (Table 5). Dendrimers **BNG1** and **BNG2** also show phosphorescence bands that, however, are quite different from one another (Figure 5.3b and 5.3c).

[a]λ_{ex} = 300 nm. [b]Delayed fluorescence in deaerated solution. [c]λ_{ex} = 270 nm.

	Fluorescence				Phosphorescence	
	298 K			77 K	77 K	
	λ_{max} / nm	Φ_{em}	τ / ns	τ / ns	λ_{max} / nm	τ / s
DMBP[a]	375[b]	-	-	-	406	3.4×10^{-3}, 17.6×10^{-3}
MeN[c]	335	0.068	10	21.0	478	1.32
DN2[c]	335	0.024	5.4 (92%) 66 (8%)	17.7	478	1.05
BNG1[c]	335	0.003	0.8 (88%) 6.4 (12%)	<0.4	- 478	- 1.13
BNG2[c]	335	0.009	2.1 (78%) 8.4 (22%)	8.2	406 478	1.2×10^{-3}, 5.4×10^{-3} 1.04

Table 5. Photophysical data in CH_2Cl_2 solution at 298 K and in $CH_2Cl_2/CHCl_3$ 1:1 (v/v) rigid matrix at 77K.

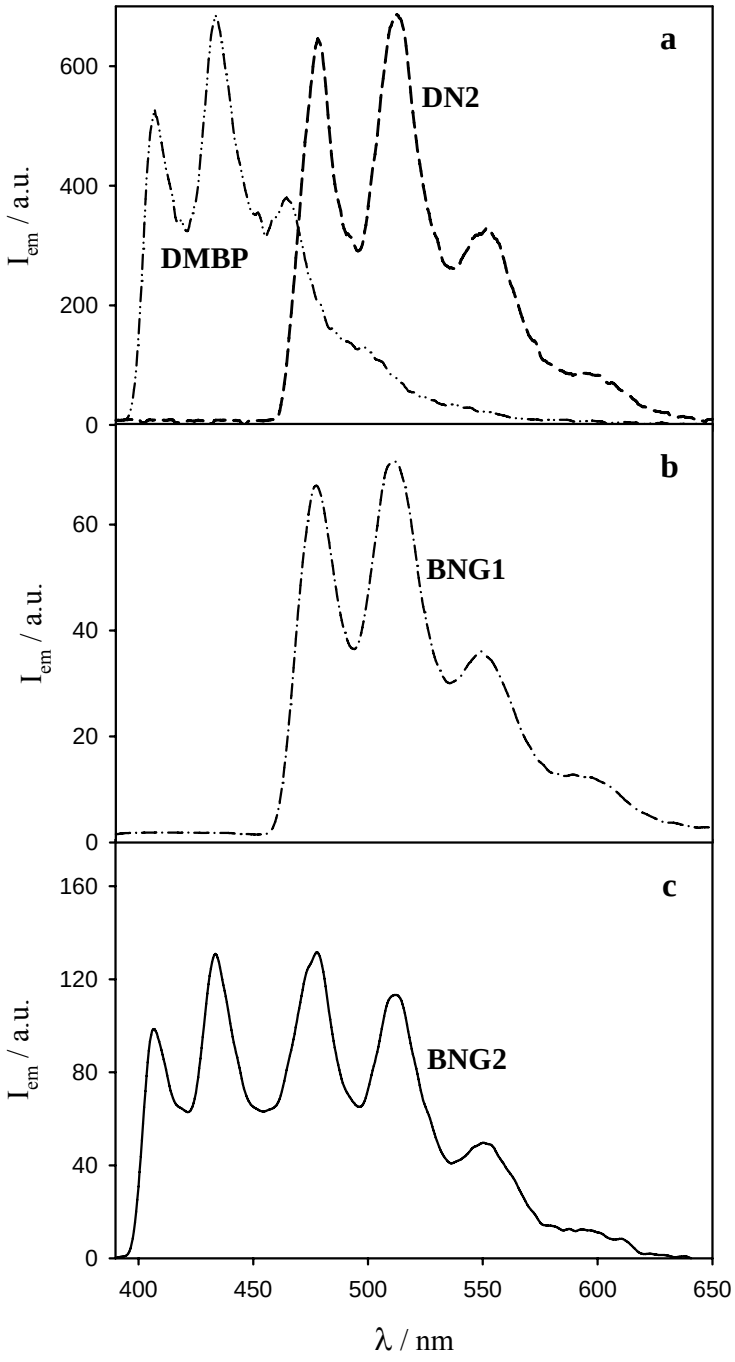

Figure 5.3. Phosphorescence spectra of (a) 4,4'-dimethoxybenzophenone **DMBP** (dashed-dotted-dotted line) and dendron **DN2** (dashed line), (b) dendrimer **BNG1** (dashed-dotted line) and (c) dendrimer **BNG2** (solid line) in $CH_2Cl_2/CHCl_3$ 1:1 (v/v) rigid matrix at 77 K. λ_{ex}=270 nm.

The phosphorescence band of dendrimer **BNG1** is very similar to that of model compound **DN2**, whereas that of **BNG2** contains the spectral features of both reference compounds, **DMBP** and **DN2**.[7] Selective excitation of the benzophenone unit of the two dendrimers at 320 nm leads to the same result. In particular, no emission at 406 nm is obtained for **BNG1**, which only exhibits the band with its highest energy feature at 478 nm. It can be noticed that the phosphorescence band of reference compound **DMBP**, as well as the corresponding spectral features of dendrimer **BNG2**, exhibit a two exponential decay. Such a behaviour is likely due to the fact that the n,π* and π,π* triplet excited states of the dimethoxybenzophenone core are very close in energy.[8] In fluid solution at 298 K, where the two states are likely thermally equilibrated, **DMBP** shows a single exponential decay (Table 5).

The relative intensity of naphthalene phosphorescence upon excitation at 270 nm is higher for the dendrimers (particularly, for **BNG1**) compared with model compound **DN2**, and for **BNG1** it is higher upon excitation at 300 nm compared with 270 nm.

5.2.3 Intradendrimer energy transfer processes

The results obtained can be rationalized on the basis of the energy level diagram shown in Figure 5.4. It can be noticed that overlap between the absorption spectra of the benzophenone core and naphthalene branches (Figure 5.1) prevents selective excitation of the naphthalene chromophoric group in the dendrimers. Therefore,

quantitative data concerning the quenching processes can better be obtained from lifetime measurements. Since phosphorescence of the naphthalene units can only be observed in rigid matrix, our discussion on the triplet-triplet energy transfer will mainly be based on the experiments carried out at 77 K.

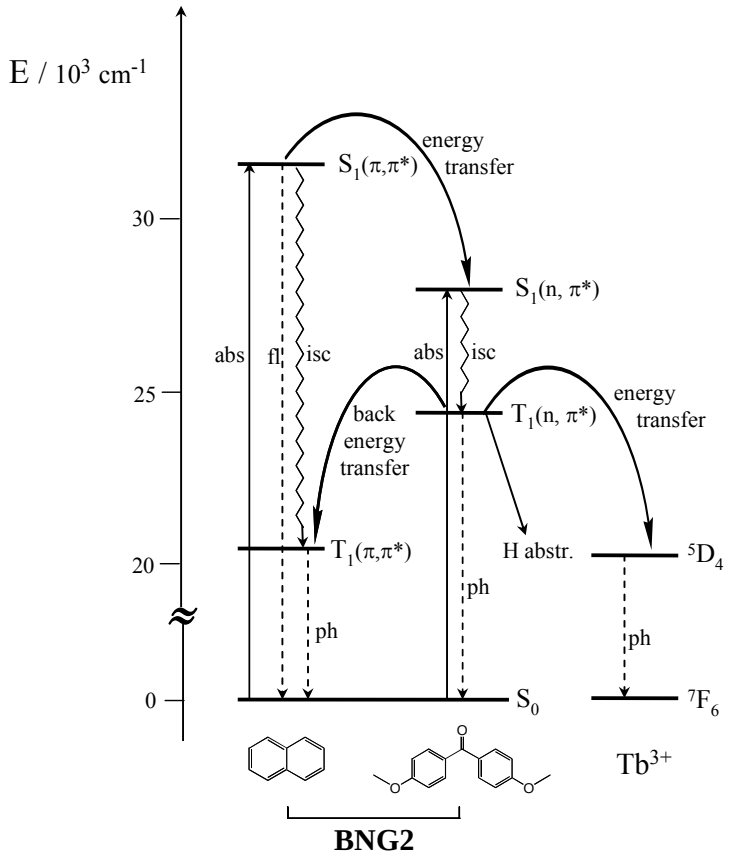

Figure 5.4. Energy level diagram showing the excited states involved in the photochemical and photophysical processes of dendrimer **BNG2**.

Excitation at 270 nm of dendrimers **BNG1** and **BNG2** leads mainly to the population of the $S_1(\pi,\pi*)$ fluorescent excited state of the naphthalene units. Comparison between the fluorescence lifetimes at 298 and 77 K of compounds

DN2, **BNG1**, and **BNG2** (as well as between the fluorescence quantum yields of the same compounds at 298 K, Table 5) shows that in the dendrimers the $S_1(\pi,\pi*)$ excited state is quenched by the presence of the benzophenone core. The quenching of the fluorescence of naphthalene-type units by benzophenone-type ones had been extensively and thoroughly investigated in a variety of dyads[9] and the conclusion was drawn that this process takes place by energy transfer from $S_1(\pi,\pi*)$ excited state of naphthalene to the $S_1(n,\pi*)$ excited state of the ketone. The rate constant of the energy transfer quenching process in dendrimers **BNG1** and **BNG2** can be estimated from the equation

$$k_{et} = 1/\tau - 1/\tau^{\circ} \qquad (1)$$

where τ° and τ are the fluorescence lifetimes of reference compound **DN2** and of the dendrimer, respectively. The values obtained are: $k_{et} = 1.1 \times 10^9\ s^{-1}$ at 298 K and $> 2.5 \times 10^9\ s^{-1}$ at 77 K for **BNG1**; $k_{et} = 2.9 \times 10^8\ s^{-1}$ at 298 K, $7 \times 10^5\ s^{-1}$ at 77 K for **BNG2**.

Upon excitation of the $S_1(n,\pi*)$ of the benzophenone core, or its population via energy transfer from the naphthalene $S_1(\pi,\pi*)$ excited state, fast and 100% efficient intersystem crossing takes place,[2] followed by triplet-triplet energy transfer from the $T_1(n,\pi*)$ excited state of the core to the $T_1(\pi,\pi*)$ excited state of the naphthalene units in the branches, as shown by the quenching of the benzophenone type phosphorescence and the sensitization of the naphthalene type one. In

particular, at 298 K for dendrimers **BNG1** and **BNG2**, the strong phosphorescence of model compound **DMBP** can no longer be observed, showing that the rate of the energy transfer process has to be at least two orders of magnitude faster than the excited state decay of the $T_1(n,\pi*)$, i.e. $k_{et} > 1 \times 10^6$ s^{-1}. In $CH_2Cl_2/CHCl_3$ rigid matrix at 77 K, dendrimer **BNG1** shows no benzophenone phosphorescence, thus $k_{et} > 6 \times 10^3$ s^{-1}. For dendrimer **BNG2**, using eq. 1 and the phosphorescence lifetimes of **DMBP** and **BNG2** (406 nm feature), the rate constant for triplet-triplet energy transfer results to be ca. 3×10^2 s^{-1}.

As shown by Figures 5.2 and 5.3, both the quenching of the naphthalene fluorescence and of the benzophenone phosphorescence is stronger in **BNG1** compared with **BNG2**.

In conclusion (Figure 5.4), the luminescence results show that excitation of the $S_1(\pi,\pi*)$ excited state of peripheral naphthalene units of dendrimers **BNG1** and **BNG2** is followed by energy transfer to the $S_1(n,\pi*)$ of the benzophenone core. This process is followed by fast intersystem crossing to the $T_1(n,\pi*)$ excited state of the core which then transfers back the energy to the $T_1(\pi,\pi*)$ excited state of the naphthalene units in the branches. Both the forward (singlet-singlet) and back (triplet-triplet) energy transfer processes are faster in **BNG1** compared to **BNG2**, as expected because of the shorter separation distance between the two types of chromophoric groups in **BNG1**.

Interestingly, the relative intensity of the naphthalene phosphorescence is higher upon excitation to the $S_1(n,\pi*)$ compared with the the $S_1(\pi,\pi*)$ one, and it is higher in the dendrimers than in model compound **DN2**. This means that the population of the $T_1(\pi,\pi*)$ excited state is more efficient via $S_0 \rightarrow S_1(\pi,\pi*) \rightarrow S_1(n,\pi*) \rightarrow T_1(n,\pi*) \rightarrow T_1(\pi,\pi*)$ than via the "shorter" $S_0 \rightarrow S_1(\pi,\pi*) \rightarrow T_1(\pi,\pi*)$ pathway because of the higher intersystem crossing efficiency of benzophenone ($S_1(n,\pi*) \rightarrow T_1(n,\pi*)$) compared with naphthalene ($S_1(\pi,\pi*) \rightarrow T_1(\pi,\pi*)$).

5.2.4 Energy transfer to Tb^{3+} ions

The above reported results show that, in dendrimers **BNG1** and **BNG2**, light excitation of the peripheral naphthalene units is followed by energy transfer to the benzophenone core, as happens in other light harvesting dendrimers.[1] In **BNG1** and **BNG2**, however, the excitation energy is then back transferred from the core to the peripheral units. Nevertheless, it should still be possible to exploit the excitation energy collected by the core before the occurrence of the back energy transfer process. In order to explore this possibility, we performed experiments using compounds **DMBP**, **DN2** and **BNG2** as energy donors towards Tb^{3+} as an energy acceptor. As shown in Figure 5.4, the lowest excited state of the Tb^{3+} ion lies below the $T_1(n,\pi*)$ excited state of the benzophenone unit and almost at the same level as the $T_1(\pi,\pi*)$ excited state of the naphthalene units. We have found that in deaerated acetonitrile solution both **DMBP** and **BNG2** sensitize the Tb^{3+} luminescence,

whereas in the case of **DN2** sensitization is almost negligible (Figure 5.5). From the concentration of Tb^{3+} (2.25×10^{-2} M), the lifetime of the $T_1(n,\pi*)$ excited state of **DMBP** in the absence (90 μs[1]) of the quencher and the ratio between the emission intensities of **DMBP** in the absence and in the presence of Tb^{3+}, we have estimated a value of k_{et}(**DMBP** $\rightarrow Tb^{3+}$) = 6.8×10^8 $M^{-1}s^{-1}$ for the energy-transfer rate constant in the case of the model compound **DMBP**. Assuming that the energy-transfer rate constant to the Tb^{3+} ion is the same for **BNG2**, from the relative intensities of the Tb^{3+} emission sensitized by **DMBP** and **BNG2** (Figure 5.5)[10] we conclude that the competing $T_1(n,\pi*) \rightarrow T_1(\pi,\pi*)$ energy transfer process has a rate constant of 3.1×10^7 s^{-1} at 298K, a value five orders of magnitude larger than that found in rigid matrix at 77 K. Such a large temperature effect is likely related to energy barriers found by the dendrimer branches to approach the core in the rigid matrix.

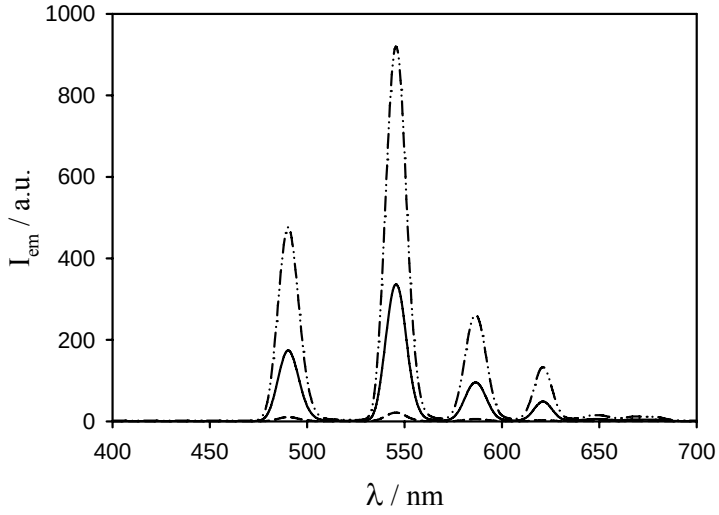

Figure 5.5. Sensitized phosphorescence spectra of a 2.25×10^{-2} M $Tb(CF_3SO_3)_3$ solution containing 4,4'-dimethoxybenzophenone **DMBP** (dashed-dotted-dotted line), dendron **DN2** (dashed line), and dendrimer **BNG2** (solid line) in deaerated acetonitrile solution at 298 K. The three solutions have the same absorbance at λ_{ex}=300 nm.

5.2.5 Delayed fluorescence and energy up-conversion

It is well known that the lowest triplet excited state of the aromatic hydrocarbons are very long lived and that the encounter between two $T_1(\pi,\pi*)$ excited molecules can lead to triplet-triplet annihilation with formation of a ground state S_0 and a $S_1(\pi,\pi*)$ excited state, thereby giving rise to a delayed fluorescence.[2,11] We thought that the preorganization of chromophoric groups in a dendrimer can be exploited to favour triplet-triplet annihilation.

We have excited isoabsorbing deaerated solutions of compounds **MeN**,[12] **DN2**, and **BNG2** in dichloromethane by a 266 nm laser source. In all cases, prompt and delayed fluorescence at 335 nm was observed, with the longer lifetime component

strongly dependent on the absorbance at the excitation wavelength and the laser intensity.[13] Under the same experimental conditions, the values of the delayed fluorescence lifetimes were: 1510 ns (**MeN**), 310 ns (**DN2**), and 320 ns (**BNG2**). The lifetime is much longer in the case of **MeN** since diffusion and encounter of two triplet excited states are necessary to observe the delayed fluorescence, while intramolecular triplet-triplet annihilation is "preorganized" in the dendritic structures. The intensity of the delayed fluorescence is higher in **MeN** because of the higher (prompt) fluorescence quantum yield (Table 5).

We have also performed the same experiment in rigid matrix at 77 K. Under such conditions, diffusion of the $T_1(\pi,\pi*)$ excited molecules is prevented and therefore no delayed fluorescence is observed for **MeN**. In the case of **DN2** and **BNG2**, however, a delayed fluorescence was again observed with lifetimes of 15 μs (**DN2**) and 8 μs (**BNG2**).

In the case of dendrimer **BNG2** delayed naphthalene fluorescence (λ_{max}=335 nm) can also be obtained upon excitation at 355 nm (benzophenone absorption band), thus leading to energy up-conversion (ΔE=0.21 eV). Energy up-conversion of this type has already been observed in the case of benzophenone and naphthalene[14] for solutions containing an excess (10^{-3} M) of the triplet donor and a small amount of the triplet acceptor (10^{-5} M).

5.2.6 Protection from photodecomposition

It is well known that the $T_1(n,\pi*)$ excited state of benzophenone and its derivatives, including **DMBP** (see chapter 4), abstracts hydrogen from donor molecules efficiently. The reaction mechanism and the nature of the products formed in such hydrogen abstraction reactions have been studied in great detail.[2a] In the case of dendrimers **BNG1** and **BNG2**, where H abstraction can also occur intramolecularly,[1] the benzophenone core is protected from hydrogen abstraction. Indeed, the $T_1(n,\pi^*)$ excited state of the benzophenone core of **BNG1** and **BNG2** has a significantly shorter lifetime (no benzophenone phosphorescence has been detected in deaerated solution under our experimental conditions) compared to model compound **DMBP** because of an efficient energy transfer to the naphthalene $T_1(\pi,\pi^*)$ excited state. Indeed, irradiation at 313 nm for 15 minutes of two isoabsorbing solutions of **DMBP** and **BNG2** in dichloromethane/2-propanol 1:1 (v/v) mixture led to an 80% decrease of the dimethoxybenzophenone absorbance in the case of **DMBP** and no observable change in the absorption spectrum of **BNG2**. Therefore, triplet-triplet energy transfer from benzophenone to naphthalene in **BNG2** is much faster than intra- and intermolecular (from solvent) H abstraction.

5.3 Conclusions

We have investigated the photochemical and photophysical behaviour of two dendrimers consisting of a benzophenone core and branches that contain four

(**BNG1**) and eight (**BNG2**) naphthalene units at the periphery. In both dendrimers, excitation of the peripheral naphthalene units is followed by fast singlet-singlet energy transfer to the benzophenone core, but on a longer time scale a back energy transfer process takes place from the triplet state of the benzophenone core to the triplet state of the peripheral naphthalene units. Selective excitation of the benzophenone unit is followed by intersystem crossing and triplet-triplet energy transfer to the peripheral naphthalene units. This sequence of processes, which is made possible by the preorganization of photoactive units in a dendrimer structure, can be exploited for several purposes. In hydrogen donating solvents, the benzophenone core is protected from degradation by the presence of the naphthalene units. In solutions containing $Tb(CF_3SO_3)_3$, sensitization of the green Tb^{3+} luminescence is observed on excitation of both the peripheral naphthalene units and the benzophenone core. Upon excitation of the naphthalene absorption band (266 nm) with a laser source, intradendrimer triplet-triplet annihilation of naphthalene excited states leads to delayed naphthalene fluorescence (λ_{max}=335 nm), that can also be obtained upon excitation of the benzophenone core at 355 nm (energy up-conversion).

References

[1] G. Bergamini, P. Ceroni, V. Balzani, F. Vögtle, S.-K. Lee, *ChemPhysChem* **2004**, *5*, 315.

[2] (a) A. Gilbert, J. Baggot, *Essential of molecular photochemistry*, Balckwell scientific publications, Oxford, **1991**. (b) N. J. Turro, *Modern Molecular Photochemistry*, The Benjamin/Cummings Publishing Co., Menlo Park, **1978**.

[3] (a) P. J. Wagner, R. J. Truman, A. E. Puchalski, R. Wake, *J. Am. Chem. Soc.* **1986**, *108*, 7727. (b) P. J. Wagner, R. J. Truman, J. C. Scaiano, *J. Am. Chem. Soc.* **1985**, *107*, 7093. (c) U. Pischel, S. Abad, L. R. Domingo, F. Boscá, M. A. Miranda, *Angew. Chem. Int. Ed.* **2003**, *42*, 2531.

[4] (a) A. Beeby, L. M. Bushby, D. Maffeo, J. A. G. Williams, *J. Chem. Soc, Perkin Trans 2* **2000**, 1281. (b) M. H. V. Werts, M. A. Duin, J. W. Hofstraat, J. W. Verhoeven, *Chem. Commun.* **1999**, 799. (c) A. P. Darmanyan, C. S. Foote, *J. Phys. Chem.* **1993**, *97*, 5032. (d) W. M. Mooreand, M. Ketchum, *J. Am. Chem. Soc.* **1962**, *84*, 1368.

[5] Previous investigations[1] have shown that benzophenone is not fully satisfactory as a model for the dendritic core.

[6] Thermally activated reverse intersystem crossing occurs between T_1 and S_1 in benzophenone and its derivatives. See e.g.: (a) A. M. Turek, G. Krishnamoorthy, K. Phipps, J. Saltiel, *J. Phys. Chem. A* 2002, 106, 6044. (b) J. Saltiel, H. C. Curtis, L. Metts, J. W. Miley, J. Winterle and M. Wrighton, Delayed fluorescence and phosphorescence of aromatic ketones in solution, *J. Am. Chem. Soc.* **1970**, *92*, 410.

[7] Notice that in CH_2Cl_2:CH_3OH 1:1 (v/v) rigid matrix at 77 K no phosphorescence of the benzophenone core was observed for **BNG2** upon excitation at 300 nm. This result suggests that in a polar matrix dendrimer **BNG2** exhibits a more compact structure that favours energy transfer.

[8] Such a situation occurs also for acetophenone: N. Ohomori, T. Suzuki, M. Ito, *J. Phys. Chem.*, **1998**, *92*, 1086.

[9] (a) R. A. Keller, L. J. Dolby, *J. Am. Chem. Soc.* **1967**, *89*, 2768. (b) A. A. Lamola, P. A. Leermakers, G. W. Byers, G. S. Hammond, *J. Am. Chem Soc*, **1965**, *87*, 2322.

[10] The ratio between the intensities of the sensitized emissions for **DMBP** and **BNG2** (3/1) has to be equal to the ratio between the lifetimes of the $T_1(n,\pi*)$ excited state of the two compounds *in the presence of the quencher*. In the case of **DMBP**, the excited state lifetime is $[1/\tau° + [Tb^{3+}]\times k_{et}(\mathbf{DMBP}\rightarrow Tb^{3+})]^{-1}$, whereas in the case of **BNG2**, the lifetime is $[1/\tau° +$

$[Tb^{3+}]\times k_{et}(\mathbf{BNG2}\rightarrow Tb^{3+}) + k_{et}(T_1(n,\pi*)\rightarrow T_1(\pi,\pi*))]^{-1}$, where $\tau°$ is the lifetime of **DMBP** in the absence of Tb^{3+}.

[11] C. A. Parker, *Adv. Photochem.* **1964**, *2*, 305.

[12] In order to have the same percentage of light absorbed by the naphthalene units, an equimolar amount of a second generation Frechét dendron functionalized with benzene units at the periphery (compound D2 in ref. 1) was added to the solution of **MeN**.

[13] In our experimental conditions, we observed a square dependence between the delayed fluorescence intensity and the laser excitation intensity, with a saturation effect at high laser power.

[14] C. A. Parker, T. A. Joyce, *Chem. Commun.* **1968**, 749.

CHAPTER 6

Cyclam-based dendrimers

6.1 Introduction

An important property of dendrimers is the presence of dynamic internal cavities.[1] This feature, coupled with the presence of coordinating moieties, has been exploited to host metal ions in the interior of dendrimers. Research on such host-guest systems has been performed for a variety of purposes which include investigation of the dendrimer structure,[2] preparation of encapsulated metal nanoparticles,[3] dioxygen binding,[4] ion transportation,[5] ion sensing,[6] light harvesting,[7] stepwise complexation,[8] reversible metal complex assembly.[9] Metal ions have also been used to assemble coordinating dendrons[10] and as branching centres in dendrimer synthesis.[11]

1,4,8,11-Tetraazacyclotetradecane (cyclam) is one of the most extensively investigated ligands in coordination chemistry. Both cyclam and its 1,4,8,11-tetramethyl derivative in aqueous solution can be protonated[12] and can coordinate metal ions such as Co(II), Ni(II), Cu(II), Zn(II), Cd(II), and Hg(II) with very large stability constants.[13,14] Furthermore, cyclam and its derivatives have been studied as carrier of metal ions in antitumor[15] and imaging[16] applications and, most recently, as anti-HIV agents.[17] In most cases, the cyclam derivatives contain

pendant functionalities to increase complex stabilities or to allow attachment of other chemical species to the macrocycle structure.

In this chapter it is presented some results of our studies on cyclam based dendrimers.

6.2 Absorption spectra, multiple luminescence and effect of protonation

Therefore we have studied two novel dendrimers (**CyG1** and **CyG2**, Scheme 6.1), synthesized by the group of Professor Vögtle, consisting of a cyclam core with appended four dimethoxybenzene and eight naphthyl units (**CyG1**) and twelve dimethoxybenzene and sixteen naphthyl units (**CyG2**). The absorption and luminescence spectra of these compounds have been investigated in acetonitrile-dichloromethane 1:1 v/v solution. For comparison purposes, the absorption and luminescence spectra of naphthalene (**Naph**), 2-naphthylmethylethylamine (**NMA**) and 1,4,8,11-tetrakis(naphthylmethyl)-cyclam (**CyG0**). Dendrimers **CyG1** and **CyG2** have been found to exhibit three types of emission bands, that have been assigned to a naphthyl localized excited state, a naphthyl excimer, and a naphthyl-amine exciplex. Titration with trifluoroacetic acid has shown that the tetraamine cyclam core undergoes two successive protonation reactions that have dramatic effects on the luminescence properties.

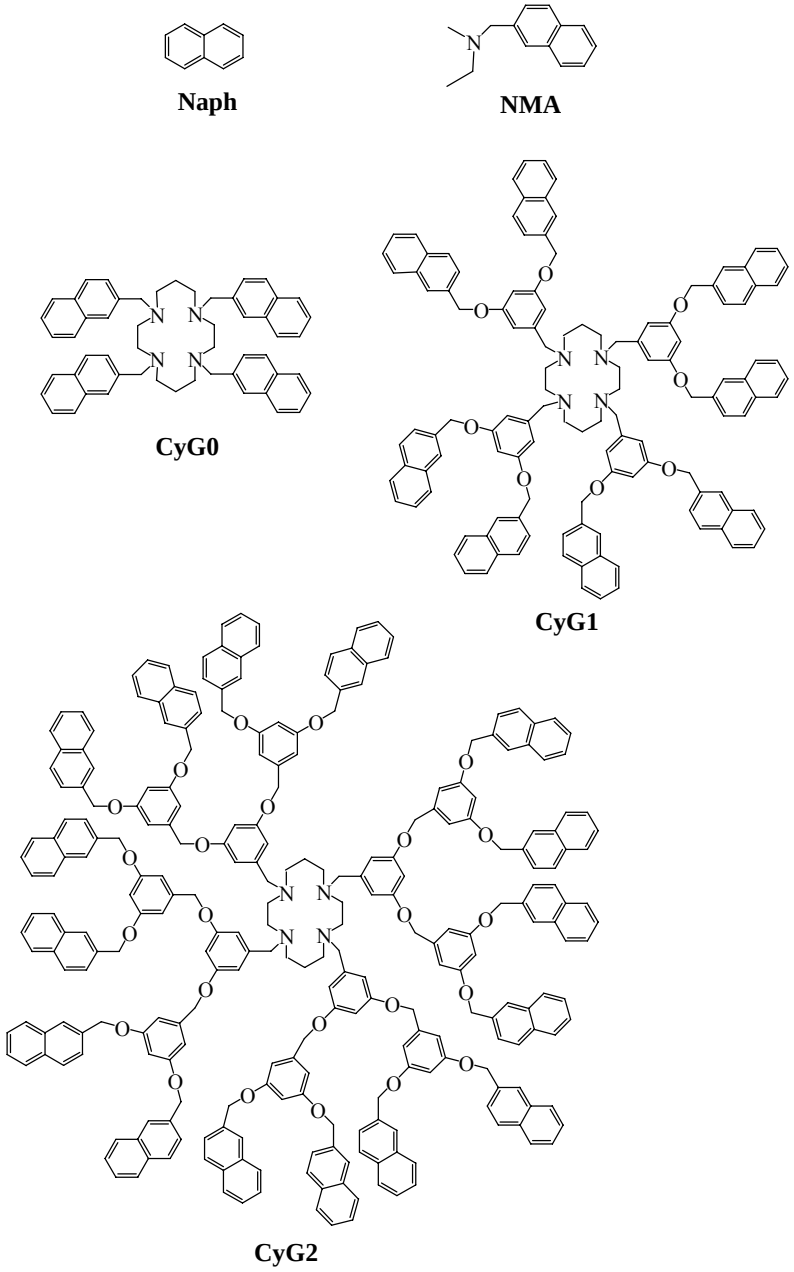

Scheme 6.1. Structure formulae of naphthalene (**Naph**), 2-naphthylmethylethylamine (**NMA**) and dendrimers **CyG0**, **CyG1** and **CyG2**

6.2.1 Unprotonated species

All the compounds are soluble in acetonitrile-dichloromethane 1:1 v/v, which has therefore been chosen as a solvent for our experiments. The X-ray structure of cyclam[14] shows that the macrocycle adopts an endodentate, centrosymmetric conformation with two three-centre hydrogen bonds. In compounds **CyG0, CyG1** and **CyG2**, of course, hydrogen bonds cannot be present because the hydrogens have been replaced by substituents.

Absorption Spectra. The absorption spectra of compounds **NMA, CyG0, CyG1** and **CyG2** are shown in Figure 6.1. The only chromophoric group present in compounds **NMA** and **CyG0** is naphthalene. Accordingly, the spectra of these compounds show the well known naphthalene bands around 270 nm ($S_0 \rightarrow S_2$ transition) and 310 nm ($S_0 \rightarrow S_1$ transition).[18] Dendrimers **CyG1** and **CyG2** contain both naphthalene and dimethoxybenzene chromophoric groups. The dimethoxybenzene unit present in the dendrimers has an absorption maximum at 275 nm with $\varepsilon = 2200\ M^{-1}\ cm^{-1}$,* much smaller than that of the naphthalene unit at the same wavelength ($6000\ M^{-1}\ cm^{-1}$ for compound **NMA**). As shown in the inset of Figure 6.1, the molar absorption coefficient at 275 nm of compounds **CyG1** and **CyG2** is higher than expected from the number of their naphthyl units because of the contribution of the dimethoxybenzene groups. If such a contribution is

* The value of the molar absorption coefficient for the dimethoxybenzene unit was obtained from the absorption spectrum of the dendron (see chapter 4).

subtracted, the molar absorption coefficients for **CyG1** and **CyG2** become slightly smaller than expected on the basis of the data obtained for **NMA** and **CyG0**, most likely because the naphthyl unit of **NMA** and **CyG0** is not a perfect model for the naphthyl unit of **CyG1** and **CyG2**, owing to the different substituents. We can conclude that the absorption spectra of the examined compounds are roughly those expected from the spectra of the component chromophoric units.

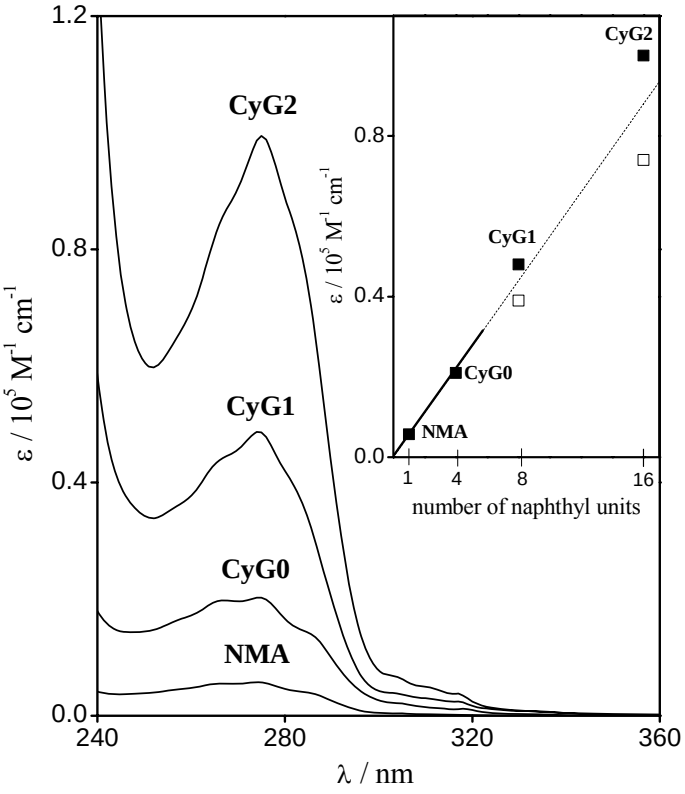

Figure 6.1. Absorption spectra of the investigated compounds in acetonitrile-dichloromethane 1:1 v/v solution at 298 K. The inset shows the molar absorption coefficients at 275 nm (dark squares). The empty squares represent the molar absorption coefficients of dendrimers **CyG1** and **CyG2** after subtraction of the expected contribution of their dimethoxybenzene chromophoric units.

Emission Spectra. Both naphthalene and dimethoxybenzene are known to exhibit fluorescence. The fluorescent excited state of dimethoxybenzene is slightly higher in energy than that of naphthalene. Therefore excitation of dimethoxybenzene can be expected to be followed by energy transfer to the naphthalene unit. In order to elucidate this point, we have compared the emission intensities observed for compound **CyG2** upon excitation at 275 nm (where 23% of the light is absorbed by the dimethoxybenzene units) and 305 nm (where absorption is only due to the naphthalene units). The results obtained show that dimethoxybenzene emission is almost completely quenched and the energy transfer does occur with efficiency $\geq$0.5.

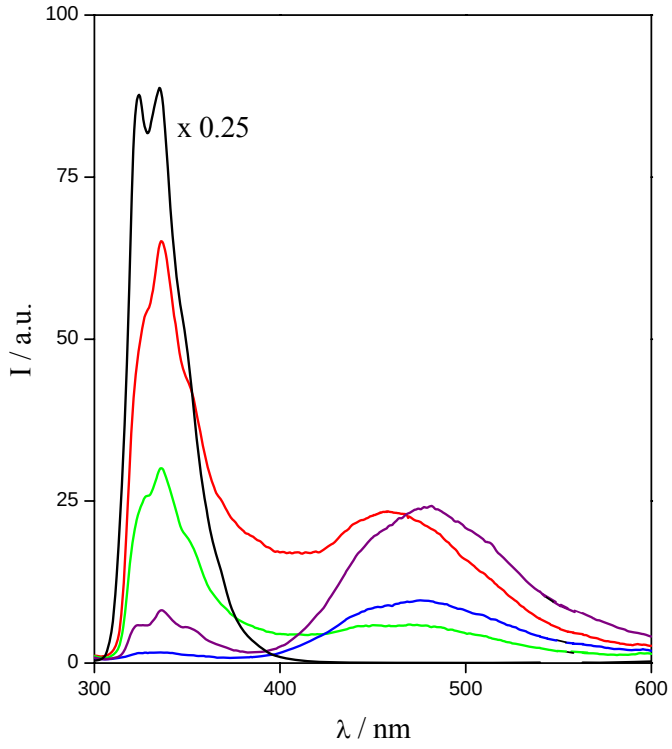

Figure 6.2. Emission spectra of **Naph** (black line), **NMA** (purple line), **CyG0** (blue line), **CyG1** (green line), **CyG2** (red line) in acetonitrile-dichloromethane 1:1 v/v solution at 298 K. The intensities are directly comparable since in all cases the excitation wavelength was 275 nm, the solution absorbance at the excitation wavelength was 0.50.

The emission spectra of compounds **NMA, CyG0, CyG1** and **CyG2** in acetonitrile-dichloromethane 1:1 v/v at 298 K are shown in Figure 6.2. In the same figure, the fluorescence spectrum of naphthalene (**Naph**) is also reported for comparison purposes. Since excitation has been performed at the same wavelength (275 nm) on solutions having the same absorbance (0.50), the intensities of the various bands are directly comparable. It can be noticed that the emission intensity

of compounds **NMA** and **CyG0** at 337 nm is only 1 or 2% that of the naphthalene,[#] and that these compounds exhibit a broad emission with maximum at about 480 nm. The quenching of naphthalene excited states by appended amine units is a well known phenomenon, usually ascribed to photoinduced electron transfer (PET) processes.[19] In several cases, the quenching occurs via formation of an intramolecular exciplex between the excited naphthyl unit and amine.[20,21,22,23] The broad band with maximum at about 480 nm can indeed be assigned to such an exciplex. A further indication of this assignment is the disappearance of this band in the emission spectrum of compound **CyG2** in butyronitrile at 77 K, where formation of exciplexes is prevented by the lack of solvent repolarisation. As shown in Figure 6.2, dendrimers **CyG1** and **CyG2** display complex emission spectra which include (i) the locally excited naphthalene band exhibiting the characteristic vibrational structure, (ii) the exciplex band shown by **NMA** and **CyG0**, slightly displaced to higher energies, and (iii) an emission band in the 400 nm region, overlapped with the other two bands, which is not present in **Naph**, **NMA**, and **CyG0**. Such an emission, which is particularly evident in the case of **CyG2**, was previously observed for other macrocyclic ligands bearing naphthyl chromophores[24,25] and can be assigned to naphthyl excimers. As it could be expected, this excimer band is almost completely absent in butyronitrile rigid

[#] It cannot be excluded that such a weak emission is due to small amounts of impurities of strongly emitting naphthalene-type compounds

matrix at 77 K. The three different types of excited states responsible for the observed emissions are schematically shown in Figure 6.3a.

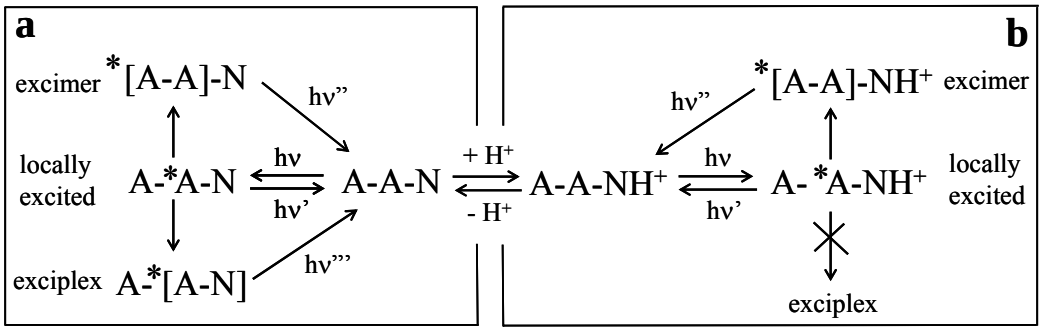

Figure 6.3. Schematic representation of the different types of excited states responsible for the observed emissions of the unprotonated (a) and protonated (b) forms of dendrimers **CyG1** and **CyG2**. A indicates a naphthalene unit and N an amine unit.

6.2.2 Effects of protonation

It is well known that cyclam undergoes protonation in aqueous solution[12,26] as well as in other solvents.[27] In aqueous solution, the four successive pK_a values are 11.6, 10.6, 1.61, and 2.42,[12] showing that cyclam can be easily mono- and di-protonated, but further protonation is difficult. It is also interesting to note that the fourth pK_a value is larger than the third one, a result related to protonation-induced structural rearrangements. In dimethylformamide solution only two successive protonation steps have been observed with pK_a values of 9.3 and 7.5.[27]

Absorption spectra. It is well known that protonation of amines engages the lone pair of the nitrogen atoms and therefore moves the n(N)→ π* charge-transfer (CT) transitions to higher energy. The lack of any spectral change upon addition of trifluoroacetic acid shows that CT transitions do not contribute to the absorption

spectrum. This finding shows that there is no appreciable interaction between amine and aromatic moieties in the ground state.

Emission spectra. Addition of trifluoroacetic acid causes strong changes in the emission spectra of compounds **NMA, CyG0, CyG1** and **CyG2**. The spectra obtained at the end of acid titration are shown in Figure 6.4. Comparison with the spectra of Figure 6.2, which have been recorded under the same experimental conditions, shows that protonation causes (i) the disappearance of the exciplex band with maximum around 480 nm in all cases, and (ii) a strong increase in the intensities of the naphthyl localized band with λ_{max} = 337 nm , particularly for compounds **NMA** and **CyG0**. Moreover, the protonated species of dendrimers **CyG1** and **CyG2** exhibit much stronger excimer bands than the corresponding isolated dendrons,[28] suggesting that excimer formation is facilitated by the folding of the dendrimer structure.

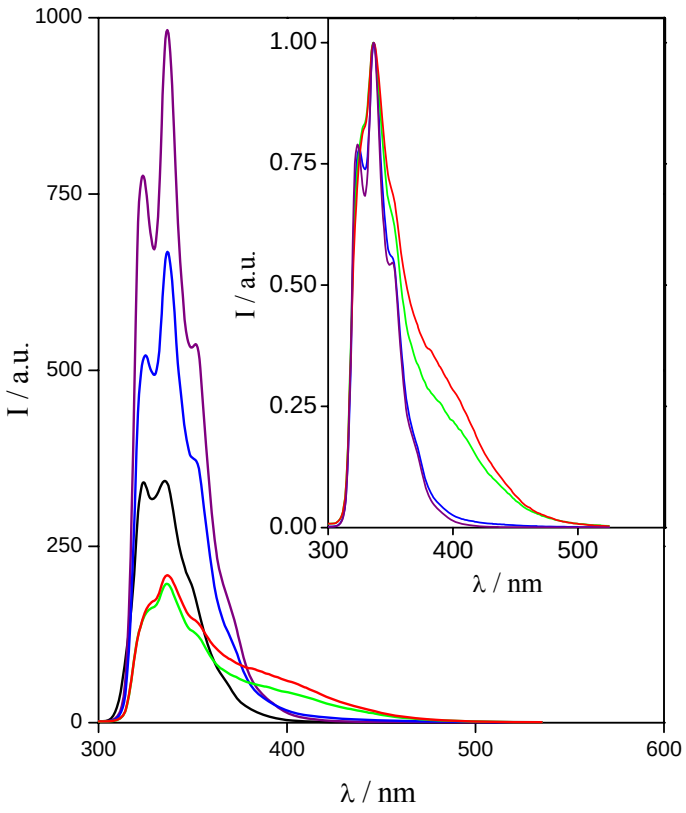

Figure 6.4. Emission spectra of **Naph** (dark line), **NMA** (purple line), **CyG0** (blue line), **CyG1** (green line), **CyG2** (red line) in acetonitrile-dichloromethane 1:1 v/v solution at 298 K at the end of the titration with trifluoroacetic acid. The intensities are directly comparable since in all cases the excitation wavelength was 275 nm, the solution absorbance at the excitation wavelength was 0.50. Direct comparison with the spectra reported in Figure 6.2 can also be made. Notice, however, the different ordinate scale of the two figures. The normalized spectra shown in the inset evidence the presence of the excimer emission in compounds **CyG1** and **CyG2**.

More details on the protonation processes can be drawn from the changes in the emission intensities observed during titration.[30a] In the case of model compound **NMA**, which contains a single naphthylamine unit, the intensity of the exciplex

band decreases and the naphthyl-localized band increases linearly with increasing acid concentration and no further change is observed after addition of one proton per nitrogen atom. For compounds **CyG0, CyG1, CyG2**, however, the intensity of the naphthyl-localized, excimer, and exciplex bands do not change linearly with increasing acid concentration. Furthermore, the spectral changes take place only during the addition of the first two equivalents of acid. These results allow us to draw the following conclusions.

(i) Under our experimental conditions (low polarity solvent), the tetraamine cyclam core apparently shows only two protonation reactions. This result is in agreement with the behaviour observed for cyclam derivatives in dimethylformamide solution.[27]

(ii) Addition of acid prevents, as expected, exciplex formation. There is no need to protonate each nitrogen atom to suppress exciplex formation, showing that protons are in some way shared by nitrogen atoms.

(iii) For all the examined compounds, the increase in the naphthyl-based fluorescence intensity (337 nm) mirrors the decrease in the emission intensity at 480 nm, showing that the species emitting at 480 nm is formed in competition with the naphthyl fluorescence decay, as expected in the case of exciplex formation. The two different types of excited states responsible for the observed emission are schematically shown in Figure 6.3b. However, the intensity of the naphthyl-localized emission at the end of the acid titration is much weaker for **CyG1** and **CyG2** than for **NMA** and **CyG0** (Figure 6.4). This effect can be ascribed to the

formation of the excimer species in the dendritic structures, which provides a deactivation pathway in competition with the naphthyl fluorescence.

(iv) For compound **CyG0**, the initial slope of the titration curve is very small and increases on increasing acid concentration until about one acid equivalent has been added. This result can be accounted for assuming that protonation of a nitrogen (or sharing a proton between two nitrogens) does not fully prevent exciplex formation between an excited naphthyl unit and a non protonated nitrogen. Formation of different types of exciplexes upon addition of acid is indicated by the slight, progressive displacement of the maximum of the exciplex band during titration.

(v) For compounds **CyG1** and **CyG2**, the slope of the titration curves based on the decrease of the exciplex band and the increase of the naphthyl band is very large at the beginning and tends to decrease on increasing acid concentration. Such a behaviour is completely different from that exhibited by compound **CyG0**. Apparently, for dendrimers **CyG1** and **CyG2** monoprotonation is sufficient to prevent most of exciplex formation. This result suggests that in dendrimers **CyG1** and **CyG2** all the four nitrogen atoms share, in some way, the first proton, a result that requires the formation of an appropriate structure.

(vi) Particularly in the case of dendrimer **CyG2**, the excimer band reaches its maximum intensity upon addition of only one proton per molecule. Since excimer formation is mostly due to folding of the dendrimer structure (see above), this result suggests that in the monoprotonated species the four dendrons lie on the

same side of the cyclam core, in a structure that could also be appropriate for the above mentioned sharing of the first proton among all the nitrogen atoms.

In an attempt to obtain further information on the protonation processes, the spectra were implemented into the SPECFIT software.[29] The resulting values for the two association constants are very large (for example, pK_1 = 7.4 and pK_2 = 7.0 for compound **CyG1**) and do not appreciably differ for compounds **CyG0, CyG1, CyG2**. The fitting procedure allows also to obtain the spectrum of the monoprotonated form. The calculated spectra of the monoprotonated forms of compounds **CyG1** and **CyG2** are very close to that of the diprotonated one, contrary to what happens for compound **CyG0**.

6.3 Cyclam cored luminescent dendrimers as ligands for Zn(II), Co(II), Ni(II) and Cu(II) ions

Continuing our investigations in the field of photoactive dendrimers containing a cyclam core, we have thus performed titrations in acetonitrile/dichloromethane 1:1 (v/v) solutions of the two dendrimers (**CyG0** and **CyG2**) with Ni(II), Co(II) and Cu(II) as nitrate salts.

The complexation of the comparison compound **CyG0** (ca. 2.5×10^{-5} M) and dendrimer **CyG2** (ca. 6.0×10^{-6} M) have been investigated in acetonitrile/dichloromethane 1:1 (v/v) solutions with Ni(II), Co(II) and Cu(II) as nitrate salts and the results have been compared with those previously obtained upon addition of $Zn(CF_3SO_3)_2$ in the same solvent mixture.[30]

6.3.1 Zn(II) complexation

Titration of **CyG0** solutions with Zn(II) causes the disappearance of the exciplex emission (470 nm) and the appearance of a strong naphthyl-localized fluorescence (337 nm); the final emission spectrum is identical in shape and intensity to the spectrum obtained upon protonation. Zn(II) coordination to the cyclam unit, engaging nitrogen lone pairs, prevents exciplex formation and switches on the usual, intense naphthyl fluorescence. The titration plot shows the formation of the 1:1 species, $[Zn(\mathbf{CyG0})]^{2+}$. Similar, but not identical results were obtained by Zn(II) titration of dendrimer **CyG2**. The emission spectrum shows the decrease of the exciplex emission and the parallel increase of the emission intensity at 337 nm (naphthyl emission) and 400 nm (excimer emission); these changes yielded coincident linear plots that reach a plateau for 0.5 equivalents of Zn(II), showing the unexpected formation of a 1:2 Zn/ligand species, $[Zn(\mathbf{CyG2})_2]^{2+}$ (Table 6.1). ^{1}H NMR experiments evidenced the gradual replacement of this species by $[Zn(\mathbf{CyG2})]^{2+}$ upon further Zn(II) addition. Fluorescence experiments were unable to evidence the formation of the latter species.

6.3.2 Ni(II) complexation

Addition of $Ni(NO_3)_2.6H_2O$ to a **CyG0** solution causes absorbance changes mainly localized in the 240-280 nm region (Figure 6.5a). The absorbance increase in this region is due not only to the added nitrate salt (this contribution has been subtracted in the plot reported in the inset of Figure 6.5a) but also to the formation

of a Ni(II) cyclam complex. In the case of **CyG2**, the use of a very low dendrimer concentration, leads to absorption changes too small to be profitably analyzed.

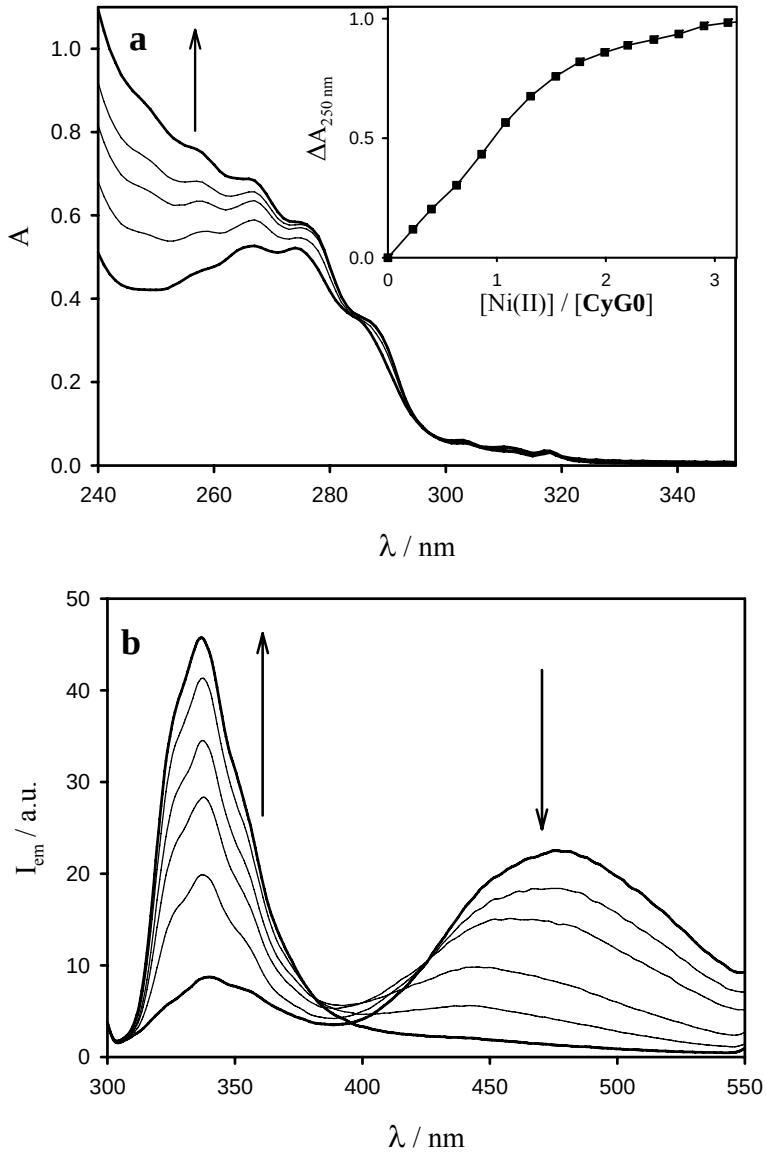

Figure 6.5. Absorption (a) and emission spectra (b) of **CyG0** upon addition of $Ni(NO_3)_2.6H_20$ in acetonitrile/dichloromethane 1:1 (v/v) solution at 298 K. Inset of panel (a) shows absorption changes at 250 nm, after correction for nitrate absorption (see text).

On the contrary, strong changes have been observed in the emission spectra of both dendrimers (see e.g. Figure 6.5b and Figure 6.6). Upon addition of Ni(II), exciplex emission band decreases and naphthyl monomer emission intensity at 337 nm increases (in the case of dendrimer **CyG2** an emission increase at 400 nm was also observed). These results were expected since it is known that Ni(II), like Zn(II), can be coordinated by cyclam nitrogens preventing exciplex formation and thus reviving naphthyl monomer emission (and excimer emission in the case of **CyG2**). However, detailed analysis of the shape and intensity of the emission bands shows that emission intensity at 337 nm is much lower than that observed upon Zn(II) complexation (Figure 6.7), especially in the case of compound **CyG0**. Moreover, exciplex emission does not completely disappear and is progressively shifted to higher energy (Figure 6.5b).[31] The low intensity of naphthyl fluorescence can be rationalized on the basis of a double-faced effect of Ni(II) coordination: on one hand, it can increase naphthyl emission, engaging nitrogen lone pairs of cyclam, and, on the other hand, it can quench it offering additional deactivation pathways to the naphthyl singlet excited state via energy or electron transfer processes. It is well known that Ni(II) has metal centred excited states[32] at energy lower than the fluorescent excited state of naphthalene (4.0 eV[33]). It is also known that this excited state is a reductant strong enough ($E°(Naph^{+}/{}^{*}Naph)$ ca. – 2.3 V[33]) to reduce Ni(II) complexes.[34] On the basis of our results, we cannot discriminate between the two mechanisms, even though we lean towards a photoinduced energy transfer pathway in agreement with the suggestion previously reported for a Ni(II) complex with 1-

(2-naphthylmethyl)-1,4,8,11-tetraazacyclotetradecane ligand on the basis of 77K measurements.[35]

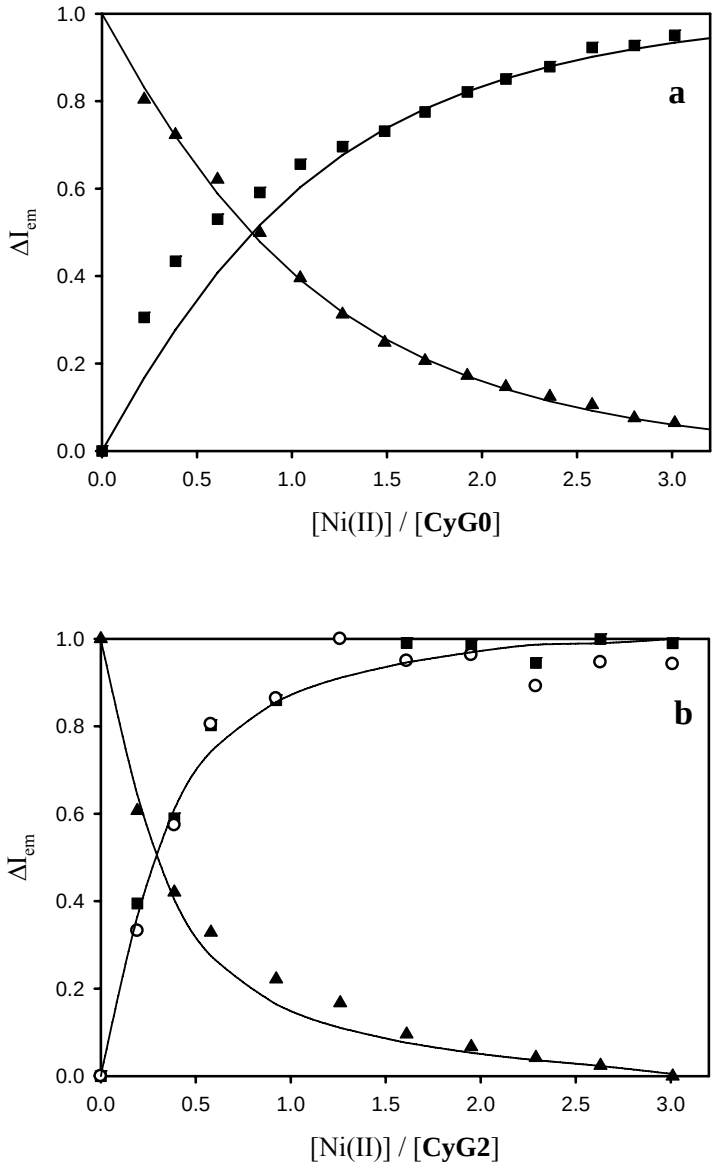

Figure 6.6. Normalized emission intensity changes observed upon addition of $Ni(NO_3)_2.6H_20$ to **CyG0** (a) and **CyG2** (b) in acetonitrile/dichloromethane 1:1 (v/v) solution (298 K, λ_{exc} = 275 nm). Emission intensity was monitored at 337 nm (squares), 380 nm (open circles, only for **CyG2**), and 480 nm (triangles). Solid lines represent the best fitting obtained by SPECFIT.[29]

As far as the incomplete disappearance (and blue shift) of exciplex emission two hypothesis can be done.

i) Free dendrimer ligands are still present at the end of the titration because of low complexation (association) constants and competition with nitrate ions and water molecules to coordinate Ni(II). Indeed, upon addition of one equivalent of Ni(II), two equivalents of nitrate ions and six equivalents of water molecules are also added.[36]

ii) Nitrate ions are good ligands for Ni(II) and high-spin hexacoordinated complexes can be formed. Indeed, it has been previously reported[35] that, in low coordinating solvents, Ni(II) forms with cyclam low-spin square-planar complexes with anions like ClO_4^-, $CF_3SO_3^-$, and high-spin pseudo-octahedral complexes with NO_3^-, Cl^-, NCS^-.

The first hypothesis can be discarded, since upon addition of an excess of metal ion, no significant change in the emission spectrum has been reported and high stability constant for Ni(II) complexes with cyclam derivatives have been reported.[13a] As to the second hypothesis, nitrate ions are likely present in the coordination sphere, therefore cyclam nitrogens are not so strongly linked to the metal ion. A fast exchange between bound and unbound cyclam nitrogen atoms takes place, so that formation of exciplexes is not completely prevented and the corresponding emission is shifted at higher energy compared to the initial one because of a partial engagement with metal ions.

In the case of **CyG2**, preventing the formation of exciplex not only naphthalene monomer but also excimer emission at 400 nm increases because more excited naphthalene units are free to deactivate by fluorescence or excimer formation.

Global analysis by SPECFIT[29] of the absorption (only for **CyG0**) and/or emission spectral changes during Ni(II) titration allows us to evaluate complex stoichiometry and association constants. For dendrimer **CyG0**, best fitting was obtained with logβ = 5.0 (Table 6.1) for a complex with 1:1 stoichiometry. In the case of the largest dendrimer, changes in the slope of the emission plots (Figure 6.6b) around 0.5 equivalents of Ni(II) per ligand indicate the formation, at low metal ion concentration, of a 1:2 metal to ligand complex, $[Ni(\mathbf{CyG2})]^{2+}$ replaced by a 1:1 complex upon further addition of Ni(II). A similar behaviour was previously observed for **CyG2** with Zn(II), and, like in that case, the formation of a 1:2 species shows the lack of an appreciable steric hindrance between the two dendrons of the same complex. Fluorescence study allows us to discriminate between $[Ni(\mathbf{CyG2})_2]^{2+}$ and $[Ni(\mathbf{CyG2})]^{2+}$, at variance with Zn(II) complexation, where the conversion between the two species could be demonstrated only by ^{1}H NMR study.[30] In the present case, the 1:1 species shows a different shape of the emission spectrum with a lower intensity of the exciplex band and, correspondingly, higher naphthyl monomer and excimer emission intensities compared to $[Ni(\mathbf{CyG2})_2]^{2+}$. This is attributable to a better engagement of cyclam nitrogen lone pairs in $[Ni(\mathbf{CyG2})]^{2+}$ compared to $[Ni(\mathbf{CyG2})_2]^{2+}$.

As expected on the basis of cyclam association constants previously reported in water solution,[13a] the obtained Ni(II) association constants (Table 6.1) are much lower than those with Zn(II), even though different counterions in the two titration experiments can play a significant role. Indeed, nitrate ions, used thoroughly the present work, compete with cyclam much more strongly than triflate ions.

6.3.3 Co(II) complexation

The changes in the absorption spectra of **CyG0** and **CyG2** upon addition of Co(II) are qualitatively similar to those observed in the case of Ni(II). As far as the emission spectra are concerned, the emission band at 337 nm (and at 400 nm in **CyG2**) increases and the exciplex band decreases, owing to the Co(II) engagement of nitrogen lone pairs of cyclam. However, compared to Zn(II) titration, the 337 nm emission intensity is lower (Figure 6.7) because of the quenching of the naphthyl singlet excited state by the complexed Co(II) ion. Also in this case, like for Ni(II), metal ion complexation simultaneously lights up and quenches the dendrimer luminescence. The naphthalene fluorescence quenching process is thermodynamically allowed either via energy or electron transfer mechanisms since the excited state of the naphthyl unit is a good energy donor (4.0 eV) and a good electron acceptor ($E(^*Naph/Naph^-)$ ca. +1.6 V[33]) and Co(II) amine complexes have low energy excited states[37] and are easy to oxidize.[38]

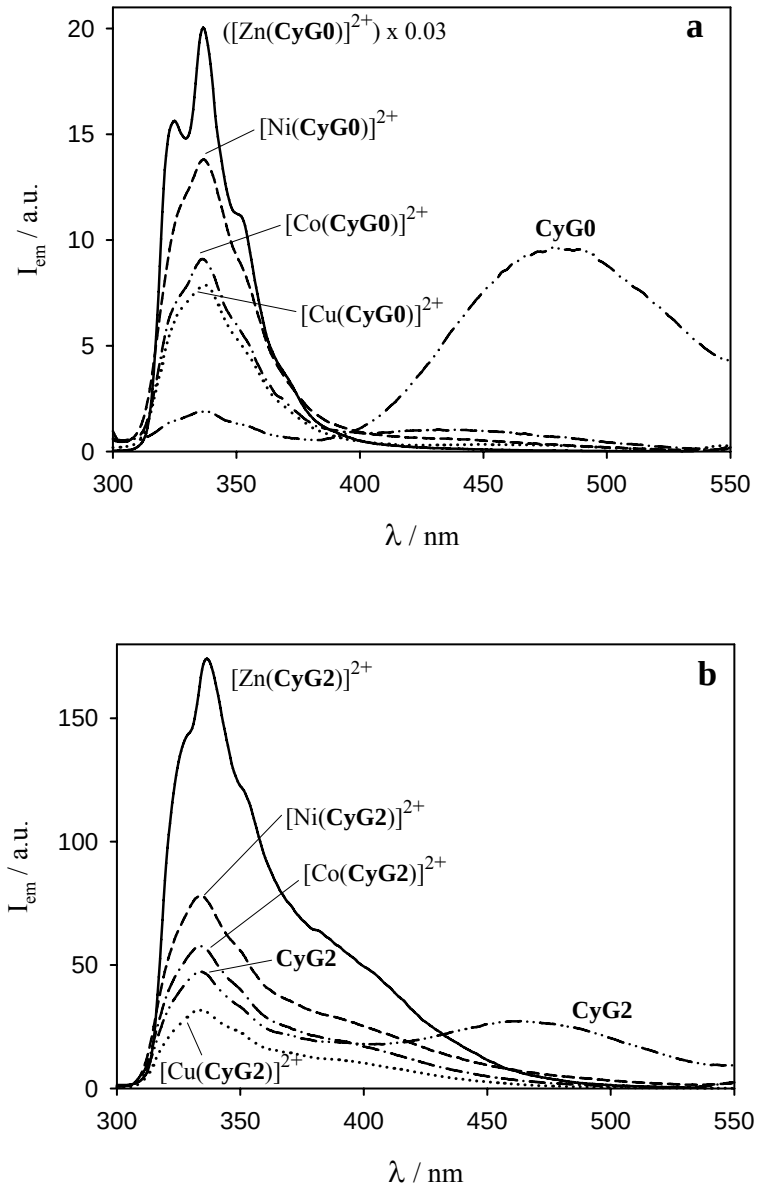

Figure 6.7. Emission spectra of **CyG0** (a) and **CyG2** (b) and their 1:1 complexes with Zn(II), Ni(II), Co(II) and Cu(II) in acetonitrile/dichloromethane 1:1 (v/v) solution at 298 K. The intensities are directly comparable since in all cases the excitation wavelength was 275 nm, the solution absorbance at the excitation wavelength was identical, and the same experimental set up was used. Note that in panel (a) emission intensity of the $[Zn(\mathbf{CyG0})]^{2+}$ complex was multiplied by 0.03 for comparison purposes.

A closer inspection of the emission spectral changes of both dendrimers upon addition of Co(II) (Figure 6.8) shows that the exciplex emission at 470 nm is reduced to about 20% of its initial value upon addition of 0.5 equivalent of metal ion per ligand, then it still decreases but with a much less steeper trend. Even the plot of the emission increase at 337 nm shows a break point at ca 0.5 equivalent of Co(II) added per dendrimer: for **CyG0** it is only a slope change (Figure 6.8a), while in the case of **CyG2**, the monomer and the excimer emission intensities (Figure 6.8b) increase up to ca 0.5 equivalent and then decrease until the end of the titration. Therefore, at the beginning of the titration when the metal ion concentration is low, a complex with 1:2 metal to ligand stoichiometry is formed in both cases. Then, increasing Co(II) concentration, this species is gradually replaced by a 1:1 complex. Luminescence spectra of the Co(II) complexes are strongly related to their stoichiometry for **CyG0** and, especially, **CyG2**. Therefore, luminescence measurements allows us to follow the progressive conversion of 1:2 metal to ligand species into 1:1 complex. In particular, this conversion causes for both dendritic ligands a better nitrogen lone pairs engagement in metal ion complexation, as testified by a slight decrease of the exciplex emission band after 0.5 equivalents of Co(II) added. However, the effect on the naphthyl monomer emission is opposite: in **CyG0**, as expected, emission intensity at 337 nm increases, while in **CyG2** it decreases together with the excimer emission band. This behaviour is difficult to rationalize: it could reflect a higher efficiency of the energy

or electron transfer quenching of naphthalene S_1 excited state, likely because of a closer donor/acceptor distance in the 1:1 species.

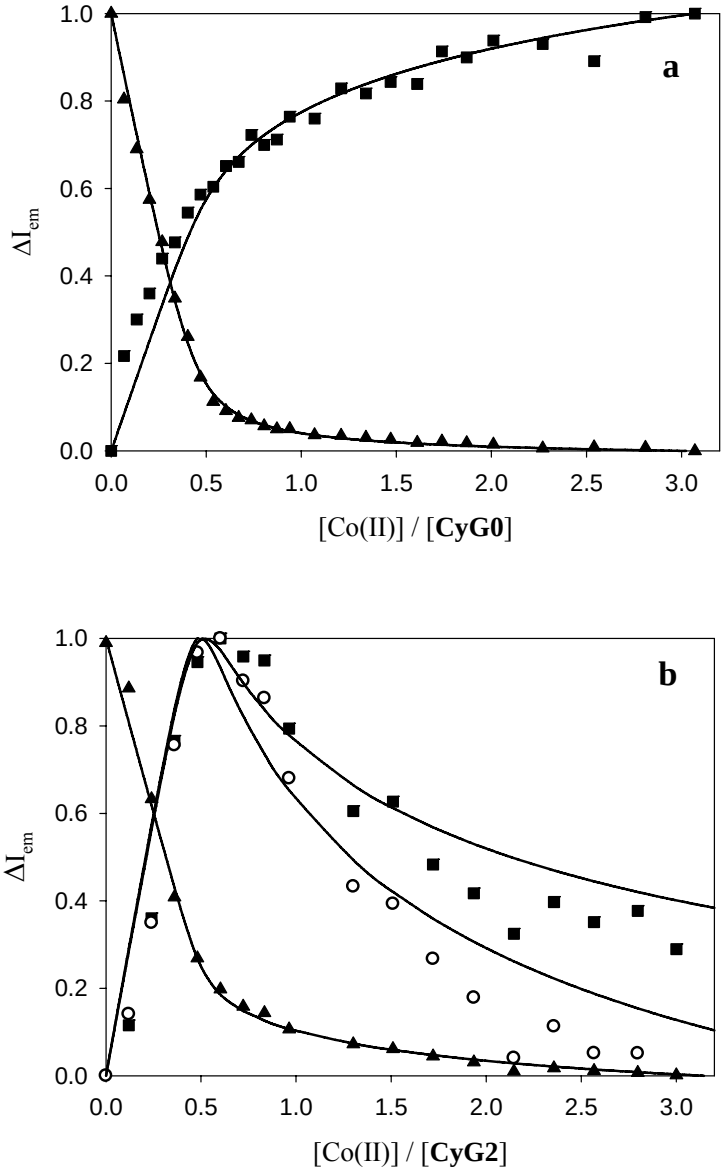

Figure 6.8. Normalized emission intensity changes observed upon addition of $Co(NO_3)_2.6H_20$ to **CyG0** (a) and **CyG2** (b) in acetonitrile/dichloromethane 1:1 (v/v) solution (298 K, λ_{exc} = 275 nm). Emission intensity was monitored at 337 nm (squares), 380 nm (open circles, only for **CyG2**), and 480 nm (triangles). Solid lines represent the best fitting obtained by SPECFIT.[29]

6.3.4 Cu(II) complexation

Upon addition of Cu(II) ions, the absorption spectra of the two dendrimers change and a new broad band with maximum at 330 nm appears (see e.g. **CyG0** in Figure 6.9). Similar bands have been previously observed for Cu(II) cyclam complexes and they were assigned to ligand-to-metal charge transfer (LMCT) transitions involving cyclam amines.[39] Therefore, we take the absorbance increase at 330 nm as a proof of the formation of a Cu(II) complex with the two dendrimers. Since $Cu(NO_3)_2$ absorbs in the same spectral region, correction are needed for a quantitative analysis of the spectral changes. In the case of **CyG0** a plot of the absorbance at 330 nm (Figure 6.10) shows a steep and linear increase until a plateau is reached for one equivalent of metal ion per ligand added. SPECFIT analysis of the absorption spectra obtained during the titration suggests the formation of a 1:1 complex (Table 6.1). The corresponding association constant is lower than that already reported[40] in tetrahydrofuran/water (70:30 v/v) mixture. In the case of **CyG2** a less linear increase of 330 nm absorption is obtained, even though a plateau is again reached with one equivalent of metal ion. SPECFIT analysis in this case gives less straightforward results, but again points toward a 1:1 complex (see Table 6.1).

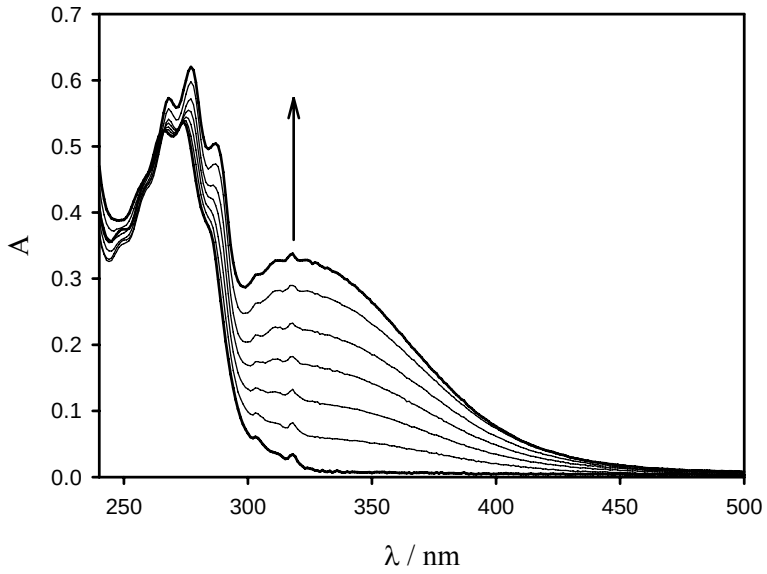

Figure 6.9. Absorption spectra of **CyG0** upon addition of $Cu(NO_3)_2.3H_20$ in acetonitrile/dichloromethane 1:1 (v/v) solution at 298 K.

The changes observed in the emission spectra of the two dendrimers are qualitatively similar to those observed for Co(II) titrations, although a lower intensity of the naphthyl localized and exciplex emission bands are found (Figure 6.7), indicative of a more efficient quenching in this case. As for the Ni(II) case, naphthalene singlet excited state can be deactivated either via energy transfer by low-lying Cu(II) excited states (LMCT and metal centered states[39]) or via reductive electron transfer to form Cu(I) complexes.

In the case of **CyG0** (Figure 6.10a), the intensity decrease of the exciplex band at 470 nm and the absorption increase of the LMCT band at 330 nm have a mirror-like behaviour, showing that exciplex competes with the formation of Cu(II)

complex; the behaviour of the emission intensities at 337 nm has not been reported because of the big uncertainties introduced by the correction for the strong reabsorption of the emitted light.

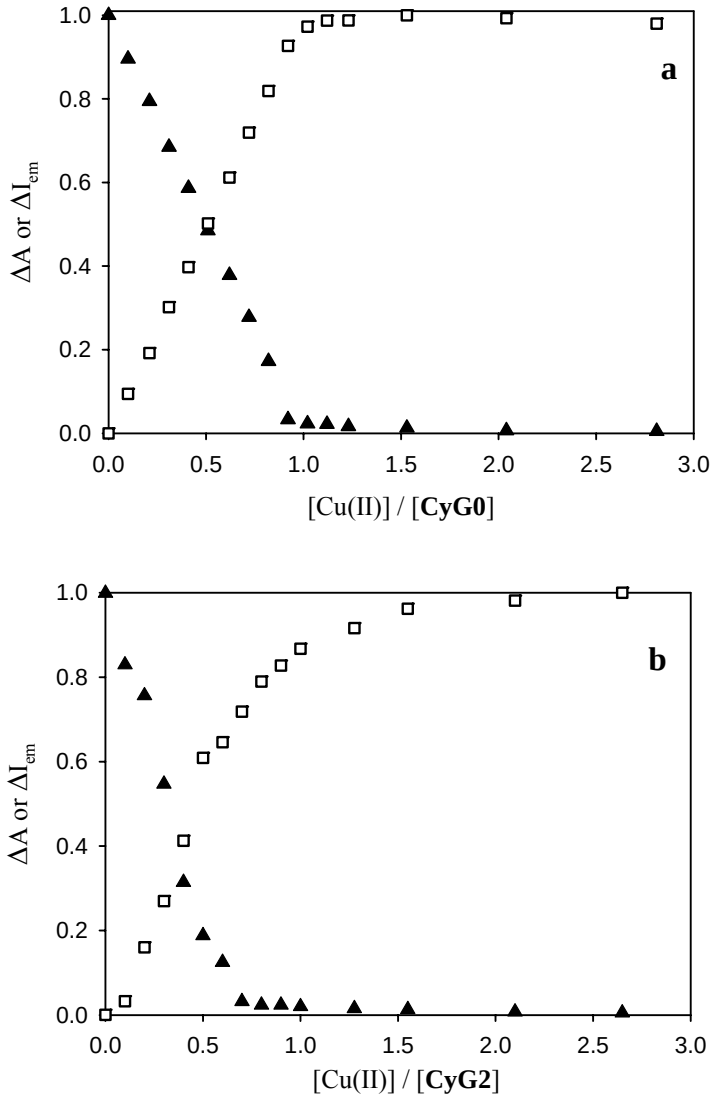

Figure 6.10. Normalized absorption and emission intensity changes observed upon addition of $Cu(NO_3)_2.3H_20$ to **CyG0** (a) and **CyG2** (b) in acetonitrile/dichloromethane 1:1 (v/v) solution (298 K, λ_{exc} = 275 nm). Absorption changes are monitored at 330 nm (open squares) after correction for $Cu(NO_3)_2.3H_20$ absorption (see text), while emission intensity was monitored at 480 nm (triangles).

In the case of **CyG2** (Figure 6.10b), the intensity of the exciplex band decreases linearly until a plateau is reached at about 0.5 equivalent of metal ion per ligand. SPECFIT analysis applied to this spectral changes suggests, in contrast with the absorption treatment, the initial formation of a $[Cu(\mathbf{CyG2})_2]^{2+}$ complex. As for **CyG0**, the emission intensities at 337 nm is affected by the reabsorption of the emitted light; for this reason quantitative consideration on its behaviour must be avoided. Nevertheless, a behaviour qualitatively similar (initial emission increase until 0.5 equivalent and then a decrease) to that observed for the titration with Co(II) suggests the formation of the $[Cu(\mathbf{CyG2})]^{2+}$ species upon further addition of Cu(II) to the initially formed $[Cu(\mathbf{CyG2})_2]^{2+}$ complex. Combining absorption and emission spectral changes allows us to discriminate between the two complexes with different stoichiometry.

[a]This value could not be obtained by fluorescence titration experiments (see text).

	Ni(II)	Co(II)	Cu(II)	Zn(II)
$[M(\mathbf{CyG0})]^{2+}$	5.0	5.6	6.6	7.5
$[M(\mathbf{CyG0})_2]^{2+}$	-	11.4	-	-
$[M(\mathbf{CyG2})]^{2+}$	3.8	7.1	7.5	-[a]
$[M(\mathbf{CyG2})_2]^{2+}$	10.9	14.2	12.2	13.4

Table 6.1. Association constants (β values) of **CyG0** and **CyG2** with Ni(II), Co(II) and Cu(II) in acetonitrile/dichloromethane 1:1 (v/v) at room temperature.

6.3.5 Conclusions

The presently investigated dendrimers show fluorescence bands that can be assigned to naphthyl localized excited states (λ_{max} = 337 nm), naphthyl-amine

exciplexes (λ_{max} = 470 nm) and, for **CyG2**, naphthyl excimers (λ_{max} ca 390 nm). The intensity and shape of these bands are strongly affected by coordination of Ni(II), Co(II) and Cu(II), as nitrate salts, to the cyclam core. Complexation with these metal ions, in contrast to the previously investigated Zn(II) complexes, has a double-faced effect: on one hand, it can increase naphthyl localized emission and suppress exciplex emission, engaging nitrogen lone pairs of cyclam; on the other hand, it can quench this fluorescence by offering additional deactivation pathways to the naphthyl singlet excited state via energy or electron transfer processes. Complexation with Cu(II) causes not only changes in the relative intensities of the fluorescence bands, but also the appearance of a new absorption band in the near UV spectral region. Analysis of the titration curves has allowed us to obtain clear evidence for formation not only of 1:1 species, but also 1:2 metal to ligand species. **CyG2** shows a clear preference, compared to **CyG0**, in forming complexes with 1:2 metal to ligand stoichiometry. This counterintuitive effect demonstrates that the bulky dendrons appended to the cyclam core do not hinder, but favour the formation of complexes with 1:2 metal to ligand stoichiometry.

6.4 Dendrimers based on a bis-cyclam core as fluorescence sensors for metal ions

In a further effort to explore the potentiality of cyclam-based fluorescent dendrimers as ligands for metal ions (and thus as fluorescent sensors), we have synthesized a novel dendrimer (**BisCyc** Scheme 6.2) based on two covalently

linked cyclam units[41,42] as a core appended with six branches, each one consisting of a dimethoxybenzene and two naphthyl units. In this paper we report the changes caused by protonation and complexation with Zn^{2+} and Cu^{2+} on the fluorescent properties of this dendrimer. The results obtained are discussed by comparison with the properties of the parent monocyclam dendrimer **CyG1**.[30a,43]

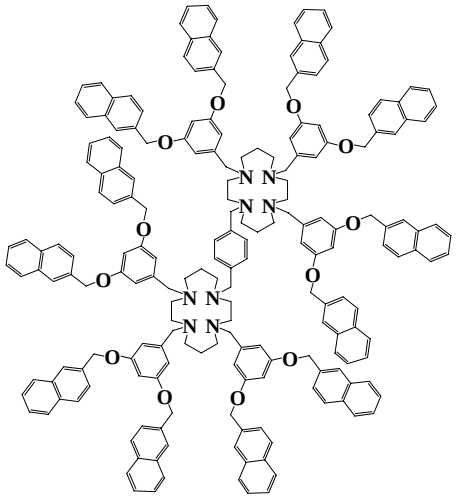

BisCyc

Scheme 6.2. Bis-cyclam dendrimer

6.4.1 Absorption and emission spectra of the bis-cyclam dendrimer (BisCyc)

The absorption spectrum of dendrimers **BisCyc** and **CyG1** are displayed in Figure 6.11. The chromophoric groups present in the two compounds (Scheme 6.2) are dimethoxybenzene (six and four, respectively) and 2-methylnaphthalene (twelve and eight, respectively). 2-Methyl naphthalene exhibits absorption bands at 275 nm ($S_0 \rightarrow S_2$ transition, $\varepsilon = 4800\ M^{-1}\ cm^{-1}$) and 310 nm ($S_0 \rightarrow S_1$ transition, $\varepsilon = 1100\ M^{-1}\ cm^{-1}$), and the dimethoxybenzene unit has an absorption maximum at 275 nm ($\varepsilon =$

2200 M^{-1} cm^{-1}). The absorption spectra of the two compounds are those expected on the basis of the component units.

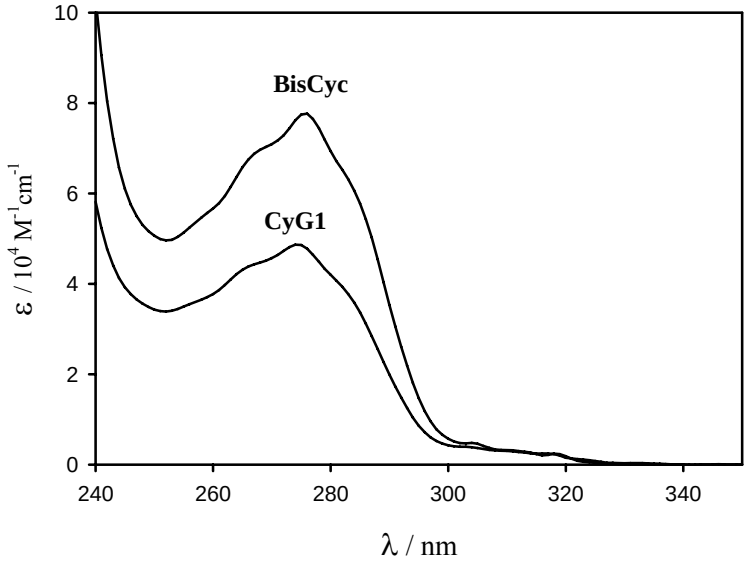

Figure 6.11. Absorption spectrum of dendrimers **BisCyc** and **CyG1** in air-equilibrated acetonitrile-dichloromethane 1:1 v/v solution at 298 K.

The emission spectrum of **BisCyc** in acetonitrile-dichloromethane 1:1 v/v at 298 K shown in Figure 6.12 is quite similar to that of **CyG1**.[30] Both 2-methylnaphthalene (λ_{max} = 335 nm, $\Phi = 6.6\times10^{-2}$) and dimethoxybenzene (λ_{max} = 300 nm, $\Phi = 1.1\times10^{-2}$) are known to exhibit fluorescence. Since the fluorescent excited state of dimethoxybenzene is higher in energy than that of 2-methylnaphthalene, excitation of dimethoxybenzene should be followed by energy transfer to the naphthyl unit. In order to elucidate this point, we have compared the emission intensities observed for compound **BisCyc** upon excitation at 275 nm (where 23% of the light is

absorbed by the dimethoxybenzene units) and 305 nm (where absorption is only due to the naphthyl units). The results obtained show that dimethoxybenzene emission is almost completely quenched and that energy transfer does occur with efficiency ≥0.5.

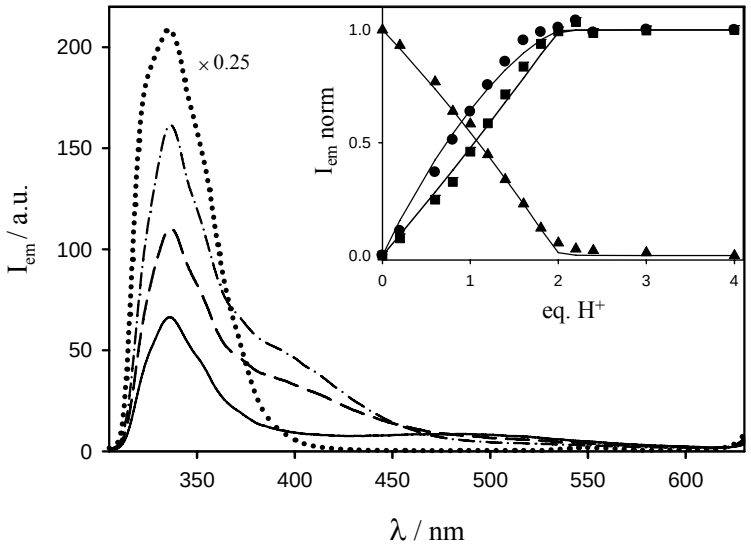

Figure 6.12. Emission spectrum of **BisCyc** (full line) and 2-methylnaphthalene (dotted line): The dashed and dotted-dashed lines are the spectra of **BisCyc** after addition of one and two equivalents of trifluoroacetic acid. Inset shows the normalized fluorescence intensity changes at 336 (■), 390 (●), and 510 (▲) nm. Experimental conditions: acetonitrile-dichloromethane 1:1 v/v solution, 298 K, λ_{exc} = 275 nm, absorbance = 0.50.

In Figure 6.12, the fluorescence spectrum of 2-methylnaphthalene is also reported for comparison purposes. Since excitation has been performed at the same wavelength (310 nm) on solutions showing the same absorbance (0.50), the emission intensities are directly comparable. As in the case of **CyG1**, the emission intensity of **BisCyc** at 336 nm is less than 10% of that exhibited by 2-

methylnaphthalene, and other bands clearly contribute to the spectrum at longer wavelengths.

The quenching of naphthyl excited states by amine units is a well known phenomenon, usually ascribed to photoinduced electron transfer (PET) processes.[44] In several cases, quenching occurs via formation of intramolecular exciplexes between excited naphthyl units and amines.[45, 46, 47, 48] The broad band exhibited by **BisCyc** with maximum at about 510 nm can indeed be assigned to such exciplexes. A further indication of this assignment is the disappearance of this band in the emission spectrum of compound **BisCyc** in butyronitrile at 77 K, where formation of exciplexes is prevented by the lack of solvent repolarisation. Careful examination of the emission spectrum of **BisCyc** shows, in fact, that it receives contribution from a third component band in the 400 nm region, overlapped with the other two bands. Such an emission, previously observed for macrocyclic ligands bearing naphthyl chromophores,[24, 25] can be assigned to naphthyl excimers. As expected, such an excimer band is almost completely absent in a butyronitrile rigid matrix at 77 K.

We would like to note that the very low intensity of the naphthyl band of **BisCyc**, compared to the intensity of 2-methylnaphthalene, can be due not only to the direct engagement of excited naphthyl units in exciplexes and excimers, but also to the deactivation of such excited units by energy transfer to the lower lying exciplex and excimer levels.

Before studying the effect of addition of acid or metal ions to solutions containing **BisCyc**, we have performed experiments on its dimethoxybinaphthyl dendron and we have found that neither protons nor metal ions cause any change in the absorption and emission spectra.

6.4.2 Effects of protonation

It is well known that cyclam undergoes protonation in aqueous solution[26] as well as in other solvents.[27] In aqueous solution, the four successive pK_a values are 11.6, 10.6, 1.61, and 2.42,[26] showing that cyclam can be easily mono- and di-protonated, but further protonation is difficult. It is also interesting to note that the fourth pK_a value is larger than the third one, a result related to protonation-induced structural rearrangements.

Protonation of amines engages the lone pair of the nitrogen atoms and therefore moves the n(N)$\rightarrow\pi^*$ charge-transfer (CT) transitions to higher energy.[44] The lack of any change in the absorption spectrum upon addition of trifluoroacetic acid to a 1.1×10^{-5} M solution of **BisCyc** shows that CT transitions do not contribute to the absorption spectrum. This finding shows that there is no appreciable interaction between amine and aromatic moieties in the ground state.

Addition of trifluoroacetic acid, however, causes strong changes in the emission spectrum of **BisCyc** (Figure 6.12), which are similar but not identical to those previously observed for **CyG1**.[30] As shown in the inset of Figure 6.12, no further change was observed after addition of two equivalents of protons per dendrimer,

i.e, after formation of a **BisCyc**($2H^+$) species; the same 2:1 proton/dendrimer ratio was observed at the end of the titration of **CyG1** which, however, contains only one cyclam unit (Scheme 6.2). These results suggest that the two cyclam units of **BisCyc** do not behave independently and that in the **BisCyc**($2H^+$) species the two protons are likely shared by the two cyclam units in a sandwich-type structure.

The spectra reported in Figure 6.11 show that protonation of **BisCyc** causes: (i) a linear increase in the intensity of the naphthyl localized band with λ_{max} = 336 nm that, however, remains much weaker than the band of 2-methylnaphthalene; (ii) a decrease, but not the disappearance, of the exciplex band with maximum around 510 nm; (iii) a moderate, slightly not linear increase in intensity of the excimer band around 390 nm. The non linear increase in intensity of the excimer band suggest that protonation causes a rearrangement in the structure of the dendrimer and the relatively small recovery of the intensity of the naphthyl fluorescence on protonation is likely related to the lack of disappearance of exciplexes and the further formation of excimers. From a SPECFIT analysis of the observed spectral changes the following values were obtained for the first and second protonation constants: $\log\beta_{1:1} = 8.1 \pm 0.6$, and $\log\beta_{2:1} = 14.1 \pm 0.6$.

6.4.3 Complex formation with Zn^{2+}

Upon addition of $Zn(CF_3SO_3)_2$ (up to three equivalents) to a 1.1×10^{-5} M solution of **BisCyc** no change was observed in the absorption spectrum, whereas strong changes were observed in the emission spectrum (Figure 6.13). Such changes are

qualitatively similar to those caused by protonation, but there are some important differences: (i) the titration plot of the naphthyl fluorescence clearly shows a discontinuity after addition of one equivalent of Zn^{2+} per dendrimer and at the end of the titration, which occurs after addition of about two equivalents of metal ion, the naphthyl band is more intense than in the case of protonation; furthermore, most of the increase in intensity of the naphthyl fluorescence band takes place after addition of one equivalent of Zn^{2+}; (ii) the exciplex band with maximum around 510 nm decreases in intensity, shows a discontinuity, and does not disappear; (iii) the increase in intensity of the excimer band at 390 nm, once corrected for the contribution of the naphthyl fluorescence, reaches a plateau after addition of one equivalent of metal ion.

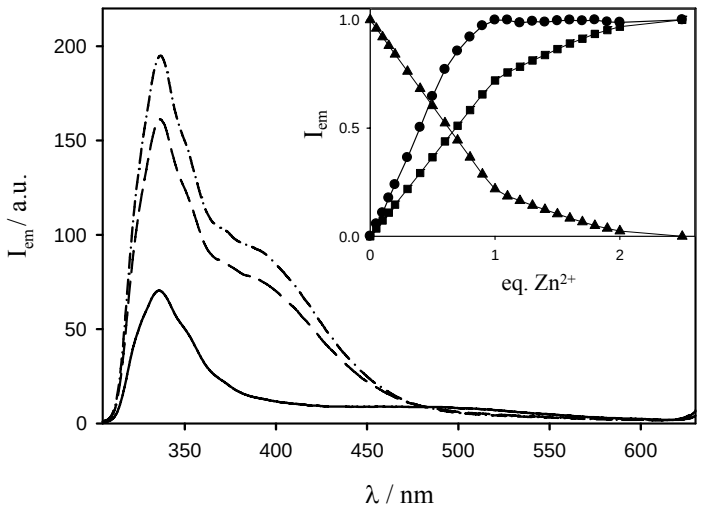

Figure 6.13. Emission spectrum of **BisCyc** before (full line) and after the addition of one (dashed line) and two (dotted-dashed) equivalents of $Zn(CF_3SO_3)_2$. Inset shows the normalized fluorescence intensity changes at 336 (■), 390 (●), and 510 (▲) nm. Experimental conditions: acetonitrile-dichloromethane 1:1 v/v solution, 298 K, λ_{exc} = 275 nm, absorbance = 0.50.

These results clearly indicate that a 1:1 complex, $[Zn(\mathbf{BisCyc})]^{2+}$, is first formed and then replaced by a 2:1 species, $[Zn_2(\mathbf{BisCyc})]^{4+}$. SPECFIT analysis yielded values of $\log\beta_{1:1} = 9.7 \pm 0.7$, and $\log\beta_{2:1} = 16.1 \pm 0.8$ for these two species, respectively. In the 1:1 complex $[Zn(\mathbf{BisCyc})]^{2+}$, both the cyclam units are likely coordinated to Zn^{2+}, as suggested by the formation of a 1:2 compound, $[Zn(\mathbf{CyG1})_2]^{2+}$, on titration of the monocyclam dendrimer **CyG1** with Zn^{2+}.[30] In the 1:1 complex of Zn^{2+} with **BisCyc**, $[Zn(\mathbf{BisCyc})]^{2+}$, the metal ion is likely sandwiched between the two cyclam units, as is thought to happen in the $[Zn(\mathbf{CyG1})_2]^{2+}$ compound. All the metal complexes of cyclam and of non dendritic cyclam derivatives reported so far have a 1:1 stoichiometry. Apparently, the dendrimer branches not only do not hinder, but in fact favour coordination of cyclam units to metal ions with respect to solvent molecules and counter ions; indeed, even evidence for formation of $[Eu(\mathbf{CyG1})]^{3+}$ has also been reported.[30] Presumably, the dendritic branches force the cyclam cores to adopt a structure in which only three N atoms are available for metal complexation. As in the case of $[Zn(\mathbf{CyG1})_2]^{2+}$, two limiting structures can be proposed for $[Zn(\mathbf{BisCyc})]^{2+}$: (i) an "inward" structure, in which the branches of the two coordinated cyclam units are intermeshed, or (ii) an "outward" structure, in which the branches of the two coordinated moieties do not interact. An inward structure with intermeshed branches should favour formation of excimers. The results obtained, however, show that in going from $[Zn(\mathbf{BisCyc})]^{2+}$ to $[Zn_2(\mathbf{BisCyc})]^{4+}$ the intensity of the excimer band does not change. It seems, therefore, more likely that in these

sandwich-type complexes the dendrimer branches extends outward and maintain the same structure in the $[Zn_2(\mathbf{BisCyc})]^{4+}$ species.

6.4.4 Complex formation with Cu^{2+}

Quite different results were obtained upon titration of a 1.1×10^{-5} M solution of **BisCyc** with $Cu(CF_3SO_3)_2$. The absorption spectrum (Figure 6.14) showed the appearance of a broad tail in the 300-400 nm region. The absorbance values increase almost linearly up to the addition of 2 equivalents of metal ion per dendrimer (Figure 6.14, inset). A quite similar absorption band, assigned to ligand-to-metal charge-transfer (LMCT) transitions, is obtained when a 2.2×10^{-5} M cyclam solution is titrated by $Cu(CF_3SO_3)_2$. Therefore we can conclude that upon addition of $Cu(CF_3SO_3)_2$ to **BisCyc**, both the cyclam units of the dendrimer coordinate a Cu^{2+} ion. SPECFIT analysis based on the changes in the absorption spectrum yielded a value of $\log \beta_{2:1} = 11.9 \pm 0.3$.

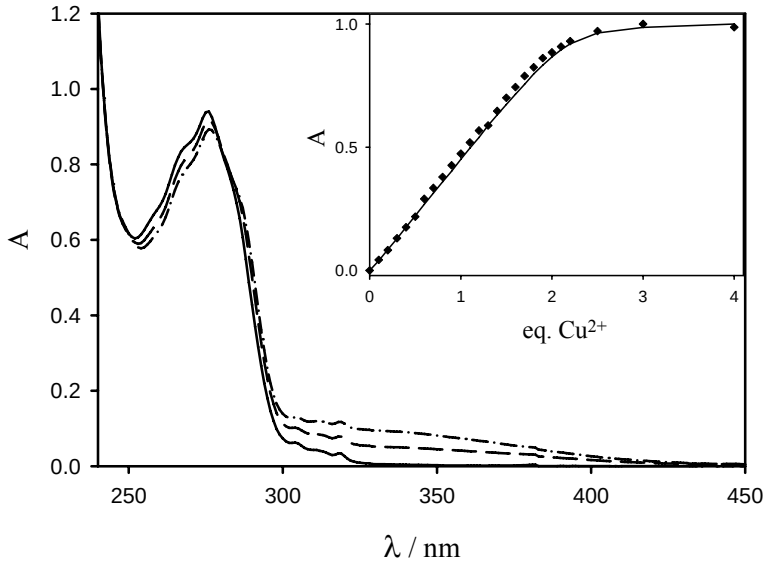

Figure 6.14. Absorption spectrum of **BisCyc** before (full line) and after the addition of one (dashed line) and two (dotted-dashed) equivalents of $Cu(CF_3SO_3)_2$. Inset shows the normalized absorption changes at 319 nm. Experimental conditions: acetonitrile-dichloromethane 1:1 v/v solution, 298 K.

More details were obtained from the changes observed in the emission spectrum (Figure 6.15), that can be summarized as follows: (i) the intensity of the naphthyl band is almost constant up to the addition of one equivalent of metal ion and then decreases slightly; (ii) the intensity of the exciplex band decreases linearly and disappears after addition of two equivalents of metal ions; (iii) the intensity of the excimer band increases at the beginning of the titration, and reaches a maximum value after addition of one equivalent of metal ion and then decreases. SPECFIT analysis was not performed in the case of the emission spectrum because of the too complex behaviour and the relatively small intensity changes.

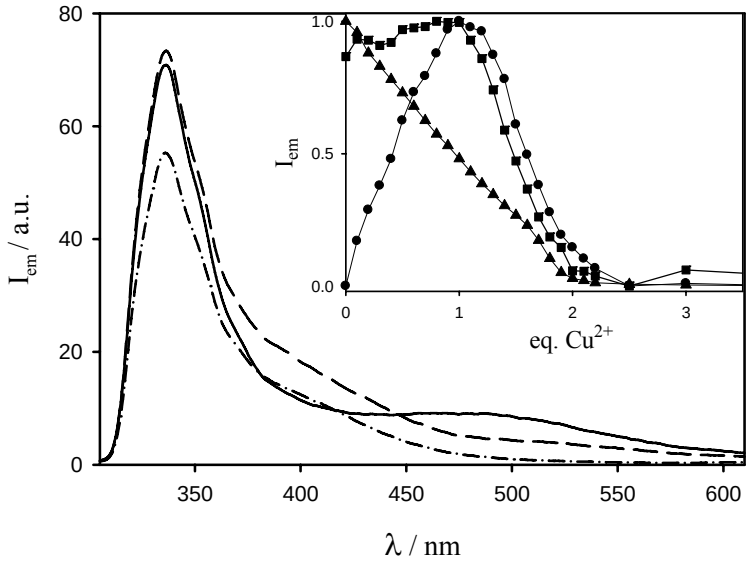

Figure 6.15. Emission spectrum of **BisCyc** before (full line) and after the addition of one (dashed line) and two (dotted-dashed) equivalents of $Cu(CF_3SO_3)_2$. Inset shows the normalized fluorescence intensity changes at 336 (■), 390 (●), and 510 (▲) nm. Experimental conditions: acetonitrile-dichloromethane 1:1 v/v solution, 298 K, λ_{exc} = 275 nm, absorbance = 0.50.

We would like to notice an important difference in the behaviour of the emission spectrum of **BisCyc** upon titration with H^+ or Zn^{2+} (Figures 6.12 and 6.13), and titration with Cu^{2+} (Figure 6.15). In the case of H^+ or Zn^{2+}, the decrease in the intensity of the exciplex emission, caused by the engagement of the cyclam N atoms by protons or metal ions, is accompanied, as expected, by an increase in the intensity of the naphthyl emission. This does not happen, however, when titration is performed with Cu^{2+}; in particular, at the end of the titration, when $[Cu_2(\mathbf{BisCyc})]^{4+}$ is formed, although exciplex formation is fully prevented by coordination of two metal ions, the naphthyl emission is clearly less intense than in the free dendrimer

BisCyc. This result can be easily rationalized considering that coordination of Cu^{2+}, while preventing deactivation of the excited naphthyl units via exciplex formation, introduces another deactivation channel related to the presence of the low energy LMCT state.

Figure 6.14 shows that from the view point of the interaction between cyclam and metal ion (i.e., from the behaviour of the MLCT absorption band), there are minor (if any) differences between the 1:1 and 2:1 species. In other words, the two cyclam units behave independently as far as the MLCT absorption is concerned. From the view point of the naphthyl units (Figure 6.15), however, it is clear that a 1:1 complex, $[Cu(\mathbf{BisCyc})]^{2+}$, is first formed, as suggested by the formation of a 1:2 compound, $[Cu(\mathbf{CyG1})_2]^{2+}$ on titration of the monocyclam dendrimer **CyG1** with Cu^{2+},[49] and then replaced by a 2:1 species, $[Cu_2(\mathbf{BisCyc})]^{4+}$.

6.4.5 Conclusions

We have prepared for the first time a dendrimer with a bis-cyclam core. Such a dendrimer (**BisCyc**) contains in its branches 12 naphthyl units and exhibits three fluorescence bands assigned to naphthyl localized excited states (λ_{max} = 336 nm), naphthyl excimers (λ_{max} ca 390 nm), and naphthyl-amine exciplexes (λ_{max} = 510 nm). Titration with H^+, Zn^{2+}, and Cu^{2+} causes strong changes in the emission spectrum and, in the case of Cu^{2+}, also in the absorption spectrum. Clear evidence for formation of 1:1 (**BisCyc**.(H^+), $[Zn(\mathbf{BisCyc})]^{2+}$, $[Cu(\mathbf{BisCyc})]^{2+}$) and 2:1 (**BisCyc**.($2H^+$), $[Zn_2(\mathbf{BisCyc})]^{4+}$, $[Cu_2(\mathbf{BisCyc})]^{4+}$) species has been obtained. The

three luminescence bands and, in the case of Cu^{2+}, also an absorption band, offer the way to monitor not only the metal-ligand coordination process, but also its consequences on the interaction between the naphthyl units contained in the dendritic branches. The spectral changes are likely too weak and too complex to be used for sensory purposes. We would like to note, however, that while the availability of dendrimers possessing a well defined ligand unit, like cyclam, opens the way to the construction of mixed-(dendritic)ligand complexes, dendrimers containing two cyclam units can be used, in principle, to construct dendrimers containing two different types of metal ions.

References

[1] M.W.P.L. Baars, E.W. Meijer, *Top. Curr. Chem* **2001**, *210*, 131.

[2] (a) M. F. Ottaviani, S. Bossamann, N.J. Turro, D. A. Tomalia, *J. Am. Chem Soc*. **1994,** *116*, 661. (b) J. D. Epperson, L.-J. Ming, B. D. Woosley, G. R. Baker, G. R. Newkome, *Inorg. Chem.*, **1999**, *38*, 4498.

[3] (a) L. Balogh, D. A. Tomalia, *J. Am. Chem. Soc.* **1998**, *120*, 7355. (b) M. Zhao, L. Sun, R. M. Crooks, *J. Am. Chem. Soc*. **1998**, *120*, 4877. (c) M. Zhao, R. M. Crooks, *Adv. Mater*. **1999**, *11*, 217; (d) M. Zhao, R. M. Crooks, *Angew. Chem. Int. Ed.* **1999**, *38*, 364. (e) V. Chechik, M. Zhao, R. M. Crooks, *J. Am. Chem. Soc.* **1999**, *121*, 4910. (f) V. Chechik, R. M. Crooks, *J. Am. Chem. Soc.* **2000**, *122*, 1243 (g) L. Zhou, D. H. Russell, M. Zhao, R. M. Crooks, *Macromol.* **2001**, *34*, 3567. (h) R. M. Crooks, M. Zhao, L. Sun, V. Chechik, L. K. Yeung, *Acc. Chem. Res.* **2001**, *34*, 181.

[4] R. J. M. K. Gebbink, A. W. Bosman, M. C. Feiters, E. W. Meijer, R. J. M. Nolte, *Chem. Eur. J*. **1999**, *5*, 65.

[5] H. Stephan, H. Spies, B. Johannsen, L. Klein, F. Vögtle, *Chem. Commun.* **1999**, 1875.

[6] (a) V. Balzani, P. Ceroni, S. Gestermann, C. Kauffmann, M. Gorka, F. Vögtle, *Chem. Commun.* **2000**, 853. (b) F. Vögtle, S. Gestermann, C. Kauffmann, P. Ceroni, V. Vicinelli, V. Balzani, *J. Am. Chem. Soc.* **2000**, *122*, 10398. (c) V. Balzani, P. Ceroni, S. Gestermann, M. Gorka, C. Kauffmann, F. Vögtle, *J. Chem. Soc., Dalton Trans* **2000**, 3765.

[7] (a) F. Vögtle, M. Gorka, V. Vicinelli, P. Ceroni, M. Maestri, V. Balzani, *ChemPhysChem* **2001**, *12*, 769. (b) V. Vicinelli, P. Ceroni, M. Maestri, V. Balzani, M. Gorka, F. Vögtle, *J. Am. Chem. Soc.* **2002**, *124*, 6461.

[8] C. Gorman, *Nature* **2002**, *415*, 487.

[9] R. van de Coevering, M. Kuil, J. M. K. Gebbink, G. van Koten, *Chem. Commun.* **2002**, 1636.

[10] M. Kawa, J. M. J. Fréchet, *Chem. Mater.* **1998**, *10*, 286.

[11] See for example, (a) V. Balzani, S. Campagna, G. Denti, A. Juris, S. Serroni, M. Venturi, *Acc. Chem. Res.* **1998**, *31*, 26. (b) B.-H. Huisman, H. Schönherr, W. T. S. Huck, A. Friggeri, H.-J. van Manenm, E. Menozzi, G. J. Vancso, F. C. J. M. van Veggel, D. N. Reinhoudt, *Angew. Chem. Int. Ed.* **1999**, *38*, 2248. (c) N.D. McClenaghan, F. Loiseau, F. Puntoriero, S. Serroni, S. Campagna, *Chem. Commun.* **2001**, 2634.

[12] R. D. Hancock, R. J. Motekaitis, J. Mashishi, I. Cukrowsky, J. H. Reibenspies, A. E. Martell, *J. Chem. Soc., Perkin Trans., 2* **1996**, 1925.

[13] (a) A. Bianchi, M. Micheloni, P. Paoletti, *Coord. Chem. Rev.* **1991**, *110*, 17. (b) E. Kimura, *Prog. Inorg. Chem.* **1994**, *41*, 443. (c) L. Fabbrizzi, M. Licchelli, P. Pallavicini, D. Sacchi, *Supramolecular Chemistry* **2001**, *13*, 569.

[14] M. Meyer, V. Dahaoui-Gindrey, C. Lecomte, R. Guilard, *Coord. Chem. Rev.* **1998**, *178*, 1313.

[15] J. W. Sibert, A. H. Cory, J. G. Cory, *Chem. Commun.* **2002**, 154.

[16] (a) E. Brucher, A.D. Sherry, in *The Chemistry of Contrast Agents in Medical Magnetic Resonance Imaging*, A.E. Merbach, E. Toth, eds., John Wiley, New York, **2001**, chapter 6. (b) P. Caravan, J. J. Ellison, T. J. McMurry, W. H. Lauffer, *Chem. Rev.* **1999**, *99*, 2293.

[17] (a) E. Kimura, T. Koike, Y. Inouye, in *Perspective on Bioinorganic Chemistry*, R.W. Hay, J.R. Dilworth, K.B. Nolan, eds., vol. 14, JAI Press. Inc., Stamford, CT, **1999**, pp.145. (b) X. Liang, J. Parkinson, M. Weishäupl, R.O. Gould, S. J. Paisey, H.-S. Park, T. M. Hunter, C. A. Blindauer, S. Parson, P. J. Sadler, *J. Am. Chem. Soc.* **2002**, *124*, 9105.

[18] H. H. Jaffé, M. Orchin, *Theory and Application of Ultraviolet Spectroscopy,* Wiley&Sons,Inc., New York, **1964**.

[19] A. P. De Silva, H.Q.N. Gunaratne, T. Gunnlaugsson, A. J. M. Huxley, C. P. McCoy, J. T. Rademacher, T. E. Rice, *Chem. Rev.*, **1997**, *97*, 1515.

[20] K. Kubo, E. Yamamoto, T. Sakurai, *Heterocycles* **1998**, *4*, 1477.

[21] G. E. Collins, L. –S. Choi, J. H. Callahan, *J. Am. Chem. Soc.* **1998**, *120*, 1474.

[22] S. Quici, A. Manfredi, M. Maestri, I. Manet, P. Passaniti, V. Balzani, *Eur. J. Org. Chem.* **2000**, 2041.

[23] P. V. Bernhard, E. G. Moore, M. J. Riley, *Inorg. Chem.* **2001**, *40*, 5799.

[24] D. Parker, J. A. G. Williams, *J. Chem. Soc., Perkin Trans. 2* **1995**, 1305.

[25] A. Beeby, D. Parker, J. A. G. Williams, *J. Chem. Soc., Perkin Trans. 2* **1996**, 1565.

[26] M. Micheloni, A. Sabbatini, P. Paoletti, *J. Chem. Soc., Perkin Trans.* **1978**, *2*, 828. (b) V. J. Thöm, G. D. Hosken, R. D. Hancock, *Inorg. Chem.* **1985**, *24*, 3378.

[27] J. R. Röper, H. Elias, *Inorg. Chem.* **1992**, *31*, 1202.

[28] For the emission spectrum of the dendron see chapter 5 or: U. Hahn, M. Gorka, F. Vögtle, V. Vicinelli, P. Ceroni, M. Maestri, V. Balzani, *Angew. Chem. Int. Ed.* **2002**, *41*, 3595.

[29] (a) R.A. Binstead, SPECFIT; Spectrum Software Associates: Chapell Hill, NC, **1996**. (b) H. Gampp, M. Maeder, C. J. Meyer, A. Zuberbulher, *Talanta* **1985**, *32*, 257.

[30] (a) C. Saudan, V. Balzani, M. Gorka, S.-K. Lee, M. Maestri, V. Vicinelli, F. Vögtle, *J. Am. Chem. Soc.* **2003**, *125*, 4424. (b) C. Saudan, P. Ceroni, V. Vicinelli, M. Maestri, V. Balzani, M. Gorka, S.-K. Lee, J. van Heyst, F. Vögtle, *Dalton Trans.* **2004**, 1597.

[31] Residual exciplex emission in the tritration of **CyG2** is difficult to appreciate because of the superimposed tail of the increased excimer emission.

[32] See e.g., (a) Y. Dong, L. F. Lindoy, P. Turner, G. Wei, *Dalton Trans.* **2004**, 1264. (b) L. Fabbrizzi, M. Licchelli, S. Mascheroni, A. Poggi, D. Sacchi, M. Zema, *Inorg. Chem.* **2002**, *41*, 6129.

[33] M. Montalti, A. Credi, L. Prodi, M. T. Gandolfi, *Handbook of Photochemistry*, 3rd ed., Taylor & Francis, CRC press, **2006**, ch. 7.

[34] For Ni(II) cyclam complexes, $E_{1/2}(Ni^{2+}/Ni^{+}) \sim -0.9$ V (vs SCE), as reported by Y. Dong, G. A. Lawrance, L. F. Lindoy, P. Turner, *Dalton Trans.* **2003**, 1567.

[35] M. Engeser, L. Fabbrizzi, M. Licchelli, D. Sacchi, *Chem. Commun.* **1999**, 1191 and references therein.

[36] F. Vögtle, S. Gestermann, C. Kauffmann, P. Ceroni, V. Vicinelli, V. Balzani, *J. Am. Chem. Soc.* **2000**, 122, 10398.

[37] C. K. Jorgensen, *Adv. Chem. Phys.* **1963**, *5*, 33.

[38] F. A. Cotton, G. Wilkinson, *Advanced Inorganic Chemistry*, Wiley, New York, **1980**, ch. 25.

[39] M. Lachkar, R. Guilard, A. Atmani, A. De Cian, J. Fischer, R. Weiss, *Inorg. Chem.* **1998**, *37*, 1575.

[40] Y. A. Shihadeh, A. Benito, J. M. Lloris, R. Martínez-Máñez, T. Pardo, J. Soto, M. D. Marcos, *J. Chem. Soc., Dalton Trans.* **2000**, 1199.

[41] M. Ciampolini, L. Fabbrizzi, A. Perotti, A. Poggi, B. Seghi and F. Zanobini, *Inorg. Chem.* **1987**, *26*, 3527.

[42] Bis-cyclam unit is extensively used in biological experiments, see, e.g.: W. Yang, C. M. Giandomenico, M. Sartori and D. A. Moore, *Tetrahedron Lett.* **2003**, *44*, 2481; X. Liang, J. A. Parkinson, M. Weishaüpl, R. O. Gould, S. J. Paisey, H.-s. Park, T. M. Hunter, C. A. Blindauer, S. Parker and P. J. Sandler, *J. Am. Chem. Soc.* **2002**, *124*, 9105.

[43] C. Saudan, V. Balzani, M. Gorka, S-K. Lee , J. van Heyst, M. Maestri, P. Ceroni, V. Vicinelli and F. Vögtle**,** *Chem. Eur. J.* **2004**, *10*, 899.

[44] A. P. De Silva, H. Q. N. Gunaratne, T. Gunnlaugsson, A. J. M. Huxley, C. P. McCoy, J. T. Rademacher and T. E. Rice, *Chem. Rev.* **1997**, *97*, 1515.

[45] K. Kubo, E. Yamamoto and T. Sakurai, *Heterocycles* **1998**, *4*, 1477.

[46] G. E. Collins, L.–S. Choi and J. H. Callahan, *J. Am. Chem. Soc.* **1998**, *120*, 1474.

[47] S. Quici, A. Manfredi, M. Maestri, I. Manet, P. Passaniti and V. Balzani, *Eur. J. Org. Chem.* **2000**, *11*, 2041.

[48] P. V. Bernhard, E. G. Moore and M. J. Riley,. *Inorg. Chem.* **2001**, *40*, 5799.

[49] See paragraph 6.3.4, pp. 111-114 in this chapter.

CHAPTER 7

A cyclam core dendrimer containing dansyl and oligoethylene glycol chains in the branches: protonation and metal coordination

7.1 Introduction

Continuing our investigations in the field of coordinating dendrimers, we have synthesized a dendrimer (**CycDans**, Scheme 7) consisting of a cyclam core appended with four benzyl substituents that carry, in the 3 and 5 positions, a dansyl amide derivative (**DEtGly**) in which the amide hydrogen is replaced by a benzyl unit that carries, in the 3 and 5 position, a oligoethylene glycol chain. Dendrimer **CycDans** contains luminescent units (8 dansyl and 8 dimethoxybenzene-type moieties) and three distinct types of multivalent basic sites (the cyclam core, the amine moieties of the 8 dansyl units of the dendrimer branches, and the 16 oligoethylene glycol chains appended in the periphery) that, in principle, can be protonated or coordinated to metal ions. We hoped that this dendrimer could have been soluble in water because of the oligoethylene glycol chains, but this was not the case. Therefore, we have studied the absorption and luminescence properties of **CycDans** and **DEtGly** in acetonitrile solution and the changes taking place upon titration with trifluoromethanesulfonic (triflic) acid and a variety of divalent (Co^{2+},

Ni^{2+}, Cu^{2+}, Zn^{2+}) and trivalent (Nd^{3+}, Eu^{3+}, Gd^{3+}) metal ions as triflate or nitrate salts.

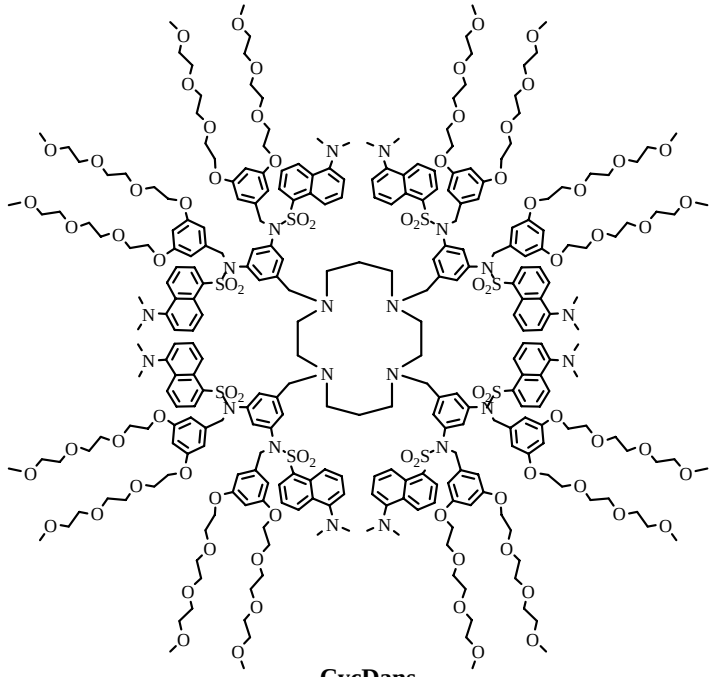

CycDans

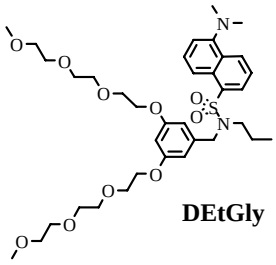

DEtGly

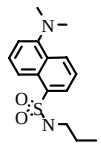

Dans

Scheme 7. Structure formulae of the dendrimer (**CycDans**) and the model compounds (**DEtGly** and **Dans**)

7.2 Absorption and emission spectra

Since the cyclam core does not show absorption bands above 240 nm, the chromophoric groups present in dendrimer **CycDans** are those contained in its

branches (**DEtGly**), namely 8 dansyl- and 8 dimethoxybenzene-type units. As shown in Figure 7.1, the spectrum of **DEtGly** is almost exactly that expected on the basis of the spectra of the reference compound **Dans** and dimethoxybenzene (**DMB**). The small red shift of the dansyl band around 340 nm, which is due to a charge-transfer transition from the amine group to the aromatic moiety, suggests that in the acetonitrile solution the dansyl unit of **DEtGly** experiences a slightly less polar environment than **Dans**, presumably because of some wrapping by the oligoethylene glycol chains.

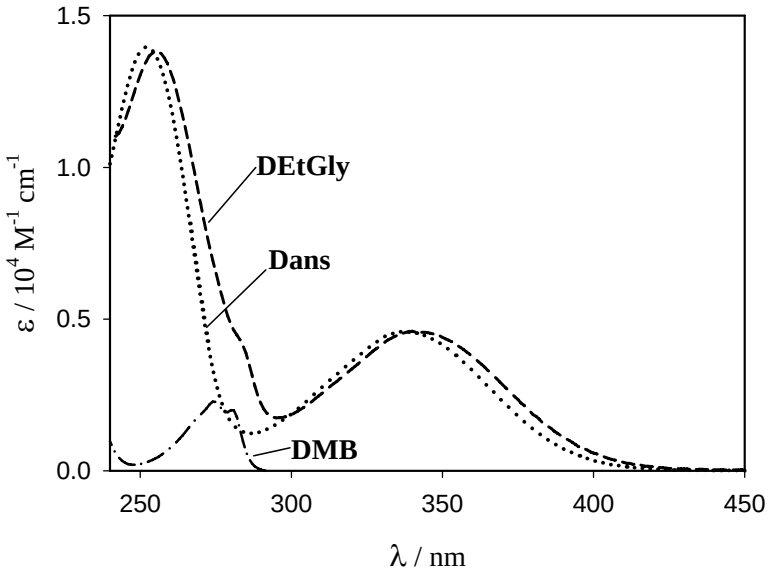

Figure 7.1. Absorption spectra of dendron **DEtGly** and reference compounds **Dans** and dimethoxybenzene (**DMB**) in acetonitrile solution at 298 K.

Figure 7.2 shows that in **CycDans** such a red-shift is more pronounced, indicating that in the dendrimer the dansyl unit indeed feels a less polar environment.

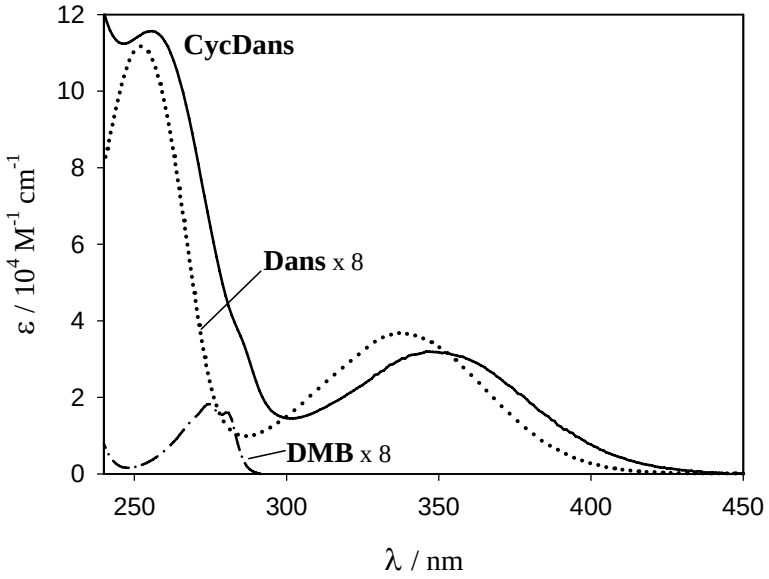

Figure 7.2. Absorption spectra of dendrimer **CycDans** compared with those of its chromophoric units in acetonitrile solution at 298 K.

As far the emission spectra are concerned (Figure 7.3), **Dans** shows the typical dansyl emission bands with λ_{max} = 505 nm, Φ = 0.30, and τ = 12 ns. Compound **DEtGly**, which contains the fluorescent dansyl and dimethoxybenzene moieties (λ_{max}= 310 nm), shows only the dansyl band, slightly red shifted (λ_{max} = 522 nm), with Φ = 0.30, and τ = 13 ns. These results indicate that the potentially fluorescent excited state of the dimethoxybenzene moiety is quenched by the nearby dansyl unit. Since the emission of the latter is not sensitized, the quenching process most likely takes place by electron transfer.[1] In dendrimer **CycDans**, the dansyl units maintain their strong fluorescence, slightly red shifted (Figure 7.3; λ_{max} = 532 nm,

Φ = 0.27, and τ = 15 ns), and, as for **DEtGly**, no dimethoxybenzene emission is present.

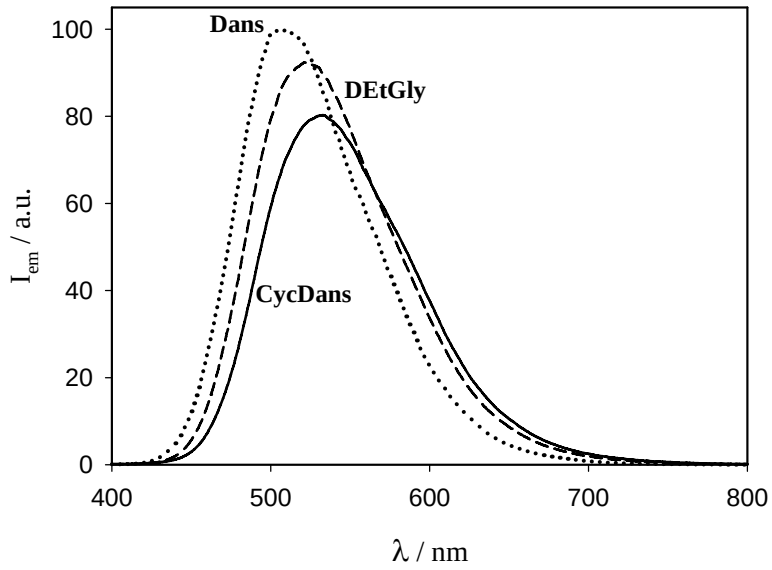

Figure 7.3. Emission spectra of the investigated compounds in acetonitrile solution at 298 K. The intensities are directly comparable since in all cases the excitation wavelength was 340 nm, the solution absorbance at the excitation wavelength was 0.20, and the same experimental set up was used.

7.3 Protonation

It is well known that cyclam undergoes protonation in aqueous solution[2, 3] as well as in other solvents.[4] In aqueous solution, the four successive pK_a values are 11.6, 10.6, 1.61, and 2.42,[3] showing that cyclam can be easily mono- and di-protonated, but further protonation is difficult. It is also interesting to note that the fourth pK_a value is larger than the third one, a result related to protonation-induced structural rearrangements. In dimethylformamide solution only two successive protonation

steps have been observed with pK_a values of 9.3 and 7.5.[4] Studies performed on other dendrimers also showed that the cyclam core undergoes only two protonation reactions in acetonitrile-dichloromethane 1:1 v/v solution.[5]

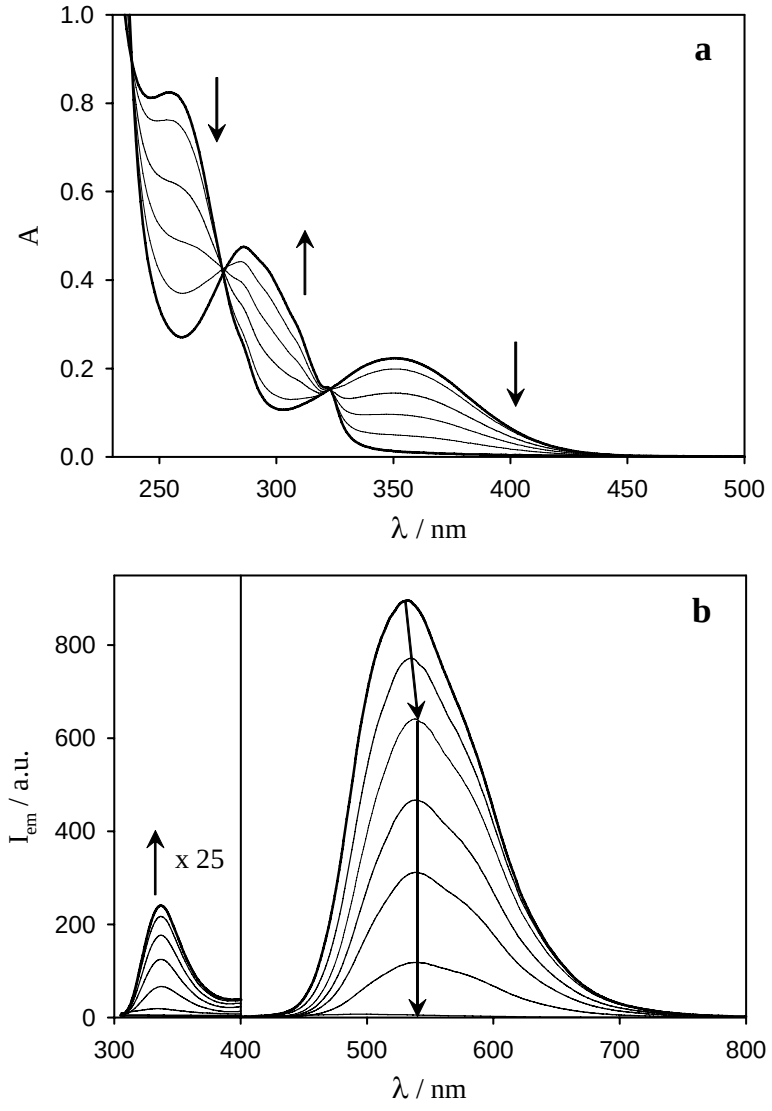

Figure 7.4. Absorption (a) and emission (b) spectra of **CycDans** recorded during the titration with triflic acid in acetonitrile solution at 298 K. The final spectrum correspond to the addition of 40 equivalents of acid. Excitation wavelength at an isosbestic point (270 nm).

It is also well known that dansyl can be protonated at its amine moiety.[6] This process causes strong changes in the absorption and emission spectra because of the charge transfer nature of the dansyl bands. More specifically, protonation of model compound **Dans** causes the disappearance of the absorption bands with λ_{max} = 337 and 252 nm, and of the emission band with λ_{max} = 505 nm, and the concomitant appearance of the absorption (λ_{max} = 287 nm) and emission (λ_{max} = 335 nm, Φ = 0.002, τ < 0.5 ns) bands of protonated dansyl. We have found similar results for dendron **DEtGly**. Qualitatively, dendrimer **CycDans** shows the same spectral changes (Figure 7.4a and 7.4b), but the titration curves reveal a much more complex behavior. In all cases, the initial spectrum could be obtained upon addition of a base (tributylamine).

In the case of the simple dansyl unit **Dans**, the titration plot (Figure 7.5) shows that upon acid addition the decrease of the dansyl absorption band around 340 nm and emission band at 516 nm is accompanied by a concomitant increase of the protonated dansyl absorption band at 284 nm and emission band at 335 nm. After addition of slightly more than one equivalent of acid, the dansyl emission is completely quenched and the protonated dansyl emission reaches a plateau. The comparison between compounds **DEtGly** and **Dans** (Figure 7.5) seems to suggest that **DEtGly** is easier to protonate than **Dans**. In the case of dendron **DEtGly** (Figure 7.5), however, the decrease of the dansyl absorption and emission bands and the increase of the protonated dansyl absorption band are not accompanied by a symmetric and parallel increase of the protonated dansyl emission. These results

show that although protonation of the dansyl moiety does take place stoichiometrically also for dendron **DEtGly**, some process interferes with the emission of the excited state of the protonated species.

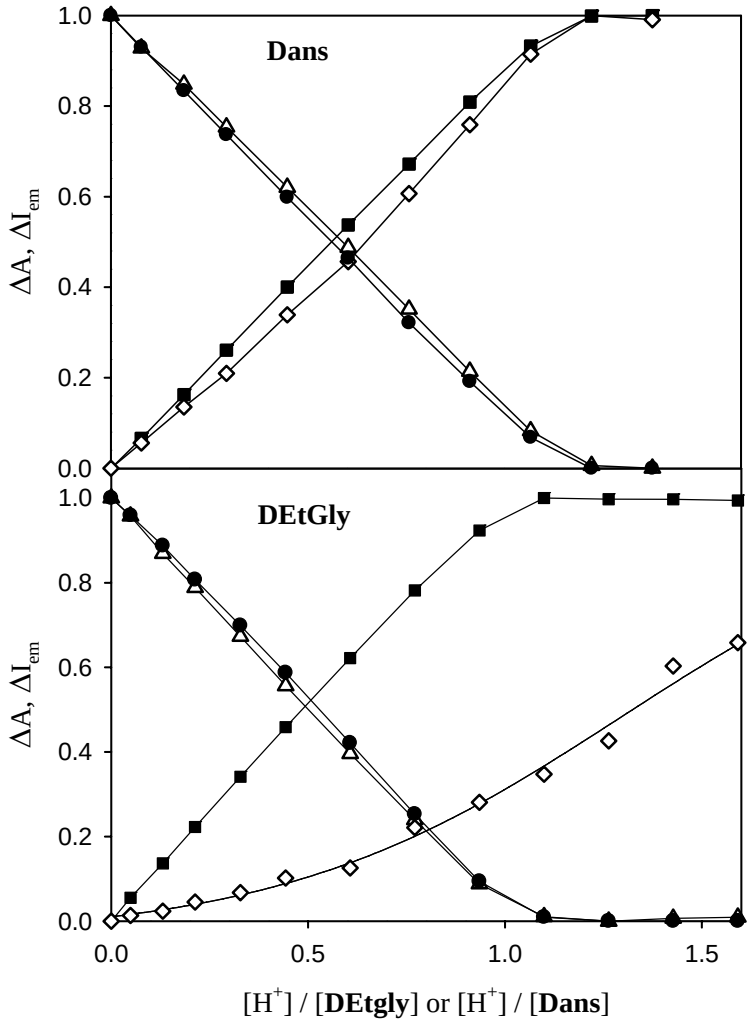

Figure 7.5. Normalized titration curves obtained for compounds **DEtGly** and **Dans** from absorption and emission measurements upon addition of triflic acid (acetonitrile solution, 298 K). Excitation at 270 nm in all cases. Absorbance values at 285 nm (full squares) and 342 nm (full circles). Emission intensity values at 335 nm (open rhombi), 505 nm (open triangles).

Interestingly, such a process cannot be a simple quenching (regardless of the mechanism) by the moiety appended to the dansyl unit because all the quantities in Figure 7.5 are normalized to the values obtained at the end of the titration, that in the case of the emission of protonated dansyl takes place after ca. one acid equivalent. The anomalous behavior of the emission of protonated dansyl could be accounted for by assuming that the excited state of protonated dansyl exhibits a lower proton affinity than the ground state. Since this is not the case for the simple dansyl unit **Dans**, the moiety appended to dansyl in **DEtGly** must be in some way responsible for the observed behavior. Our interpretation is that in **DEtGly** the protonated dansyl unit is partially enfolded by the oligoethylene glycol chains that can help the excited state deactivation by the well known reversible proton transfer mechanism.[7] As the concentration of acid increases, the oligoethylene glycol chains become more and more involved in ground state proton interactions and their interference on the deactivation of the excited state of protonated dansyl decreases.

The titration plot of **CycDans** (Figure 7.6) reveals an even more complex behavior. First of all, the absorbance at λ_{max} = 348 nm of the dansyl units (Figure 7.2) is only slightly affected by acid addition until two protons have been added. In parallel, almost no increase at 286 nm is observed, showing that protonated dansyl units are not formed. These results can be straightforwardly explained by the fact that the first two added protons associate with the nitrogens of the cyclam core (vide supra). The very small decrease of the dansyl absorbance at 348 nm caused by the first two protons (Figure 7.6) is actually due to a small red shift of the band, that can be

ascribed to the effect of the positively charged core on the charge transfer transition of the appended dansyl units. For more than two protons added, the parallel decrease at 348 nm and increase at 286 nm in absorption show that protonation of the eight dansyl units progressively takes place. It is worth noting that protonation of four out of eight dansyl units in the dendrimer (corresponding to 50% of absorbance change in Figure 7.6) is performed upon addition of six equivalent of acid. This result indicates that the first four dansyl units are protonated independently. As expected, protonation of the remaining dansyl units becomes more and more difficult as the overall charge of the dendrimer increases: complete protonation is obtained after addition of about 30 equivalents of acid, as mentioned above. The titration plots (Figure 7.6) also show that the decrease in intensity of the dansyl emission does not parallel the decrease of dansyl absorption. In fact, the emission intensity decreases even during the addition of the first two protons, i.e. when protonation takes place at the cyclam core. Furthermore, the emission intensity becomes negligible after addition of ca 10 protons, i.e. when, as shown by the absorption spectrum, 20% of the dansyl units are still unprotonated. The first result is ascribed to the influence of the positively charged core on the charge-transfer emission band, that actually undergoes a small red shift. As we will see later, a similar effect is also observed upon metal ion coordination by the cyclam core. The larger than expected decrease of the dansyl emission intensity is due to electron transfer quenching of the dansyl excited states by protonated dansyl units, as previously observed for other partially protonated polydansyl dendrimers.[8]

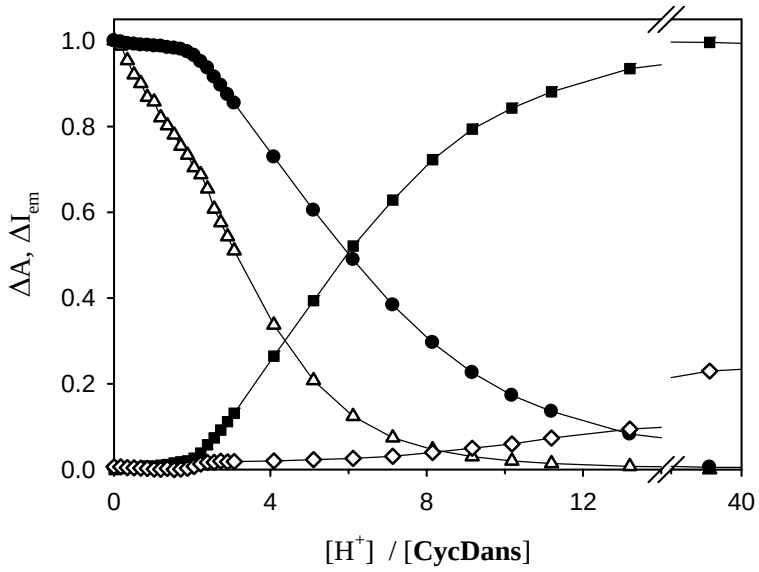

Figure 7.6. Normalized titration curves obtained for dendrimer **CycDans** from absorption and emission measurements upon addition of triflic acid (acetonitrile solution, 298 K). Excitation at 270 nm in all cases. Absorbance values at 286 nm (full squares) and 348 nm (full circles). Emission intensity values at 335 nm (open rhombi), 532 nm (open triangles).

Finally, it can be noticed that the emission of the protonated dansyl units increases very slowly on addition of acid. In fact, when, according to the changes in the absorption intensity, about 80% of the dansyl units are protonated, less than 5% of the protonated dansyl emission intensity is observed. As in the case of compound **DEtGly**, this effect can be ascribed to the fact that the protonated dansyl moieties of **CycDans** are enfolded, presumably by a greater extent than in **DEtGly**, by the oligoethylene glycol chains that can help the excited state deactivation by reversible proton transfer.

7.4 Metal ion coordination

As mentioned in the introduction, dendrimer **CycDans** contains three distinct types of multivalent, potentially coordinating sites: the cyclam core, the 16 oligoethylene glycol chains appended in the periphery, and the 8 amine moieties of the dansyl units. Comparison with the behavior of dendron **DEtGly** and reference compound **Dans** can throw some light on the role played by each type of coordination sites. We have titrated **CycDans**, **DEtGly**, and **Dans** in acetonitrile solution with Co^{2+}, Ni^{2+}, Cu^{2+}, Zn^{2+}, Nd^{3+}, Eu^{3+}, and Gd^{3+}, as nitrate and/or triflate salts. In each experiment, the changes in the absorption and emission spectra of the dansyl moieties have been monitored.

One can expect that coordination of the metal ion to the amine moiety of a dansyl chromophore has an effect similar to protonation, i.e. a decrease in intensity of the absorption and emission bands at 337 and 505 nm, and the appearance of absorption and emission bands at 287 and 335 nm, respectively (vide supra). If the coordinated metal has low lying metal-centered levels (e.g., Co^{2+}, Ni^{2+}, Cu^{2+}), and/or it is easy to reduce (e.g., Cu^{2+}), which implies the presence of low energy ligand-to-metal charge-transfer levels, quenching of the coordinated dansyl emission band at 532 nm could also occur. Coordination of a metal ion to the cyclam core or the oligoethylene glycol chains of the dendrimer is also expected to affect the absorption and emission bands of dansyl. The vicinity of a charged metal ion could perturb the transition moments, thereby altering the intensities of the dansyl absorption and emission bands. Furthermore, oligoethylene glycol or

cyclam complexes appended to the dansyl units could quench dansyl emission by energy and also by electron transfer, since dansyl can be easily oxidized ($E_{1/2}$ = 0.9 V vs SCE).[8]

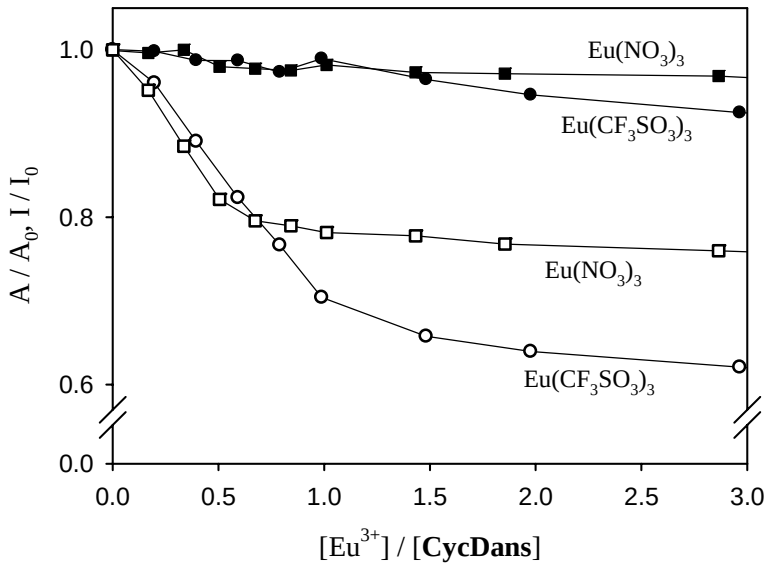

Figure 7.7. Changes in absorption (340 nm, full symbols) and emission (530 nm, open symbols) intensities observed for dendrimer **CycDans** upon addition of Eu^{3+} trifalte or nitrate (acetonitrile solution, 298 K). Excitation at 270 nm in all cases.

The results obtained indeed show that titration of dendrimer **CycDans** and reference compounds **DEtGly** and **Dans** with metal ions affects the dansyl absorption and emission bands in various ways. First of all it should be noted that, in order to form metal complexes, ligands **CycDans**, **DEtGly**, **Dans** must compete with solvent molecules and counter anions of the added metal ions. We have found indeed that the interaction of the metal ions with ligands **CycDans**, **DEtGly**, **Dans** is much stronger when the counter ion is triflate compared with nitrate (Figure 7.7). In fact,

nitrate salts have been found to interact only with dendrimer **CycDans**, not with compounds **DEtGly** and **Dans**.

Figure 7.8 shows the titration plots obtained on addition of Eu^{3+} (as triflate salt) to the "ligands" **CycDans**, **DEtGly**, and **Dans**. These results show that each of the **CycDans**, **DEtGly**, **Dans** ligands can coordinate Eu^{3+}. Analogous titration plots have been obtained in the case of Nd^{3+} and Gd^{3+} and a qualitatively similar behavior was exhibited by Zn^{2+}.

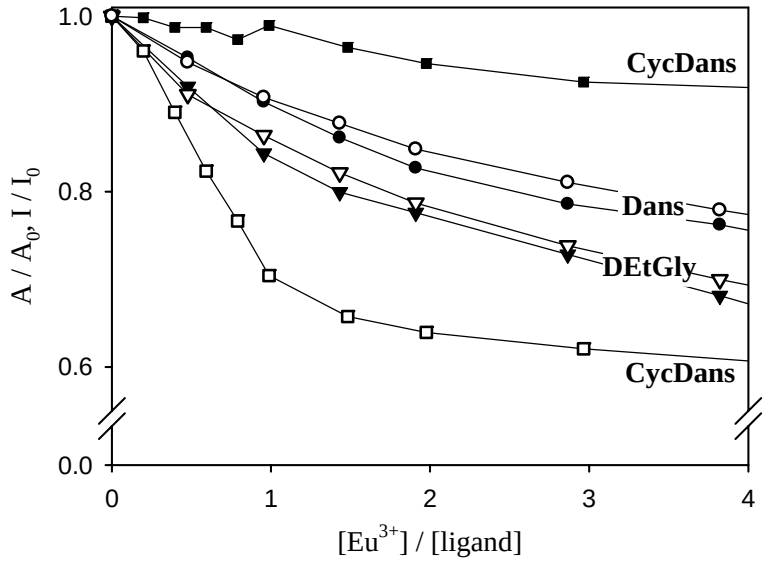

Figure 7.8. Changes in absorption (340 nm, full symbols) and emission (530 nm, open symbols) intensities observed for compounds **CycDans**, **DEtGly**, and **Dans** upon addition of Eu^{3+} trifalte (acetonitrile solution, 298 K). Excitation at 270 nm in all cases.

For compounds **DEtGly** and **Dans**, metal ion (as triflate salts) complexation causes parallel decrease in the intensities of the absorption and emission bands of dansyl as it happens upon dansyl protonation (vide supra). The appearance of an absorption

band around 285 nm, and, in the case of **Dans**, also of an emission band at 335 nm, again similar to that found for protonated dansyl, is also observed. These results indicate that both **DEtGly** and **Dans** are able to coordinate metal ions by means of the amine moiety of the dansyl unit, albeit with a small association constant. Apparently, **DEtGly** is a slightly better ligand than **Dans**, presumably because the oligoethylene glycol chains help in keeping the metal ion coordinated to dansyl.

In the case of **CycDans**, completely different results have been obtained (Figure 7.8): (i) a discontinuity can be observed in the titration plots at one equivalent of added metal ion, whereas no such discontinuity is found in the case of **DEtGly** and **Dans**; (ii) up to one equivalent, addition of the metal ion has quite different effects on absorption and emission, which was not the case for **DEtGly** and **Dans**; (iii) the effect on the absorption band in **CycDans** is smaller than in **DEtGly** and **Dans**, whereas the reverse is true for emission band; (iv) after addition of one equivalent of metal ion, the slopes of the absorption and emission plots in the case of **CycDans** become smaller than those found for **DEtGly** and **Dans**. All these results demonstrate that in the case of dendrimer **CycDans** the first equivalent of added metal ion is not coordinated by the dansyl moieties as for **DEtGly** and **Dans**, but by the cyclam core. It seems likely that the access of metal ion to the cyclam core is facilitated by transient complexation with the oligoethylene glycol chains. The presence of the charged metal ion in the core has a small effect on the dansyl absorption band, but a strong influence on the emission band which becomes weaker and slightly red-shifted. It can also be noted that once the cyclam core has

hosted a metal ion, further addition of metal ions implies coordination to the dansyl units, as shown by the decrease in intensity of both the absorption and emission dansyl bands with approximately the same slopes (Figure 7.8). Such slopes at high metal ion concentration are smaller than those found for **DEtGly** and **Dans**, presumably because the presence of a positively charged metal ion in the cyclam core makes more difficult coordination of another positively charged metal ion by the dansyl units of the branches.

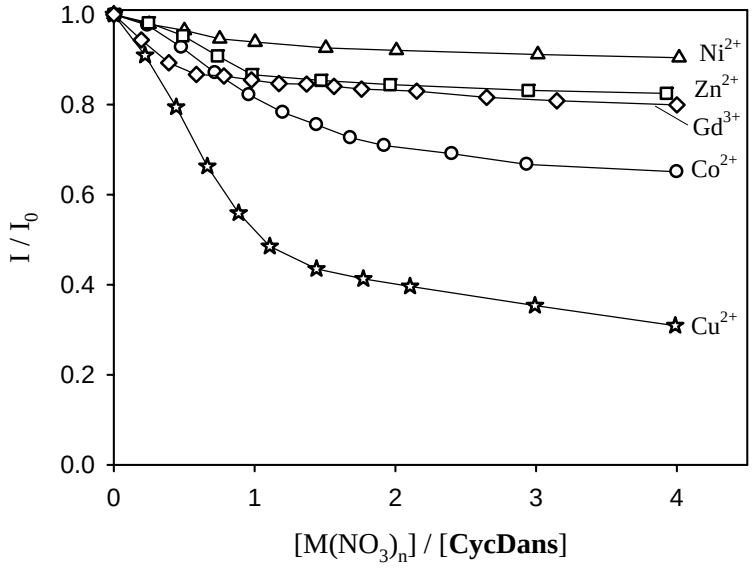

Figure 7.9. Changes in emission (530 nm) intensities observed for dendrimer **CycDans** upon addition of nitrate salts (acetonitrile solution, 298 K). Excitation at 270 nm in all cases.

Figure 7.9 compares the results obtained monitoring the intensity of the dansyl emission band upon titration of dendrimer **CycDans** with various metal ions as nitrate salts. Somewhat similar results have been obtained upon titration with

triflate salts. Clearly, there are effects strongly dependent on the chemical nature of the metal ion, with Cu^{2+} showing a quite distinct behavior that will be discussed below. In all cases, perhaps except for Co^{2+}, there is some discontinuity around one equivalent of added metal ion, as already discussed for the titration with triflate salts (see, e.g., the curve for **CycDans** in Figure 7.8). This result suggests again that the first dendrimer site to be involved in metal coordination is the cyclam core. It should be pointed out that the slopes of the titration curves depend on two parameters, namely the association constant and the ability of the coordinated metal ion to quench, by any mechanism, the emission intensity of the dansyl units. As mentioned above, three quenching mechanisms can be expected for metal ions coordinated to the cyclam core, namely (i) an effect of the positive charge of the metal ion on the emission transition moment, (ii) an energy transfer quenching when the metal ion has low-lying excited states, and (iii) an electron transfer quenching for metal ions that can be easily reduced (the oxidation potential of excited dansyl is ~ –1.9 V vs SCE).[9] Energy and electron transfer quenching, of course, will play a role only if they can compete with the excited state lifetime of dansyl (ca. 15 ns). It should also be considered that the counter ion, particularly in the case of nitrate salts, could play a role. Because so many parameters are involved, it is not easy to rationalize the results obtained. Among the metal ions used, $Zn^{2+}$and Gd^{3+} do not have low lying metal-centered levels and are too difficult to oxidize or reduce. Therefore, when coordinated to the cyclam core, they should affect the dansyl emission only by a charge perturbation effect that is slightly

stronger (Figure 7.9) for the metal carrying a higher charge (i.e., Gd^{3+}). The larger effect observed for Cu^{2+} could be attributed to either energy or electron transfer quenching. However, since Ni^{2+} and Co^{2+}, which have low lying metal-centered excited states like the Cu^{2+}complexes, behave similarly to Zn^{2+}, we can conclude that the ability of Cu^{2+} to quench the dansyl excited state is related to the occurrence of an electron transfer process. The lack of energy transfer quenching is also apparent from the very similar behavior of Gd^{3+} and Nd^{3+}, and the fact that Eu^{3+} behaves like Gd^{3+} and Nd^{3+} suggests that quenching by electron transfer is not effective for Eu^{3+}. Other details of the observed results are difficult to interpret. For example, both Ni^{2+} and Co^{2+}, which have low lying metal centered levels, would be expected to exhibit a larger quenching effect that Zn^{2+}.

7.5 Conclusions

We have synthesized dendrimer **CycDans** that contains 16 potentially luminescent moieties (8 dansyl- and 8 dimethoxybenzene-type units) and three distinct types of multivalent sites (the cyclam nitrogens, the amine moieties of the 8 dansyl units, and the 16 oligoethylene glycol chains) that, in principle, can be protonated or coordinated to metal ions. We have investigated the absorption and luminescence properties of **CycDans** in acetonitrile solution and the changes taking place upon titration with acid and a variety of divalent (Co^{2+}, Ni^{2+}, Cu^{2+}, Zn^{2+}), and trivalent (Nd^{3+}, Eu^{3+}, Gd^{3+}) metal ions as triflate and/or nitrate salts. The first site to be involved in the protonation (two equivalents of H^{+}) and metal coordination (one

equivalent of metal ion) is the cyclam core, followed by the dansyl units. Once hosted by cyclam, the metal ion interacts with the appended dansyl units. The nature and extent of interaction depend in a complex way on the nature of the metal ion and of the counter ion.

The results obtained show that: (i) cyclam is an ideal core for obtaining dendrimers capable of associating protons and metal ions; (ii) the dansyl chromophoric group is a useful unit to construct dendrimers sensitive to environment perturbations; (iii) it is possible to design and construct dendrimers that, thanks to the integration of the properties of suitable components, can perform complex functions that derive from the integration of the specific properties of the constituent moieties. Therefore, such design is interesting for understanding relations between complex structure and multiple functionality.

References

[1] For the 1,3-dimethoxybenzene unit, the energy of the fluorescent excited state, as estimated from the onset of the emission band, is about 4.3 eV. Electrochemical experiments in acetonitrile solution have shown that it undergoes a chemically irreversible one-electron oxidation process (E_{pa} = 1.5 V vs SCE, at 0.2 V/s), while dansyl unit is reduced at $E_{1/2}$ = -2.02 V (vs SCE). It follows that upon excitation of the dimethoxybenzene unit an electron transfer process from dimethoxybenzene to dansyl moiety is thermodynamically allowed.

[2] (a) M. Micheloni, A. Sabbatini, P. Paoletti, *J. Chem. Soc., Perkin Trans.* **1978**, *2*, 828. (b) V. J.Thöm, G. D. Hosken, R. D. Hancock, *Inorg. Chem.* **1985**, *24*, 3378.

[3] R. D. Hancock, R. J. Motekaitis, J. Mashishi, I. Cukrowsky, J. H. Reibenspies, A. E. Martell, *J. Chem. Soc., Perkin Trans., 2* **1996**, 1925.

[4] J. R. Röper, H. Elias, *Inorg. Chem.* **1992**, *31*, 1202.

[5] (a) C. Saudan, V. Balzani, P. Ceroni, M. Maestri, M. Gorka, V. Vicinelli, F. Vögtle, *Tetrahedron* **2003**, *59*, 3845. (b) G. Bergamini, P. Ceroni, V. Balzani, L. Cornelissen, J. van Heyst, S.-K. Lee, F. Vögtle, *J. Mater. Chem.* **2005**, *15*, 2959.

[6] H.F.M. Nelissen, F. Venema, R.M. Uittenbogaard, M.C. Feiters, R.J.M. Nolte, *J. Chem. Soc. Perkin Trans. 2*, **1997**, 2045.

[7] P. Suppan *Chemistry and Light*, Royal Society of Chemistry, **1994**, Cambridge, UK, ch. 6.

[8] F. Vögtle, S. Gestermann, C. Kauffmann, P. Ceroni, V. Vicinelli, L. De Cola, V. Balzani, *J. Am. Chem. Soc.* **1999**, *121*, 12161.

[9] F. Vögtle, S. Gestermann, C. Kauffmann, P. Ceroni, V. Vicinelli, V. Balzani, *J. Am. Chem. Soc.* **2000**, *122*, 10398.

CHAPTER 8

Proton-driven self-assembled system based on cyclam-cored dendrimers and [Ru(bpy)(CN)$_4$]$^{2-}$

8.1 Introduction

The challenge for chemists engaged in artificial self-assembly processes resides in the "programming" of the system,[1,2] i.e., in the design of components which carry, within their structures, the pieces of information necessary not only for the construction of the desired supramolecular architecture, but also for the performance of the required function. Since the function to be performed upon light excitation is often related to the occurrence of a reversible assembly/disassembly process,[2] the system has to be programmed so as to be able not only to *self-assemble* under thermodynamic control, but also to *disassemble* under a suitable energy input. For information processing, even more interesting are those systems that are capable of existing in three or more forms that are interconverted by means of different stimuli.[3,4] In fact, systems which respond to a given combination of multiple stimuli open the way to more complex switches (logic gates) at the molecular scale.[3] From this viewpoint, fluorescence is an ideal output because of its ease of detection even at the single-molecule limit.[5] Another remarkable feature of fluorescent signals is that they do not need to be wired to

operate. Light can indeed bridge the gap between the world of molecules and our macroscopic world.[6]

Here we report the results of an investigation carried out on the assembling/disassembling of the luminescent dendritic hosts **CyG0** and **CyG2** with the luminescent metal complex $[Ru(bpy)(CN)_4]^{2-}$ (Scheme8). The assembly process is proton driven and leads to formation of $\{[Ru(bpy)(CN)_4]^{2-}\bullet(2H^+)\bullet$ **CyG0**$\}$ and $\{[Ru(bpy)(CN)_4]^{2-}\bullet(2H^+)\bullet$ **CyG2**$\}$ adducts with strong effects on the luminescence properties. The adducts can then be disassembled both by addition of a base, namely 1,4-diazabicyclo[2.2.2]octane (DABCO), and of an excess of triflic acid, giving rise to two different optical outputs that behave according to an XOR and XNOR logic.

8.2 Dendrimers CyG0 and CyG2

The absorption and luminescence spectra of these host compounds CyG0 and CyG2 (Scheme 8) in acetonitrile-dichloromethane 1:1 v/v solution have been previously investigated and reported in the previous chapters.[7] Also the protonation of **CyG0** and **CyG2** has been extensively reported and analize in the previous chapters.

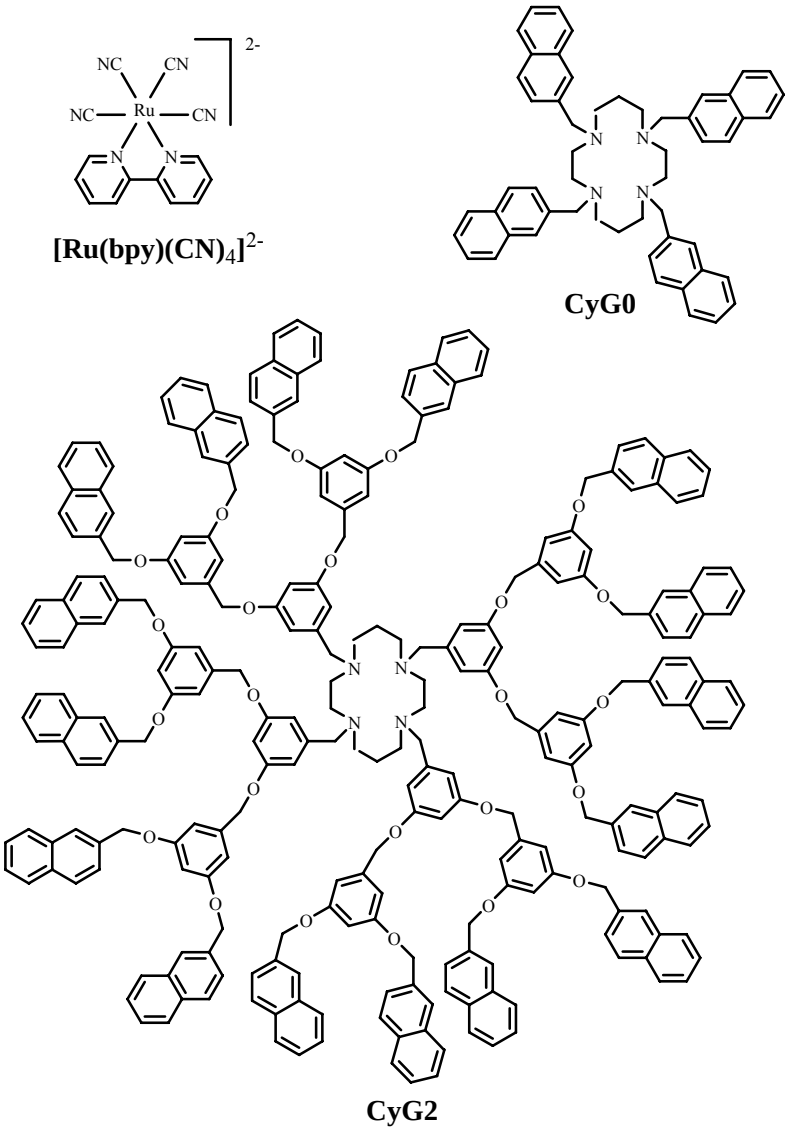

Scheme 8. Structure formulae of the dendrimers **CyG0** and **CyG2** and the complex $[Ru(bpy)(CN)_4]^{2-}$.

8.3 $[Ru(bpy)(CN)_4]^{2-}$

The absorption and emission spectra of this complex have been thoroughly investigated by Scandola and co-workers in water and acid solution.[8] The low energy absorption bands and the weak luminescence band exhibited in the visible

region are related to metal-to-ligand (bpy) charge-transfer (MLCT) excited states (spin-allowed states for the absorption bands; the lowest spin-forbidden state for the emission band). The energies of these excited states are strongly dependent on the interaction of the CN^- ligands with solvents or protons. In aqueous solution, addition of sulphuric acid starting from pH 3 causes successive protonation of the four CN^- ligands as shown by the progressive displacement of the absorption and emission bands to higher energies. The four protonation steps, however, are not separable and no definite emission spectra for the various protonated forms can be obtained.[8b]

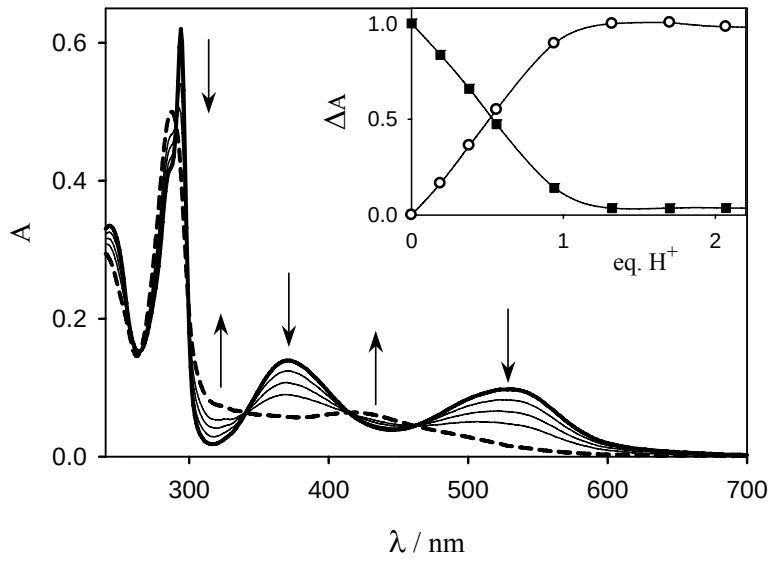

Figure 8.1. Changes observed in the absorption spectrum of $[Ru(bpy)(CN)_4]^{2-}$ (2.25×10^{-5} M) in acetonitrile-dichloromethane 1:1 v/v solution at 298 K upon addition of trifluoroacetic acid. The thick solid line is the spectrum before acid addition, and the thick dashed line the spectrum obtained after addition of 1 eq. of acid. Inset shows the normalized absorbance changes at 318 (o) and 535 nm (■).

In acetonitrile-dichloromethane 1:1 v/v solution, $[Ru(bpy)(CN)_4]^{2-}$ shows two moderately intense MLCT absorption bands at 373 and 535 nm (Figure 8.1) and a very weak emission band at 770 nm (Figure 8.2). Upon titration with trifluoroacetic acid, the absorption bands move to higher energies with an isosbestic point that is maintained until one equivalent of acid has been added. Strong changes are also observed in the emission spectra (Figure 8.2) where a band arises at 630 nm upon addition of acid. The intensity of such a band increases linearly up to a plateau value that is reached at about one equivalent of acid. Addition of large amounts of acid causes further changes in the absorption spectra with a second family of isosbestic points and the corresponding emission band further shifts to higher energy and increases in intensity. Analysis by the SPECFIT software[9] of the titration plots shown in the insets of Figures 8.1 and 8.2 yielded the following values for the first and second acidity constants: $pK_{a1} = 7.1$, pK_{a2} ca. 4.[10]

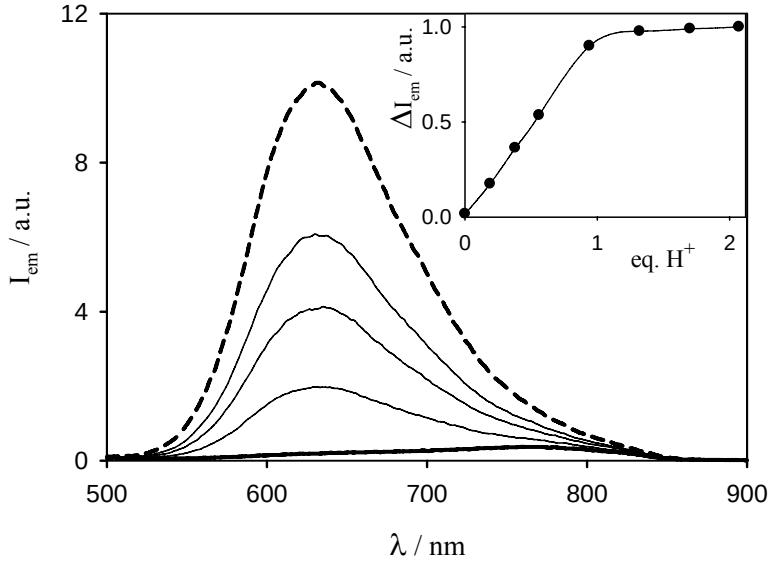

Figure 8.2. Changes observed in the emission spectrum of $[Ru(bpy)(CN)_4]^{2-}$ (2.25×10^{-5} M) in acetonitrile-dichloromethane 1:1 v/v solution at 298 K upon addition of trifluoroacetic acid. The thick solid line is the spectrum before acid addition, and the thick dashed line the spectrum obtained after addition of 1 eq. of acid. Inset shows the normalized intensity changes at 630 nm. λ_{ex} = 300 nm.

8.4 Assembling

Formation of adducts between protonated polyazamacrocycles and $[Ru(bpy)(CN)_4]^{2-}$ was previously exploited for promoting intercomponent energy-transfer processes.[11] The aims of our study were (i) to see whether the cyclam core of dendrimers is accessible to large potential guests, (ii) to understand whether the excitation energy collected by the dendrimer chromophoric units can be funneled to such a guest, and (iii) to explore whether the effect of adduct assembling/disassembling on the luminescence properties could be used for light-signal processing. Since the behavior of the two examined systems

$[Ru(bpy)(CN)_4]^{2-}$ and **CyG0**, and $[Ru(bpy)(CN)_4]^{2-}$ and **CyG2** is quite similar, we will mainly concentrate our discussion on that involving dendrimer **CyG2**.

The absorption spectrum of a 1:1 mixture of $[Ru(bpy)(CN)_4]^{2-}$ and **CyG2** (3.0×10^{-5} M) is displayed in Figure 8.3. Comparison with the spectra of the two separated components (Figures 6.1 and 8.1) shows that there is no interaction between the two compounds in the ground state. Lack of interaction in the excited state, as well, is demonstrated by the emission spectrum (Figure 8.4) which exhibits the characteristic bands of the isolated dendrimer (Figure 6.1) and metal complex (Figure 8.2).

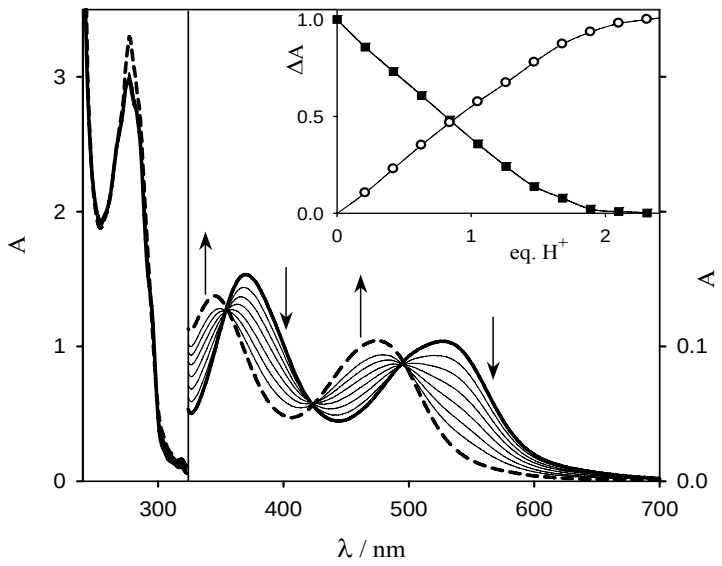

Figure 8.3. Changes observed in the absorption spectrum of a 1:1 mixture of $[Ru(bpy)(CN)_4]^{2-}$ and **CyG2** (3.0×10^{-5} M) in acetonitrile-dichloromethane 1:1 v/v solution at 298 K upon addition of trifluoroacetic acid. The thick solid line is the spectrum before acid addition, and the thick dashed line the spectrum obtained after addition of 2 eq. of acid. Inset shows the normalized absorbance changes at 445 (o) and 535 nm (■). Note the different absorbance scale for the left and right part of the figure.

Titration of the above mentioned mixture with trifluoroacetic acid causes strong changes in the absorption and emission spectra. In the absorption spectrum (Figure 8.3) the two bands of $[Ru(bpy)(CN)_4]^{2-}$ at 373 and 535 nm move to higher energies (345 and 476 nm), but less than in the case of protonation (Figure 8.1) and isosbestic points are maintained up to the addition of two equivalents of acid. These results suggest that addition of acid promotes association of $[Ru(bpy)(CN)_4]^{2-}$ and **CyG2** and that after addition of two equivalents of protons a $\{[Ru(bpy)(CN)_4]^{2-} \bullet (2H^+) \bullet$ **CyG2**$\}$ adduct is formed, where the two protons bridge the cyclam core of the dendrimer to the CN^- ligands of the metal complex (Figure 8.6). The behavior of the emission spectrum upon acid addition (Figure 8.4 and 8.5) confirms the hypothesis of the proton-driven formation of an adduct between $[Ru(bpy)(CN)_4]^{2-}$ and **CyG2**. Addition of acid up to two equivalents to the 1:1 mixture of $[Ru(bpy)(CN)_4]^{2-}$ and **CyG2** causes a decrease of the exciplex band at 450 nm which is accompanied by a decrease of the naphthyl band at 335 nm (Figure 8.4; excitation was performed at 288 nm, where ca 80% of the absorbed light causes naphthyl excitation). Such a behavior is different from that observed upon addition of acid to a solution containing **CyG2** alone (decrease of the exciplex band and increase of the naphthyl band, see chap. 6). On excitation at 490 nm (where 100 % of the absorbed light causes excitation of the metal complex), addition of acid causes the appearance of a band with maximum around 680 nm (Figure 8.5), red-

shifted compared with the band originated by addition of acid to $[Ru(bpy)(CN)_4]^{2-}$ alone (Figure 8.2).

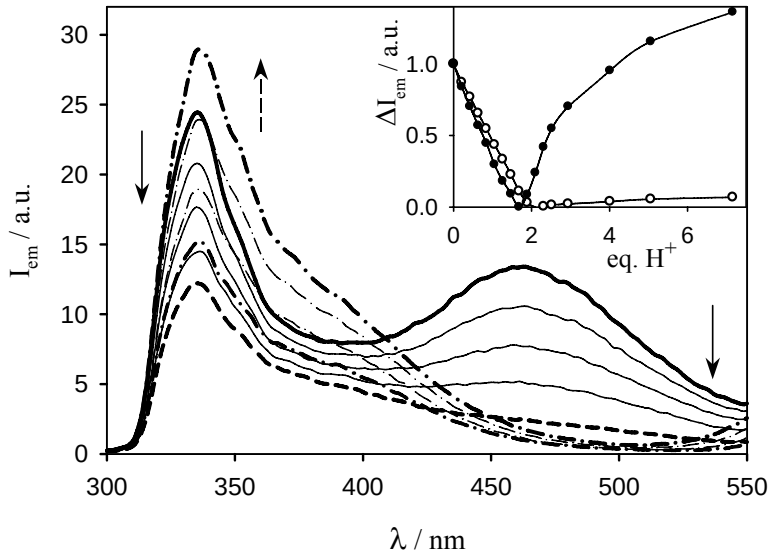

Figure 8.4. Changes in the emission spectra in the naphthyl region of a 1:1 mixture of $[Ru(bpy)(CN)_4]^{2-}$ and **CyG2** (3.0×10^{-5} M) in acetonitrile-dichloromethane 1:1 v/v solution at 298 K upon addition of trifluoroacetic acid: 0 eq. (thick solid line), 2 eq. (thick dashed line), 2.5-6 eq. (dashed-dotted line). λ_{ex} = 288 nm. Inset shows the normalized intensity changes at 335 (•) and 460 nm (o).

We have also performed titrations of $[Ru(bpy)(CN)_4]^{2-}$ solutions by the diprotonated forms of **CyG0** and **CyG2**, namely $(\mathbf{CyG0}.2H)^{2+}$ and $(\mathbf{CyG2}.2H)^{2+}$. The results obtained were fully consistent with those reported above. The absorption bands were displaced to higher energies, isosbestic points were observed up to the addition of ca. 1 equivalent of $(\mathbf{CyG2}.2H)^{2+}$, and the absorption spectrum after addition of one equivalent of $(\mathbf{CyG2}.2H)^{2+}$ was equal to that obtained upon addition of two equivalents of H^+ to the 1:1 mixture of $[Ru(bpy)(CN)_4]^{2-}$ and **CyG2** (Figure

8.3). Similar results were obtained when $(\mathbf{CyG0}.2H)^{2+}$ was used in the place of $(\mathbf{CyG2}.2H)^{2+}$.

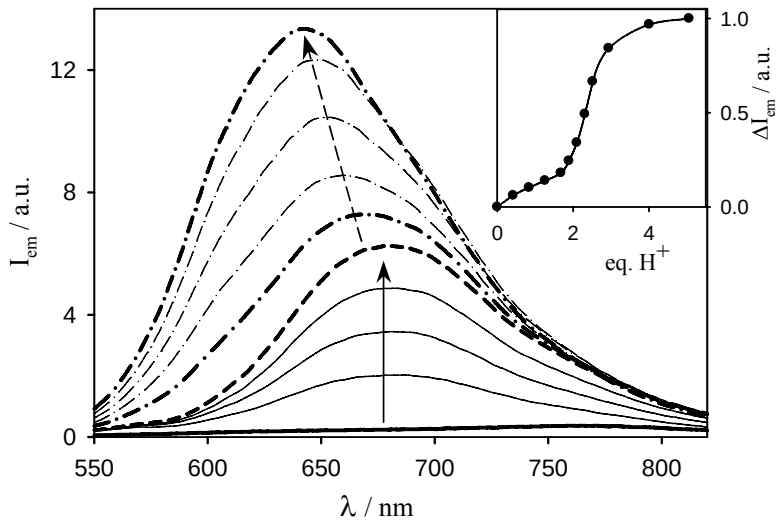

Figure 8.5. Changes in the emission spectra in the $[Ru(bpy)(CN)_4]^{2-}$ region of a 1:1 mixture of $[Ru(bpy)(CN)_4]^{2-}$ and **CyG2** (3.0×10^{-5} M) in acetonitrile-dichloromethane 1:1 v/v solution at 298 K upon addition of trifluoroacetic acid: 0 eq. (thick solid line), 2 eq. (thick dashed line), 2.5-6 eq. (dashed-dotted line). λ_{ex} = 490 nm. Inset shows the normalized intensity changes at 620 nm.

Indeed, all the results obtained are consistent with formation of $\{[Ru(bpy)(CN)_4]^{2-}\bullet(2H^+)\bullet$ **CyG0**$\}$ and $\{[Ru(bpy)(CN)_4]^{2-}\bullet(2H^+)\bullet$ **CyG2**$\}$ adducts. In such assemblies, the Ru complex must share the protons with the cyclam core of the dendrimer (Figure 8.6), which explains why the absorption and emission band of the metal complex are less shifted to higher energies than those of the protonated metal complex. As far as luminescence is concerned (Figure 8.4), on adduct formation the exciplex band of the dendrimer decreases because the cyclam core shares protons

with the metal complex; however, the intensity of the naphthyl band does not increase, as it would be expected upon disappearance of the exciplex, but decreases (to 15% of the fully protonated species). This shows that a new deactivation channel, namely energy transfer to the lower lying excited state of the metal complex, is available for deactivation of the naphthyl units in the adduct. In order to estimate the energy transfer efficiency, we prepared two solutions of $\{[Ru(bpy)(CN)_4]^{2-}\bullet(2H^+)\bullet$ **CyG2**$\}$ of different concentration, exhibiting the same absorbance at 287 and 374 nm. Excitation of these solutions mainly in the naphthyl bands (at 287 nm) and in the MLCT bands (at 374 nm), shows a metal complex emission intensity at 680 nm that is 88% lower in the former compared to the latter case.[12] Taking into account that 20% of the light is directly absorbed by the Ru complex at 287 nm, it follows that the intra-adduct energy transfer efficiency is 85%. In the case of compound **CyG0**, the behavior is qualitatively similar, but the energy transfer efficiency is higher, ca. 100%. In conclusion, both dendrimers play the role of light harvesting hosts that, in the adducts, transfer the collected energy to the metal complex guest.

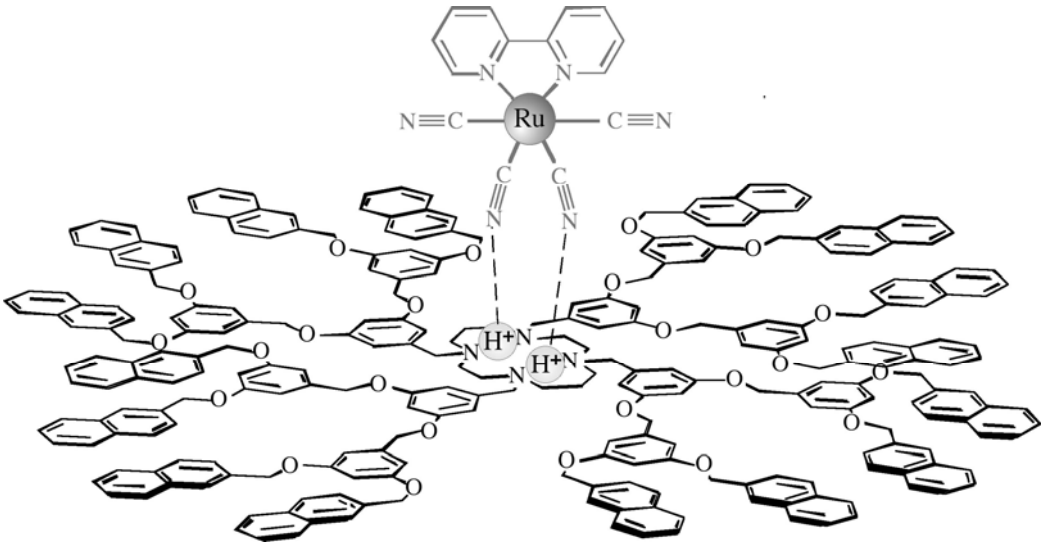

Figure 8.6. Schematic representation of the {$[Ru(bpy)(CN)_4]^{2-}$•$(2H^+)$•**CyG2**} adduct.

8.5 Disassembling

The above described spectral changes upon acid titration are fully reversed by successive addition of a stoichiometric amount of a base, namely 1,4 diazabicyclo[2.2.2]octane (DABCO), indicating an assembling/disassembling reversible behavior.

We have also found that, upon further addition of an excess of acid to {$[Ru(bpy)(CN)_4]^{2-}$•$(2H^+)$• **CyG0**} and {$[Ru(bpy)(CN)_4]^{2-}$•$(2H^+)$• **CyG2**}, novel spectral changes are observed. For example, the isosbestic points of the absorption spectra disappear, the intensity of the naphthyl type emission at 335 nm increases (Figure 8.4), and the metal complex based emission at 680 nm increases in intensity and moves to higher energies (Figures 8.5). This behavior can be easily explained considering that both $[Ru(bpy)(CN)_4]^{2-}$ and **CyG2** (or **CyG0**) are Lewis bases, so

that when excess acid is present they do not need to share protons, but they are stabilized as independent protonated species, namely $[Ru(bpy)(CN)_{2-n}(CNH)_{2+n}]^{n+}$ (n from 0 to 2) and $(\mathbf{CyG2}.2H)^{2+}$ or $(\mathbf{CyG0}.2H)^{2+}$ species. As shown by the inset to Figure 8.4, adduct formation between $[Ru(bpy)(CN)_4]^{2-}$ and **CyG2** upon acid addition exhibits an *on-off-on* behavior, i.e. the system performs as a luminescent threshold[13] device.

Energy transfer from a dendritic host to guest molecules or metal ions has already been reported,[14] as well as reversible assembling and disassembling of the supramolecular system. For example, in a dendrimer consisting of a hexaamine core surrounded by 8 dansyl-, 24 dimethoxybenzene-, and 32 naphthalene-type units[15] a very efficient energy transfer takes place from all the chromophoric groups of the dendrimer to an eosin guest molecule. In such a system, assembling requires extraction of eosin from acidic (pH=5-7) aqueous solution by shaking with a dichloromethane solution of the dendrimer, and disassembling requires shaking a dichloromethane solution of the adduct with a basic (pH>12) aqueous solution. Clearly, the assembling/disassembling process is much easier in the present system.

In conclusion the $\{[Ru(bpy)(CN)_4]^{2-}\bullet(2H^+)\bullet$ **CyG0**$\}$ and $\{[Ru(bpy)(CN)_4]^{2-}\bullet(2H^+)\bullet$ **CyG2**$\}$ adducts can be disrupted (i) by addition of a base (DABCO), yielding the starting species $[Ru(bpy)(CN)_4]^{2-}$ and **CyG0** or **CyG2**, or (ii) by addition of triflic acid, with formation of $(\mathbf{CyG0.}2H)^{2+}$ or $(\mathbf{CyG2.}2H)^{2+}$ and protonated forms of

$[Ru(bpy)(CN)_4]^{2-}$. This means that the adducts behave as systems that respond to two different chemical inputs.

8.6 Light-signal processes

Upon 270 nm excitation (90% of the light is absorbed by naphthyl units), a solution of the {$[Ru(bpy)(CN)_4]^{2-}$•$(2H^+)$• **CyG2**} adduct (3.0×10^{-5} M) shows emission bands at 335 and 680 nm (Figure 8.4 and 8.5). The intensities of these two optical channels (outputs) change upon addition of base or acid (inputs) as shown in Table 8. Let us consider first emission at 335 nm. In a binary logic scheme,[3] a threshold value of 25 can be fixed for the emission intensity and, in a positive logic convention, a 0 can be used to represent a signal that is below the threshold value and a 1 can be employed to indicate a signal that is above. We can thus write the truth table shown in Figure 8.7a, that shows that the system behaves as an XOR logic gate. Conversely, one can monitor the emission at 680 nm, establish a threshold value of 1.5 for the emission intensity, and use a 0 and a 1 to indicate intensity values below and above the threshold value, respectively.

The truth table reported in Figure 8.7b shows that using this output channel the system behaves as an XNOR logic gate.

[a]DABCO, 30 equiv. [b]triflic acid, 30 equiv.

compound	$I_{335\ nm}$ / a.u.	$I_{680\ nm}$ / a.u.
$\{[Ru(bpy)(CN)_4]^{2-}\bullet(2H^+)\bullet$**CyG2**$\}$	12	3.2
$\{[Ru(bpy)(CN)_4]^{2-}\bullet(2H^+)\bullet$ **CyG2**$\}$ + base[a]	29	0.4
$\{[Ru(bpy)(CN)_4]^{2-}\bullet(2H^+)\bullet$ **CyG2**$\}$ + acid[b]	76	0.2
$\{[Ru(bpy)(CN)_4]^{2-}\bullet(2H^+)\bullet$ **CyG2**$\}$ + acid[a] + base[b]	15	2.8

Table 8. Emission intensities of $\{[Ru(bpy)(CN)_4]^{2-}\bullet(2H^+)\bullet$**CyG2**$\}$ under different experimental conditions in acetonitrile:dichloromethane 1:1 v/v solution.

a

IN_1 (acid)	**IN_2** (base)	**OUT** ($I_{335\ nm}$)
0	0	0
0	1	1
1	0	1
1	1	0

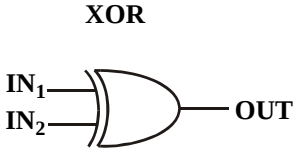

b

IN_1 (acid)	**IN_2** (base)	**OUT** ($I_{680\ nm}$)
0	0	1
0	1	0
1	0	0
1	1	1

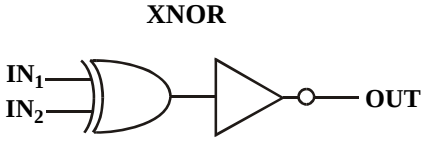

Figure 8.7. Truth table and symbol of the (a) XOR and (b) XNOR logic gate.

8.7 Conclusions

We have shown that the luminescent cyclam-based hosts **CyG0** and **CyG2** can be assembled with the luminescent metal complex $[Ru(bpy)(CN)_4]^{2-}$ by a proton-driven process that causes strong changes in the luminescence properties. In the $\{[Ru(bpy)(CN)_4]^{2-}\bullet(2H^+)\bullet$ **CyG0**$\}$ and $\{[Ru(bpy)(CN)_4]^{2-}\bullet(2H^+)\bullet$ **CyG2**$\}$ adducts formed in this way, very efficient energy transfer takes place from the naphthyl units of **CyG0** and **CyG2** to the metal complex.

We have also shown that the $\{[Ru(bpy)(CN)_4]^{2-}\bullet(2H^+)\bullet$ **CyG0**$\}$ and $\{[Ru(bpy)(CN)_4]^{2-}\bullet(2H^+)\bullet$ **CyG2**$\}$ adducts can be disrupted by two distinct chemical inputs, namely addition of DABCO, yielding the starting species $[Ru(bpy)(CN)_4]^{2-}$ and **CyG0** or **CyG2**, or addition of triflic acid, with formation of $(\mathbf{CyG0.}2H)^{2+}$ or $(\mathbf{CyG2.}2H)^{2+}$ and protonated forms of $[Ru(bpy)(CN)_4]^{2-}$. Such processes cause strong changes in the luminescent properties. In particular, in the case of $\{[Ru(bpy)(CN)_4]^{2-}\bullet(2H^+)\bullet$ **CyG2**$\}$ there are two optical output channels, emission at 335 and 680 nm, that behave as XOR and XNOR logic gates, respectively.

A large number of dendrimers playing the role of antennas for light harvesting have been reported in the literature.[15] The system investigated in this paper is an example of a light harvesting antenna in which the energy collecting units can be reversibly assembled to/disassembled from the dendrimer core.[11b,c] This behavior introduces

more flexibility in view of the construction of systems useful for artificial photosynthesis.

References

[1] J.-M. Lehn, Supramolecular Chemistry; Concepts and Perspectives; Wiley-VCH: Weinheim, **1995**.

[2] V. Balzani, A. Credi, M. Venturi, *Proc. Natl. Acad. Sci.* **2002**, *99*, 4814.

[3] V. Balzani, M. Venturi, A. Credi, *Molecular Devices and Machines- A journey into the Nanoworld*, Wiley-VCH: Weinheim, **2003**, chapter 8.

[4] (a) G. Cooke, V. M. Rotello, *Chem. Soc. Rev.* **2002**, *31*, 275. (b) G. Cooke, *Angew. Chem. Int. Ed.* **2003**, *42*, 4860. (c) F. Pina, M. Maestri, V. Balzani, In *Handbook of Photochemistry and Photobiology*, M. S. A. Abdel-Mottaleb, H. S. Nalwa, Eds.; American Scientific Publishers: Stevenson Ranch, USA, **2003**; Vol. 3, pp. 411-450.

[5] *Single Molecule Detection in Solution*; C. Zander, J. Enderlein, R. A. Keller, Eds.; Wiley-VCH, Berlin, **2002**.

[6] A. P. De Silva, N. D. McClenaghan, C. P. McCoy, In *Stimulating Concepts in Chemistry*; M. Shibasaki, J. F. Stoddart, F. Vögtle, Eds.: Wiley-VCH, Weinheim, **2001**, Vol. 5, p.156.

[7] C. Saudan, V. Balzani, P. Ceroni, M. Maestri, M. Gorka, V. Vicinelli, F. Vögtle, *Tetrahedron* **2003**, *59*, 3845.

[8] (a) C. A. Bignozzi, C. Chiorboli, M. T. Indelli, M. A. Rampi Scandola, G. Varani, F. Scandola, *J. Am. Chem. Soc.* **1986**, *108*, 7872. (b) M. T. Indelli, C. Bignozzi, A. Marconi, F. Scandola, In *Photochemistry and Photophysics of Coordination Compounds*; Yersin, H.; Vogler, A. Springer-Verlag: Berlin, **1987**, pp. 159-164. (c) F. Scandola, M. T. Indelli, *Pure Appl. Chem.* **1988**, *60*, 973. (d) M. T. Indelli, M. Ghirotti, A. Prodi, C. Chiorboli, F. Scandola, N. D. McClenaghan, F. Puntoriero, S. Campagna, *Inorg. Chem.* **2003**, *42*, 5489.

[9] (a) R. A. Binstead, SPECFIT; Spectrum Software Associates: Chapell Hill, NC, **1996**. (b) H. Gampp, M. Maeder, C. J. Meyer, A. Zuberbulher, *Talanta* **1985**, *32*, 257.

[10] The reported value for pK_{a2} is a rough estimate since the second protonation step is not well resolved from the following ones.[8c]

[11] (a) M. A. Rampi, M. T. Indelli, F. Scandola, *Inorg. Chem.* **1996**, *35*, 3355. (b) N. R. M. Simpson, M. D. Ward, A. F. Morales, B. Ventura, F. J. Barigelletti, Chem. Soc., *Dalton Trans.* **2002**, 2455. (c) F. Loiseau, G. Marzanni, S. Quici, M. T. Indelli, S. Campagna, *Chem. Commun.* **2003**, 286.

[12] The emission intensity signals were corrected for the number of exciting photons by using $[Ru(bpy)_3]^{2+}$ as a standard.

[13] For an interesting example of threshold devices, see e.g.: F. Pina, M. J. Melo, M. Maestri, P. Passaniti, V. Balzani, *J. Am. Chem. Soc.* **2000**, *122*, 4496.

[14] (a) M. Kawa, J. M. J. Fréchet, *Chem. Mater.* **1998**, *10*, 286. (b) A. P. H. J. Schenning, E. Peeters, E. W. Meijer, *J. Am. Chem. Soc.* **2000**, *122*, 4489. (c) M. Kawa, T. Takahagi, *Chem. Mater*. **2004**, *16*, 2282.

[15] U. Hahn, M. Gorka, F. Vögtle, V. Vicinelli, P. Ceroni, M. Maestri, V. Balzani, *Angew. Chem. Int. Ed.* **2002**, *41*, 3595.

CHAPTER 9

Mechanisms for fluorescence depolarization in dendrimers

9.1 Introduction

We have selected four types of dendrimers to illustrate the different fluorescence anisotropy mechanisms that can be observed depending on the nature and position of the luminescent unit(s) in the dendritic structure (Gn is the dendrimer generation number).

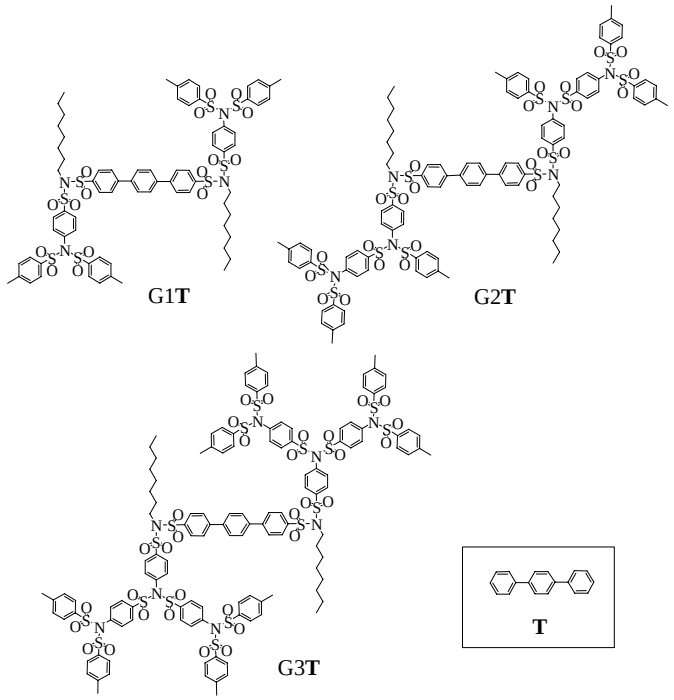

Scheme 9.1. Dendrimers with a terphenyl **T** core.

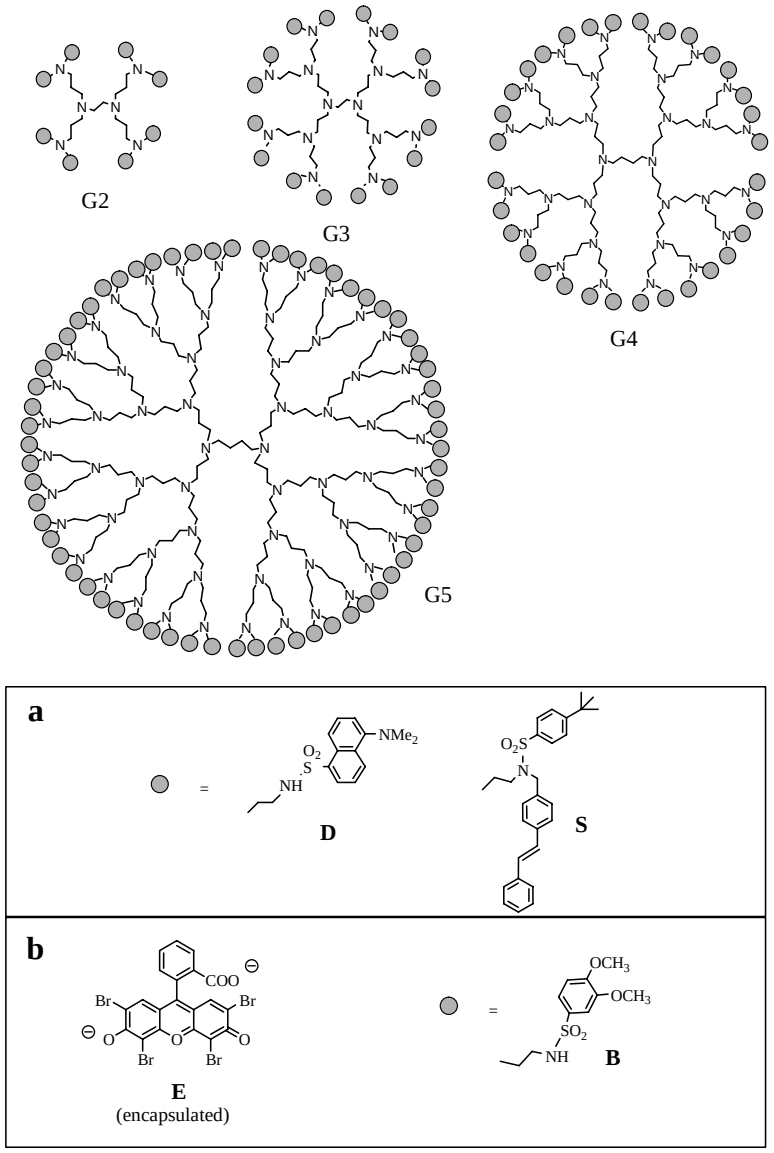

Scheme 9.2. Poply(propylene amine) dendrimers with (a) dansyl **D** and stylbenyl **S** peripheral units; (b) eosin **E** encapsulated in G4 carrying 1,2-dimethoxybenezene **B** peripheral units.

As shown in Schemes 9.1 and 9.2, the four selected systems are based on four different luminophores, namely terphenyl (**T**), dansyl (**D**), stilbenyl (**S**), and eosin (**E**). In the case of **T** (Scheme 9.1), the dendrimers have a single fluorescent

moiety, i.e. the **T** core. In the cases of **D** and **S** (Scheme 9.2a), multiple fluorescent units are appended in the periphery of poly(propylene amine) dendritic structures. In the case of **E** (Scheme 9.2b), the investigated luminophore does not belong to the dendritic structure, but is encapsulated in cavities of the low luminescent fourth generation poly(propylene amine) dendrimer G4**B** containing 1,2-dimethoxybenzene (**B**) units at the periphery.

9.2 Fluorescence anisotropy

For a simple molecular species, fluorescence anisotropy depends on the different orientation of the absorption and emission transition moments. The fluorescence anisotropy is defined as

$$r = (I_{\parallel} - I_{\perp}) / (I_{\parallel} + 2I_{\perp}) \quad (1)$$

where $I_{\parallel}$ and $I_{\perp}$ are the emission intensities registered when the emission and excitation polarizers are oriented parallelly or perpendicularly, respectively. For randomly oriented molecules, directly after excitation, the anisotropy (r_0) will be 0.4 if the transition dipole moments of the excited and the fluorescent states have the same orientation. The value of the anisotropy decreases if the transition moments are not collinear and when the molecule undergoes a change in orientation during the excited state lifetime.

The fluorescence anisotropy decay can be fitted by a monoexponential model (2):

$$r(t) = r_0 e^{-t/\theta} \quad (2)$$

where θ is the rotational relaxation time.

The rotational relaxation time θ can be related to the hydrodynamic volume V_h by the Stokes-Einstein-Debye equation. In particular, for compounds having a van der Waals volume much bigger than the volume of the solvent molecules, “sticking” boundary conditions are applicable, i.e. the form of the rotor has no influence since it moves together with solvent molecules, and θ can be expressed as

$$\theta = V_h \eta / k_B T \qquad (3)$$

where η is the viscosity of the solvent, k_B the Boltzmann constant, T the absolute temperature.

If a supramolecular system contains *only one* fluorescent unit, fluorescence depolarization takes place, as for simple molecular species, if the absorption and emission transition moments are intrinsically non collinear, and as a result of change in orientation of the fluorophore during the excited state lifetime. Such a dynamic change in orientation may be caused by (i) rotation of the supramolecular system as a whole, and (ii) local motions of the fluorophore, in the case of a flexible supramolecular architecture. For a supramolecular system that contains *more than one* identical fluorescent unit with different orientations, fluorescence depolarization can also occur by (iii) energy migration from the originally excited unit to a differently oriented one. Of course, the rates of global rotation, local movements, and energy migration must compete with the rate of deactivation of the fluorophore excited state. At constant temperature, the rate of global rotation depends on the size of the species and the viscosity of the solvent, the rate of local movements depends on the specific position of the fluorophore in the

supramolecular structure and on the nature of the bonds that link the fluorophore to the supramolecular scaffold, and the rate of energy migration depends on the overlapping between the absorption and emission spectra of the fluorophore.

As mentioned in the introduction, it is possible to construct dendrimers of different size that contain one or more selected fluorescent units in predetermined sites of the dendritic architecture. Furthermore, it is possible to incorporate fluorescent molecules in the dendritic cavities. We have exploited these possibilities to make systems that exhibit different fluorescence depolarization properties controlled by the three above mentioned mechanisms (global rotation, local motion, and energy migration).

9.3 Dendrimers with a *p*-terphenyl core

The absorption and emission properties of the G1**T**, G2**T**, and G3**T** dendrimers (Scheme 9.1) are similar to those of *p*-terphenyl **T**.[1] In dichloromethane (DCM)/propylene glycol (PGly) 1:1 (v/v) solution, all the dendrimers exhibit the characteristic absorption and emission bands of the **T** unit with maximum at 300 and 355 nm, respectively. The fluorescence quantum yield of the dendrimers is very high (close to unity) and the fluorescence decay is slightly shorter (ca. 0.6 ns) than that previously found in dichloromethane (DCM) solutions (0.8 ns).[1]

Steady state properties. Figure 9.1 shows the fluorescence anisotropy spectrum of **T** and dendrimers G1**T**, G2**T**, and G3**T** in dichloromethane. The steady state anisotropy r_{ss} is constant throughout the emission band, is practically zero for **T**

and increases with increasing mass of the dendrimer. In these compounds, depolarization channels related to energy migration are not available since the terphenyl core is the unique fluorescent component and the lowest excited state of the system. Furthermore, fluorescence depolarization via local motions is unlikely because the fluorescent unit is the core of the dendritic structure and even rotation of the terphenyl moiety around its molecular axis would not substantially change the relative orientation of the longitudinal absorption and emission transition moments.[2] Therefore, fluorescence anisotropy has to be related to global rotation of the dendrimer that is affected by solvent viscosity.

The maximum anisotropy value (r_0) for **T**, measured in polystyrene matrix where rotation is prevented, is 0.33[3] because of the relative orientation of the absorption and emission dipoles. As shown in Figure 9.1, the *p*-terphenyl molecule undergoes full depolarization during the emission lifetime in dichloromethane solution,[1] showing that rotation is faster than the excited state lifetime. In the more viscous mixture of dichloromethane/propylene glycol 1:1 (v/v), rotation is slowed down and, correspondingly, an higher value of r_{ss} has been observed for **T** (Table 9.1). The G1**T**, G2**T**, and G3**T** dendrimers in the same viscous mixture of solvents exhibit a steady-state anisotropy that is higher than that observed in dichloromethane, and increases with dendrimer generation. These results confirm that depolarization takes place by global rotation of the dendrimer. In the case of G3**T** the value of r_{ss} (Table 9.1) is very close to the maximum value of terphenyl

anisotropy (r_0 = 0.33), since rotation is almost prevented during the excited state lifetime by both solvent viscosity and dendrimer size.

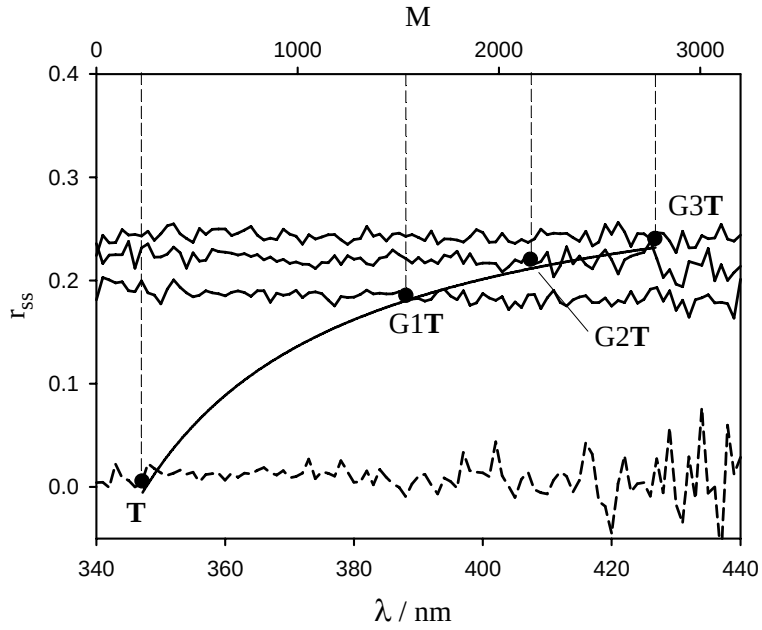

Figure 9.1. Steady state fluorescence anisotropy r_{ss} in dichloromethane solution of compounds G1**T**, G2**T**, G3**T** and **T** at 298 K. The curve represents the interpolation of the r_{ss} values upon increasing molecular mass (M) considering as a limiting value r_0 = 0.33 (open circle), typical of **T** in rigid matrix.

Time dependent properties. The fluorescent decay curves for the G1**T**, G2**T**, and G3**T** dendrimers in dichloromethane solution were collected under 0° and 90° polarization angles upon excitation at 300 nm and analyzed globally. The fluorescence anisotropy decay can be fitted to a monoexponential model (eq. 2) for all compounds. As expected, rotational relaxation times θ increase with dendrimer generation (Table 9.1), demonstrating a slower rotation for larger molecules. These

values are in good agreement with those calculated assuming a spherical rotor with a single fluorescence lifetime: [4]

$$r_{ss} = \frac{r_0}{1+\frac{\tau}{\theta}} \qquad (4)$$

The rotational relaxation time θ can be related to the hydrodynamic volume V_h by the Stokes-Einstein-Debye equation (eq. 3). The calculated V_h values increase with dendrimer generation (Table 9.1) without reaching a plateau value: this demonstrates that there is no collapse of the dendrimer structure upon increasing generation.[5] These values are in fair agreement with the ones obtained by molecular modeling, considering the non-spherical shape of the examined compounds.[6]

No reliable data on the relaxation time θ in propylene glycol/dichloromethane mixtures could be obtained with our instrumental equipment because of the too short excited state lifetime of the terphenyl fluorophore under these experimental conditions.

In conclusion, fluorescence depolarization in G1**T**, G2**T**, and G3**T** can be essentially related to global rotation of the dendrimer.

9.4 Dendrimers with dansyl units at the periphery

Dendrimers G2**D**, G3**D**, G4**D**, and G5**D** (Scheme 9.2) contain 8, 16, 32, and 64 peripheral dansyl units **D**, respectively. Experiments were carried out in dichloromethane and propylene glycol mixtures. As mentioned above, in such systems depolarization can in principle occur by (i) global rotation of the dendrimer, (ii) local motions of the **D** fluorophores, and (iii) energy migration among the **D** units. In practice, however, the last mechanism is not highly efficient in these compounds because dansyl shows a very large Stokes shift between the absorption (λ_{max}= 340 nm) and emission (λ_{max}= 515 nm) bands. Indeed, according to Förster equation,[7] the integral overlap between absorption and emission spectra J is 3×10^{-18} cm^3 M^{-1} and the distance value where the rate of energy transfer and of intrinsic deactivation are equal (R_0) is about 1.1 nm, as reported in Table 9.2. To estimate the energy migration efficiency, R_0 should be compared to the average distance between two dansyl units in the Gn**D** dendrimer family. Although to estimate this distance is difficult because of the high conformational flexibility of this dendrimer type, in the case of G4**D** in DCM a radius of about 2 nm has been calculated,[8] that would lead to an average distance of about 1.3 nm, substantially larger than R_0. Therefore, energy migration is not very efficient compared to intrinsic deactivation and is not supposed to significantly contribute to fluorescence depolarization.

Steady state properties. Figure 9.2 shows the fluorescence anisotropy spectrum of the dansyl reference fluorophore **D** and of the largest dendrimer G5**D** in

dichloromethane. The steady-state anisotropy values obtained for the examined compounds are gathered in Table 9.1. As one can see, r_{ss} is constant throughout the emission band, is practically zero for **D** and increases with increasing dendrimer generation (filled circles in Figure 9.3).

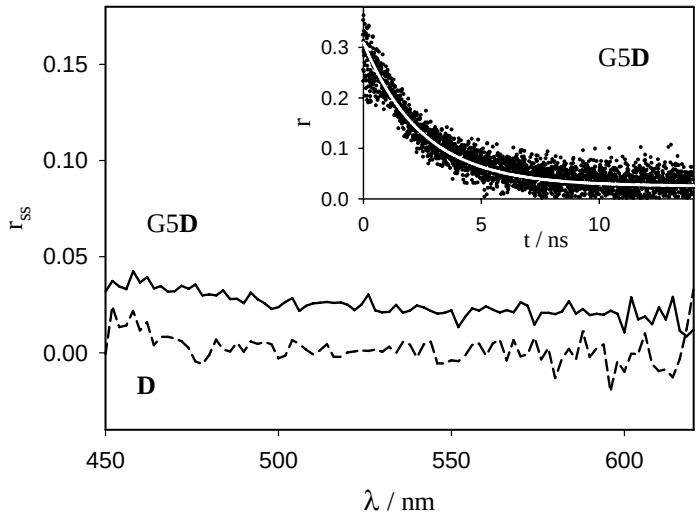

Figure 9.2. Steady state fluorescence anisotropy r_{ss} in dichloromethane solution of compounds **D**, and G5**D** at 298 K. Inset shows r (black points) as a function of time for compound G5**D**. λ_{ex} = 405 nm; λ_{em} = 500 nm.

In a dichloromethane/propylene glycol 1:30 (v/v) mixture, r_{ss} (Table 9.1) is higher than in pure dichloromethane because of the increased viscosity. Indeed, also in the case of model compound **D** and the smallest investigated G2**D** dendrimer, non-zero values of r_{ss} have been measured, at variance with results in dichloromethane solution. The steady-state anisotropy measured for the dendrimers Gn**D** is: (i) much lower (ca. 0.2) than the maximum anisotropy value r_0 = 0.31 for dansyl fluorophore,[9] suggesting that motion is still present under these experimental

conditions, (ii) increase with dendrimer molecular mass, (iii) but are much less sensitive to this parameter, compared to dichloromethane solution (the same r_{ss} values have been obtained for G3**D**-G5**D**, squares in Figure 9.3). These results suggest that anisotropy decay takes place by two processes, a slower one whose rate decreases with increasing dendrimer generation, and a faster one that is not largely dependent on dendrimer generation and that is the dominant one in more viscous solvents. We assign the slow process to the global rotation of the dendrimer, and the fast one to local motions of the peripheral dansyl units appended to the dendritic scaffold. The close similarity of steady-state anisotropy observed for G3**D**, G4**D** and G5**D** in the more viscous mixture of solvents is because local motions are not strongly influenced by the dendrimer generation and they are mainly responsible for fluorescence depolarization.

Time dependent properties. In dichloromethane solution the anisotropy decay of **D** is too fast to be measured with our equipment since it undergoes full depolarization during the excited state lifetime. For the dendrimers, the rotational relaxation time θ (Table 9.1) can be obtained by fitting the anisotropy data with a mono exponential decay (see e.g., inset of Figure 9.2) and upon setting the time-zero anisotropy r_0 equal to that of the dansyl unit, 0.31. The obtained θ values are not strongly different going from G2**D** to G5**D** (from 0.6 to 2.4 ns, Table 9.1), despite the large variation in molecular mass and volume. Furthermore, these values are not in agreement with those predicted for a spherical rotor from equation 4. The hydrodynamic volume V_h calculated from equation 3 increases with dendrimer

generation (Table 9.1), but the corresponding values are quite close and too small for the larger dendrimers. For example, in the case of G4**D** a radius of 1.6 nm is estimated by the corresponding hydrodynamic volume, while molecular model suggest a more expanded structure (r ca. 2 nm).[10] These results iindicate that this family of dendrimers may not be considered as simple spherical rotors. Indeed, as evidenced by steady-state measurements, the local motion is an additional process that contributes to depolarize fluorescence and shorten rotational relaxation times.

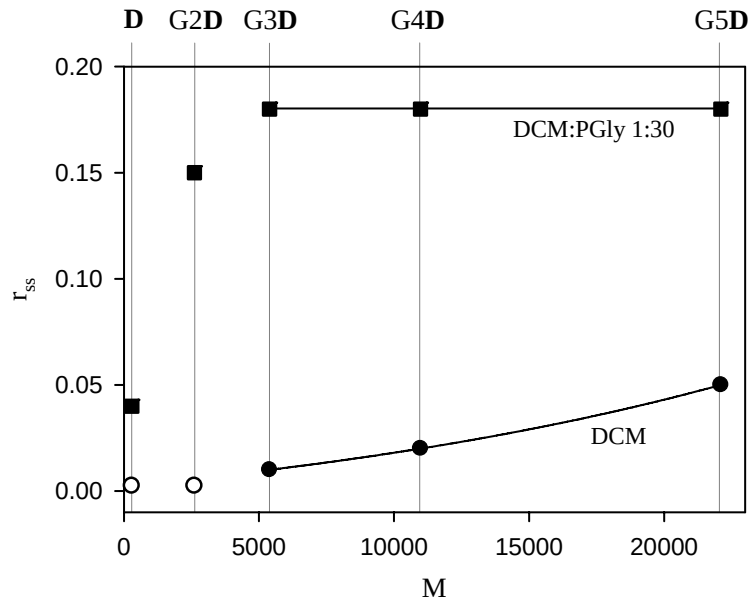

Figure 9.3. Steady state anisotropy r_{ss} in DCM (circles) and DCM:PGly 1:30 (v/v) (squares) solutions of dendrimers Gn**D** and model compound **D** at 298 K. λ_{ex} = 405 nm; λ_{em} = 500 nm. Note that empty circle refers to anisotropy values below the detection limit of 0.05.

Time-dependent data are not presented in dichloromethane/propylene glycol mixtures since in this solvent mixture a double exponential decay is observed, which prevents fitting of the corresponding anisotropy decays.

[a]λ_{ex} = 300 nm. λ_{em} = 370 nm. [b]Rotational relaxation time θ cannot be measured accurately because of the very short lifetime of the corresponding emitting excited state (ca. 0.6 ns). [c]λ_{ex} = 405 nm. λ_{em} = 500 nm. [d]Double-exponential decay of fluorescence precluded an accurate determination of the corresponding θ values. [e]λ_{ex} = 290 nm. λ_{em} = 330 nm. [f]λ_{ex} = 405 nm. λ_{em} = 550 nm.

	solvent	r_{ss}	θ (ns)	V_h (nm^3)
T[a]	DCM	<0.01	< 0.5	
	DCM/PGly 1:1	0.01	-[b]	
G1**T**[a]	DCM	0.19	1.1	10.1
	DCM/PGly 1:1	0.26	-[b]	-
G2**T**[a]	DCM	0.22	1.7	15.6
	DCM/PGly 1:1	0.29	-[b]	-
G3**T**[a]	DCM	0.24	2.8	25.6
	DCM/PGly 1:1	0.31	-[b]	-
D[c]	DCM	< 0.01	< 0.5	
	DCM:PGly 1:30	0.04	-[d]	
G2**D**[c]	DCM	< 0.01	0.6	5.8
	DCM:PGly 1:30	0.15	-[d]	-
G3**D**[c]	DCM	0.01	1.3	12.6
	DCM:PGly 1:30	0.18	-[d]	-
G4**D**[c]	DCM	0.02	1.8	17.4
	DCM:PGly 1:30	0.18	-[d]	-
G5**D**[c]	DCM	0.05	2.4	23.3
	DCM:PGly 1:30	0.18	-[d]	-
S[e]	AN	0.21	-[b]	
	AN:PGly 1:30	0.30	-[b]	
G2**S**[e]	AN	0.16	-[b]	
	AN:PGly 1:30	0.16	-[b]	
E[f]	DCM	< 0.01	-	
E ⊂ G4**B** (0.1:1)[f]	DCM	0.09	-[d]	
E ⊂ G4**B** (7:1)[f]	DCM	0.03	-[d]	

Table 9.1. Steady-state and time-resolved anisotropy of fluorescence.

9.5 Dendrimer with stilbenyl units at the periphery

Similarly to the Gn**D** family, the poly(propylene amine) dendrimer G2**S** contains identical fluorescent units (in this case, stilbenyl units **S**) appended in the periphery. Therefore, also for G2**S** depolarization can in principle occur by (i) global rotation of the dendrimer, (ii) local motions of the peripheral **S** fluorophores, and (iii) energy migration among the **S** units. Contrary to what happens for the Gn**D** dendrimers, in the case of G2**S** energy migration is expected to be fast because of the strong overlap between the absorption (λ_{max}= 310 nm) and emission (λ_{max}= 353 nm) bands of the stylbenyl moiety,[11] as demonstrated by the much higher values of J and R_0 reported for stylbenyl rather than dansyl fluorophores (Table 9.2). Experiments were performed on reference compound **S** and dendrimer G2**S** in various acetonitrile and propylene glycol mixtures.

Since the excited state lifetime is very short (<200 ps)[11] for both reference compound **S** and dendrimer G2**S**, the fluorescence anisotropy decay could not be measured with our equipment. Interesting results, however, have been obtained by measuring steady state anisotropy in different solvent mixtures.

Steady state properties. As shown in Figure 9.4a, the fluorescence anisotropy of the reference compound **S** increases upon increasing the fraction of propylene glycol in the solvent mixtures (from pure acetonitrile to 1:30 (v/v) acetonitrile/propylene glycol). This is an expected result since in such a molecular system the fluorescence anisotropy depends on the competition between excited state lifetime and rotational relaxation time, with the latter increasing upon increasing solvent

viscosity (eq. 3). On the other hand, for dendrimer G2**S** an increase in solvent viscosity does not cause any appreciable increase in fluorescence anisotropy (Figure 9.4b), maintaining a r_{ss} value around 0.16 at 330 nm. The fact that the fluorescence anisotropy of the dendrimer is not affected by rotational dynamics means that another mechanism is responsible for depolarization, i.e. local motions of the **S** fluorophores appended at the dendrimer periphery and/or energy migration among the eight **S** units. In order to elucidate which mechanism is actually involved, we studied the behaviour of the corresponding dansylated second generation dendrimer, G2**D**, in the same mixture of solvents. This dendrimer is supposed to have roughly the same dimensions as G2**S**, as well as the same local flexibility for random motions of the fluorophores. We have found that, contrary to what happens to G2**S**, in going from acetonitrile to acetonitrile/propylene glycol 1:30 (v/v), the fluorescence anisotropy of G2**D** is strongly affected and it increases approximately by a factor of ten. These results show that the lack of increase in the fluorescence anisotropy of G2**S** with increasing solvent viscosity can be attributed to a faster depolarization mechanism independent on solvent viscosity, i.e. energy migration among the **S** units, consistent with the previously reported formation of excimers[11] between nearby **S** units.

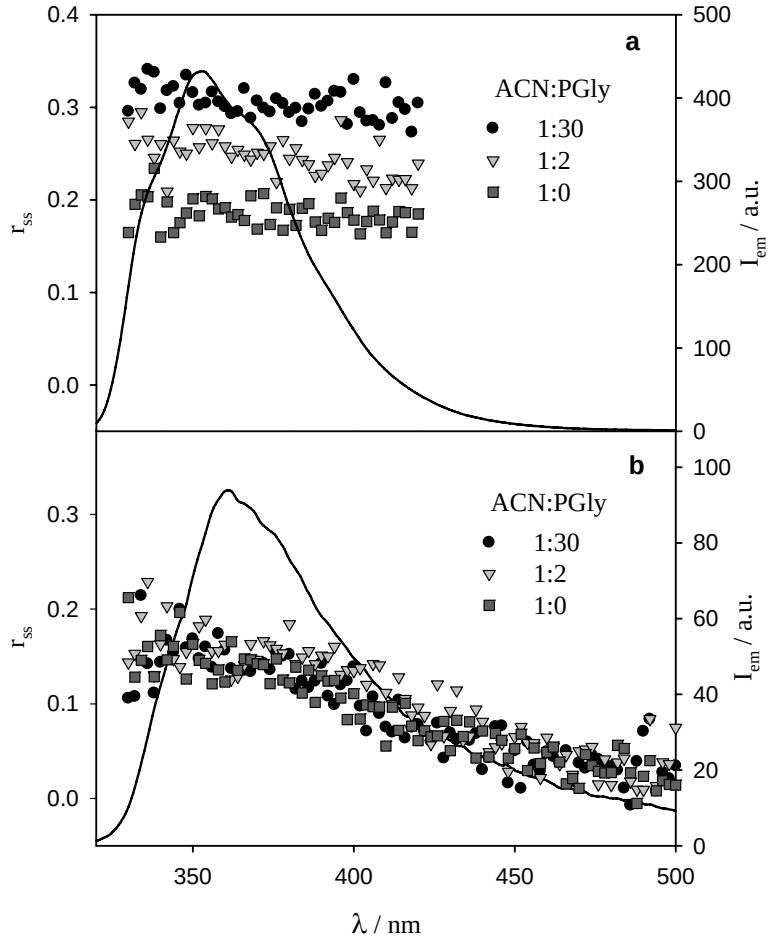

Figure 9.4. Steady state anisotropy r_{ss} in ACN (squares), ACN:PGly 1:2 (v/v) (triangles), ACN:PGly 1:30 (v/v) (circles) solutions at 298 K of compounds **S** (a) and G2**S** (b). Emission spectra in acetonitrile solution are also reported. λ_{ex} = 290 nm.

Another interesting feature of G2**S** fluorescence anisotropy spectrum (Figure 9.4b) is that it is not constant all over the investigated spectral region: it decreases from 0.16 at 330 nm to ca. 0.02 at 500 nm. This result is consistent with the fact that in the spectral region from 330 to 550 nm two different species, stilbenyl monomers and excimers, are emitting light with different emission lifetimes (τ_1 < 200 ps for

the emission band at 350 nm and τ_2 = 3.5 ns corresponding to the tail at lower energy).[11] The lower r_{ss} value observed for G2**S** (Figure 9.4b) compared to **S** (Figure 9.4a) in acetonitrile solution is indicative of the fact that the rate of energy migration among stilbenyl units in G2**S** is higher than that of rotation of **S** in acetonitrile solution.

9.6 Eosin molecules enclosed in a dendrimer

It is well known[12, 13] that poly(propylene amine) dendrimers in dichloromethane solution can extract eosin from aqueous solution. We have performed experiments on systems made of fluorescent eosin molecule(s) encapsulated in the cavities of the fourth generation poly(propylene amine) dendrimers G4**D** and G4**B** (Scheme 9.2). For technical reasons related to excitation wavelength and spectral overlap,[14] the experiments made with G4**B** were easier than those with G4**D**, although the results obtained for the two systems were comparable. Both dendrimers can host one or more eosin molecules, depending on the relative concentrations of dendrimer and eosin in the dichloromethane and aqueous solutions used for the extraction. In all cases, the average number of eosin molecules per dendrimer can be determined by measuring the absorbance of the water solution at 515 nm, where eosin shows an intense absorption band (ε = 70000 M^{-1} cm^{-1}).

Steady state properties. Eosin (as tetrabutyl ammonium salt) in dichloromethane does not show any fluorescence anisotropy (r_{ss} < 0.01). This means that rotational depolarization occurs faster than the excited state lifetime. The steady state

anisotropy values for dichloromethane solutions of eosin hosted in G4**B** with 0.1:1 and 7:1 eosin/G4 concentration ratios are shown in Figure 9.5. For solutions with 0.1:1 eosin/G4**B** ratio, where no more than one eosin molecule is hosted inside a G4**B** dendrimer, a steady state fluorescence anisotropy of 0.09 can be observed. However, solutions with 7:1 eosin/G4**B** ratio, in which 7 eosin molecules, as an average, are encapsulated in each dendrimer, exhibit a much smaller (0.03) steady state anisotropy. Since there is no reason that rotational depolarization is faster when more eosin molecules are contained into the dendrimer cavities, the strongly reduced anisotropy observed for the solution with 7:1 eosin/G4**B** concentration ratio is assigned to the occurrence of a fast energy migration among the eosin molecule hosted in the same dendrimer. This result is consistent with the small Stokes shift between absorption (λ_{max}= 515 nm) and emission (λ_{max}= 546 nm)[13] and the consequent high values of J and R_0 (Table 9.2).

[a]Data from ref. 13a. [b]Data from ref. 11.

fluorophore	solvent	Φ_{em}	τ / ns	J / 10^{-15} cm^3 M^{-1}	R_0 / nm
D	DCM	0.46[a]	16[a]	0.03	1.1
S	AN	0.05[b]	0.1[b]	3.4	1.7
E	DCM	0.65[a]	3.8[a]	55.2	4.2

Table 9.2. Photophysical parameters and integral overlap between absorption and emission spectra, J, and distance at which energy transfer has 50% efficiency (R_0), calculated according to Förster equation7 for energy transfer between identical fluorophores.

Time dependent properties. In dichloromethane solution the anisotropy decay of **E** (as tetrabutyl ammonium salt) is too fast to be measured with our equipment, since

it undergoes full depolarization during the excited state lifetime. The anisotropy decays for eosin encapsulated in G4**B** with 0.1:1 or 7:1 ratio are shown in the inset of Figure 9.5. The rotational relaxation time is lower when more eosin molecules are encapsulated inside a dendrimer, but estimation of reliable θ values is precluded by the biexponantional nature of the eosin fluorescence decay, as previously observed.[13] These qualitative time-resolved results and the steady-state measurements suggest that (i) when, at most, one eosin molecule is encapsulated inside G4**B** its motion is slowed down, so that r_{ss} and θ values are higher than in pure dichloromethane solution, and (ii) upon encapsulation of more than one eosin molecule per dendrimer an additional mechanism, i.e. energy migration, contributes to depolarize fluorescence.

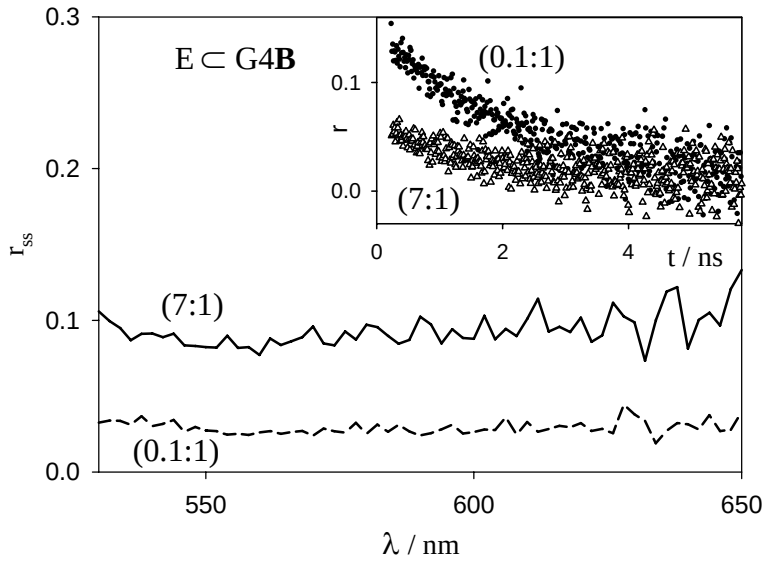

Figure 9.5. Steady state anisotropy r_{ss} and anisotropy decay as functions of time (inset) in dichloromethane solution of **E** ⊂ G4**B** with ratio 0.1:1 and 7:1 at 298 K. λ_{ex} = 405 nm; λ_{em} = 550 nm.

9.7 Conclusions

The four dendritic systems presented in this paper, based on four different luminophores, namely terphenyl (**T**), dansyl (**D**), stilbenyl (**S**), and eosin (**E**), provide representative examples of different mechanisms of fluorescent depolarization.

In the first case, the fluorophore **T** constitutes the core of the dendrimer and fluorescence depolarization is due to global rotation of the dendrimer. In the second and third cases, multiple **D** and **S** luminophoric units, respectively, are appended in the periphery of poly(propylene amine) dendritic structures. However, the photophysical properties of **D** and **S** are so different that energy migration is very efficient only among the **S** units. In the more viscous mixtures of solvents, fluorescence depolarization occurs mainly by local motion for the Gn**D** family and by energy migration for the G2**S** dendrimer. In the fourth case, the investigated luminophore (**E**) is non-covalently encapsulated in cavities of a fourth generation poly(propylene amine) dendrimer G4**B**, containing 1,2-dimethoxybenzene (**B**) units at the periphery. In this case, the study of fluorescence anisotropy of eosin evidenced that eosin rotation inside G4**B** dendrimer cavities is restricted and that when, as an average, more than one eosin is encapsulated inside a dendrimer, efficient energy migration takes place.

Fluorescence anisotropy reveals once more a very useful tool to investigate dendrimer structures and energy migration processes.

References

[1] G. Bergamini, P. Ceroni, V. Balzani, M. Del Mar Villavieja, R. Kandre, I. Zhun, O. Lukin, *ChemPhysChem* **2006**, *7*, 1980.

[2] H. H. Jaffé, M. Orchin, *Theory and application of ultraviolet spectroscopy*, John Wiley and Sons, Inc. London, **1964**, ch. 12.

[3] B. Schartel, V. Wachtendorf, M. Grell, D. D. C. Bradley, M. Hennecke, *Phys. Rev. B* **1999**, *60*, 277.

[4] J. R. Lakowicz, *Principles of Fluorescence Spectroscopy*, Kluwer Academic/Plenum Publishers, New York, **1999**.

[5] M. S. Matos, J. Hofkens, W. Verheijen, F. C. De Schryver, S. Hecht, K. W. Pollak, J. M. J. Fréchet, B. Forier, W. Dehaen, *Macromolecules* **2000**, *33*, 2967.

[6] Dendrimer structures were optimized by MM2 (Chem 3D Pro 8.0).

[7] Förster, Th. *Discuss. Faraday Trans*. **1959**, *27*, 7.

[8] G. Teobaldi, F. Zerbetto, *J. Am. Chem. Soc.* **2003**, *125*, 7388.

[9] L. Serrano, A. Horovitz, B. Avron, M. Bycroft, A. R. Fersht, *Biochemistry* **1990**, *29*, 9343.

[10] G. Teobaldi, F. Zerbetto, *J. Am. Chem. Soc.* **2003**, *125*, 7388.

[11] V. Vicinelli, P. Ceroni, M. Maestri, M. Lazzari, V. Balzani, S.-K. Lee, J. van Heyst, F. Vögtle, *Org. Biomol. Chem.* **2004**, *2*, 2207.

[12] U. Hahn, M. Gorka, F. Vögtle, V. Vicinelli, P. Ceroni, M. Maestri, V. Balzani, *Angew. Chem. Int. Ed.* **2002**, *41*, 3595.

[13] (a) V. Balzani, P. Ceroni, S. Gestermann, M. Gorka, C. Kauffmann, F. Vögtle, *Tetrahedron* **2002**, *58*, 629. (b) V. Balzani, P. Ceroni, S. Gestermann, M. Gorka, C. Kauffmann, M. Maestri, F. Vögtle, *ChemPhysChem*. **2000**, *4*, 224.

[14] Excitation of eosin at ca. 500 nm, corresponding to the lower energy band in the absorption spectrum, is precluded by our instrumental setup for time-resolved anisotropy measurements. Therefore, we have excited at 405 nm, where not only eosin but also dansyl absorbs light, so that data obtained with eosin encapsulated in G4**B** are easier to interpret than those obtained with eosin inside G4**D**.

CHAPTER 10

A novel synthesis of small gold nanoparticles: Au(I) disproportionation catalyzed by a persulfurated coronene dendrimer

10.1 Results and discussion

Two of the most exciting topics in the field of nanoscience are those of dendrimers[1,2] and nanoparticles.[3,4] It has already been shown[5] that these two research areas can profitably overlie to yield a variety of intradendrimer encapsulated[6] and interdendrimer stabilized[7] nanoparticles.

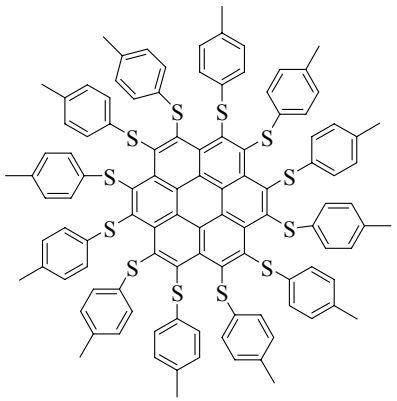

CPG1

Scheme 10. Structure formulae of the persulforated coronene dendrimer **CPG1**

Gold nanoparticles are usually obtained[8] by reducing $HAuCl_4$ with $NaBH_4$, but reduction of $HAuCl_4$ by a stabilizing polymer[9] or by light excitation in ethylene glycol,[10] and reduction of Au(I) phosphine complexes by a borane complex[11] have also been reported. In this paper we describe the synthesis of gold nanoparticles by a novel method, i.e. the disproportionation of Au(I) catalyzed by a dendrimer (**CPG1**, Scheme 10) consisting of a coronene-core appended with 12 thiophenyl units.

Compound **CPG1** is a member of a large family of dendrimers obtained by persubstitution of aromatic cores with thiophenyl units.[12] The coronene chromophoric unit that constitutes the core of dendrimer **CPG1** is strongly perturbed by the appended thiophenyl substituents, as evidenced by comparing the absorption spectrum of **CPG1** with that of coronene (Figure 10.1).

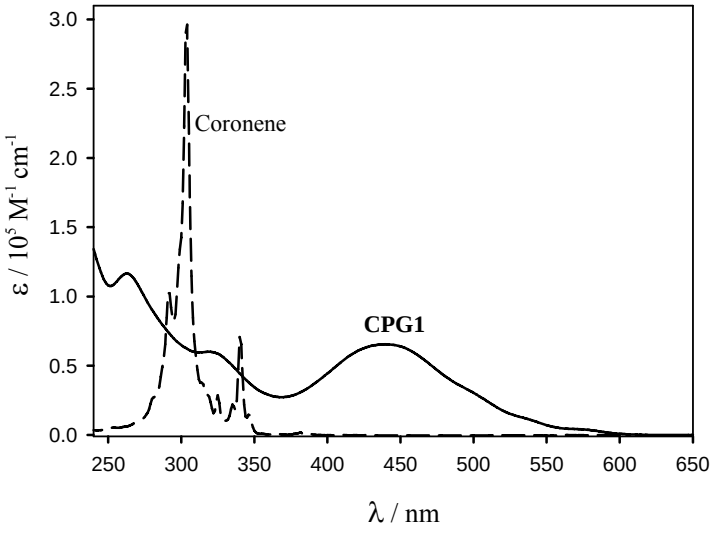

Figure 10.1. Absorption spectra of coronene (dashed line) and dendrimer **CPG1** (full line) in dichloromethane solution at 298 K.

Dendrimer **CPG1**, as well as other members of the same family, can coordinate a variety of soft metals ions.[13] Titration of **CPG1** dissolved in dichloromethane (7.5×10^{-6} M) with an acetonitrile solution of $HAuCl_4$ (2.5×10^{-3} M) causes the spectral changes displayed in Figure 10.2a. A substantial perturbation of the dendrimer bands at 320 and 435 nm is accompanied by the formation of a broad band in the near infrared spectral region (λ_{max}= 840 nm, $\varepsilon_{max} \approx 1500$ M^{-1} cm^{-1}, Figure 10.2a). The two isosbestic points at 390 and 460 nm are no longer maintained after addition of about 1.5 equivalents of $HAuCl_4$, demonstrating that dendrimer **CPG1** coordinates Au^{3+} to give a stable 1:1 species

$$\mathbf{CPG1} + Au^{3+} \rightleftharpoons \mathbf{CPG1}\supset Au^{3+} \qquad (1)$$

Since Au^{3+} can be easily reduced[14] and **CPG1** undergoes oxidation at 0.72 V vs NHE, we assign the new weak and broad band with λ_{max} = 840 nm to ligand-to-metal charge-transfer transitions. Such an assignment is supported by the fact that upon titration with $HAuCl_4$ of the analogous benzene-cored dendrimer, which is much more difficult to oxidize ($E_{1/2}$ = 1.08 V vs NHE), a similar band is formed with maximum at 565 nm. Dendrimer solutions titrated with an excess of $HAuCl_4$ show an absorption spectrum in which the isosbestic points are no longer maintained. Experiments on these solutions by high resolution transmission electron microscopy (HR-TEM) did not show any evidence of nanoparticle formation.

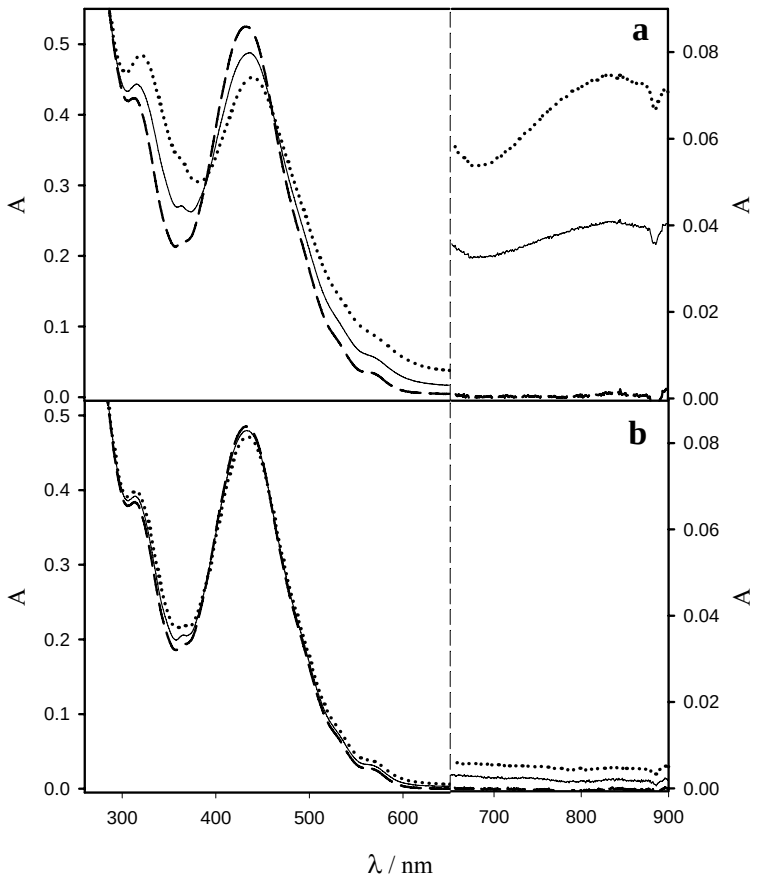

Figure 10.2. Spectral changes observed upon titration of compound **CPG1** in dichloromethane (7.5×10^{-6} M) with (a) an acetonitrile solution of $HAuCl_4$ (2.5×10^{-3} M), and (b) an acetonitrile solution of AuCl (2.2×10^{-3} M): 0 equivalent of gold ions (dashed line), 1.5 equivalents of gold ions (dotted line).

Titration of **CPG1** in dichloromethane solution (7.5×10^{-6} M) with up to 1.5 equivalents of an acetonitrile solution of AuCl (2.2×10^{-3} M) caused only very minor spectral changes in the region of the dendrimer bands and the formation of a tail at lower energy (Figure 10.2b). The small spectral changes in the 300-600 nm region are qualitatively similar to those observed upon titration with $HAuCl_4$

(Figure 10.2a). Because of the well known tendency of AuCl solutions to undergo disproportionation,[15] we assign such spectral changes to the presence of small amounts of Au(III)[16] species in the AuCl solution used for titration. Apparently, **CPG1** either does not coordinate Au^{+} or, more likely, coordination does not substantially affect the dendrimer bands.

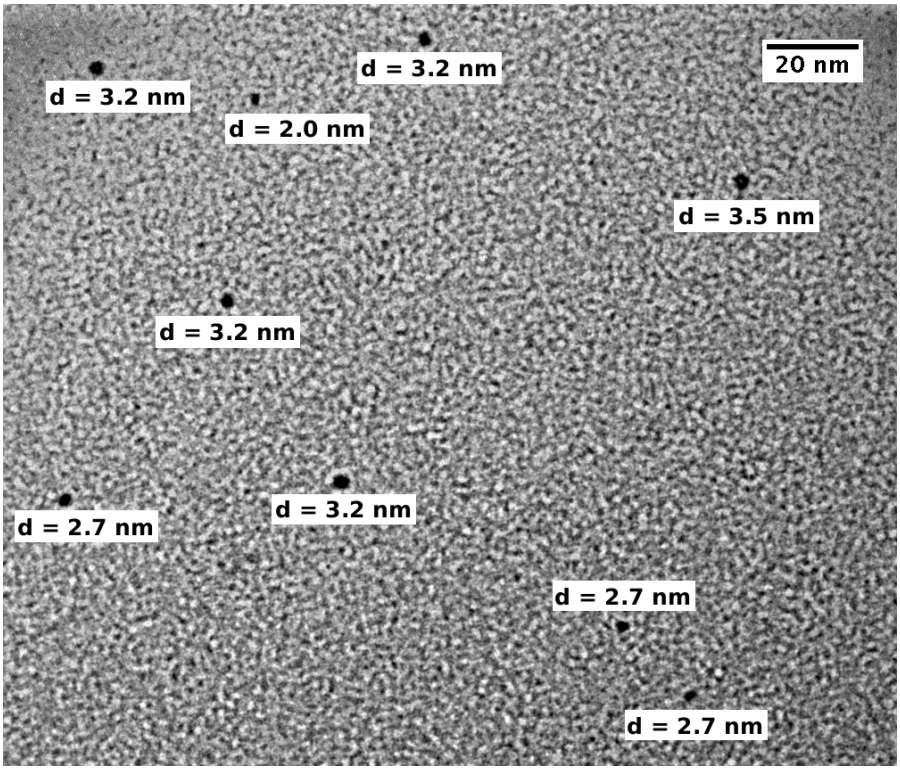

Figure 10.3. HR-TEM images of gold nanoparticles formed upon titration of a dichloromethane solution of dendrimer **CPG1** with 30 equivalents of AuCl.

Isosbestic points in the absorption spectra are maintained upon addition of 30 equivalents of AuCl per dendrimer and a proportional increase of the tail at low energy is observed. This tail present is consistent with formation of dispersed nanoparticles. Examination of the titrated solution with HR-TEM indeed showed

the presence of nanoparticles with size ranging from 1.5 to 3.5 nm (Figure 10.3). EDX (Energy Dispersive X-ray) spectra clearly indicated that the observed particles were made of gold. Magnification of the TEM images (Figure 10.4) has evidenced linear arrays of gold atoms with an interlayer distance of 0.234 nm, consistent with Au (101) crystals, and the presence in the particles with greater size of several twins (Figure 10.4b). The small size of the nanoparticles is consistent with the absence of the plasmon resonance band in the absorption spectrum typical of larger nanoparticles.[17]

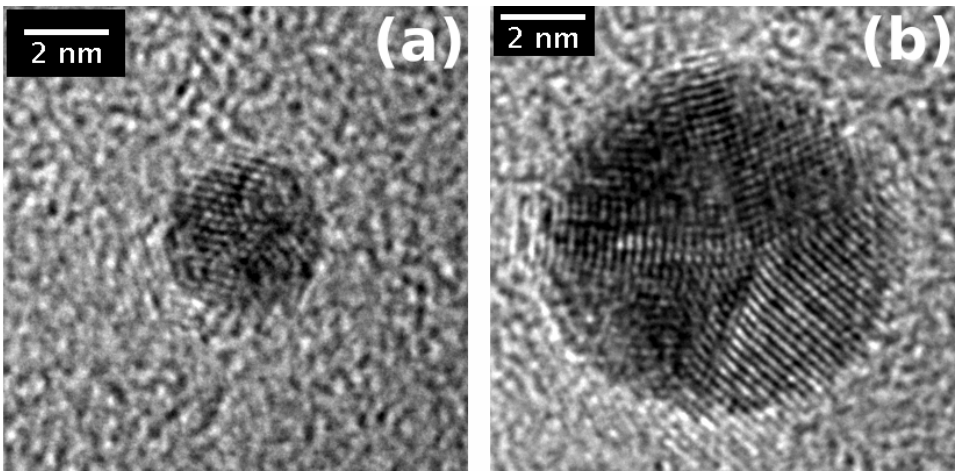

Figure 10.4. Detailed view of two nanoparticles: (a) the interlayer distance (0.234 nm) is consistent with that of Au (101) crystals; (b) the presence of several twins is clearly evident in nanoparticles of greater size.

Since the observed gold nanoparticles have been directly obtained by titration of **CPG1** with AuCl without addition of any reductant, two reaction mechanisms can be taken into consideration, namely: (i) reduction of Au^{+} by the dendrimer, and (ii) disproportionation of Au^{+} to Au^{0} and Au^{3+}. Mechanism (i) is plausible since

formation of nanoparticles upon "spontaneous" reduction of $HAuCl_4$ by a stabilizing polymer has been previously reported.[9] For our system, however, involvement of the dendrimer as a reductant seems unlikely for the following reasons: a) judging from the absorption spectra, formation of nanoparticles upon titration with AuCl is not accompanied by a decrease of the dendrimer concentration since isosbestic points are maintained upon addition of up to 30 equivalents of Au^+ per dendrimer; b) addition of an excess of 11-mercapto-1-undecanol liberates dendrimers molecules, as evidenced by the fact that the absorption spectrum of the dendrimer is completely recovered. Therefore, we believe that the observed gold nanoparticles are formed from the disproportionation of Au^+ to Au^0 and Au^{3+}, with a mechanism similar to that proposed by Eustis and El-Sayed to interpret generation of gold nanoparticles by photochemical reduction of $HAuCl_4$.[10]

In blank experiments we have verified that nanoparticles are generated neither from **CPG1** and Au^{3+} nor from Au^+ alone. We must conclude that formation of nanoparticles requires participation of species in which Au^+ ions are coordinated by the dendrimer, e.g. **CPG1**$\supset Au^+$. Since gold nanoparticles have been obtained from solutions containing an excess (10 to 30 times) of AuCl compared to the dendrimer concentration, the formation of polinuclear species, particularly of **CPG1**$\supset(Au^+)_2$, cannot be excluded.

In our system, the first step could be the coordination of Au^+ by **CPG1** (for the sake of simplicity, the Cl^- counter ions, which can play the role of ancillary ligands, are not indicated hereafter):

$$\mathbf{CPG1} + Au^+ \rightleftharpoons \mathbf{CPG1}\supset Au^+ \qquad (2)$$

A disproportionation reaction of the Au^+ species should then follow either in the form of reactions 3a

$$\mathbf{CPG1}\supset Au^+ + \mathbf{CPG1}\supset Au^+ \rightarrow \mathbf{CPG1}\supset Au^{2+} + \mathbf{CPG1}\supset Au^0 \qquad (3a)$$

followed by dissociation of the complex between dendrimer and gold atom

$$\mathbf{CPG1}\supset Au^0 \rightleftharpoons \mathbf{CPG1} + Au^0 \qquad (3b)$$

or of the equivalent reactions 4 and 5:

$$\mathbf{CPG1}\supset Au^+ + Au^+ \rightarrow \mathbf{CPG1}\supset Au^{2+} + Au^0 \qquad (4)$$

$$\mathbf{CPG1}\supset (Au^+)_2 \rightarrow \mathbf{CPG1}\supset Au^{2+} + Au^0 \qquad (5)$$

The disproportionation of Au^+ is known to be very slow for Au^+ halides[18] because, as pointed out by Eustis and El-Sayed,[10] it requires formation of a bimolecular species involving a gold-gold bond. In our system the dendrimer could favor encounters of two Au^+ species (eqs. 3a and 4) or, more likely, of two Au^+ ions in polymetallic species like **CPG1**$\supset(Au^+)_2$ (eq. 5), thereby catalyzing disproportionation. Encounters of Au atoms should then rapidly lead to formation of gold nanoparticles, most likely stabilized by dendrimer molecules:

$$nAu^0 \rightarrow (Au^0)_n \qquad (6)$$

The **CPG1**$\supset Au^{2+}$ species formed in eq. 3a, 4 and 5 should undergo disproportionation to the initial **CPG1**$\supset Au^+$ and the stable **CPG1**$\supset Au^{3+}$ complexes, as it happens for other Au^{2+} species.[10]

$$\textbf{CPG1}\supset Au^{2+} + \textbf{CPG1}\supset Au^{2+} \rightarrow \textbf{CPG1}\supset Au^{+} + \textbf{CPG1}\supset Au^{3+} \qquad (7)$$

Stability of the gold nanoparticles in the presence of dendrimer **CPG1** is demonstrated by the fact that TEM experiments do not show any substantial variation in the nanoparticle size distribution with aging of the solutions or by removal of the solvent and redissolution.

In conclusion, we have discovered a new route to obtain gold nanoparticles of 1.5 to 3.5 nm size. The process is based on the disproportionation of Au^{+} in the presence of the relatively simple dendrimer **CPG1** that not only favors encounters between Au^{+} ions, but also protects the resulting small nanoparticles from further aggregation. The effects of reactant concentrations, dendrimer generation, and nature of the dendrimer core on the efficiency of the process and on the size of the resulting particles are under investigations.

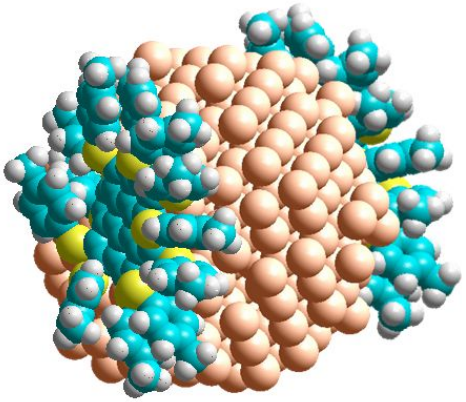

References

[1] (a) G. R. Newkome, F. Vögtle, *Dendrimers and Dendrons*, Wiley-VCH, Weinheim, **2001**; (b) *Dendrimers and Other Dendritic Polymers* (Eds.: J. M. J. Fréchet, D. A. Tomalia), Wiley, New York, **2001**; (c) D. A. Tomalia and J. M. J. Fréchet, Eds. Special Issue: Dendrimers and Dendritic Polymers. In: *Prog. Polym. Sci.* **2005**, *30 (3-4)*.

[2] For some recent reviews, see: (a) P.A. Chase, R. J. M. Klein Gebbink, G. van Koten, *J. Organomet. Chem.* **2004**, *689*, 4016; (b) W. Ong, M. Gomez-Kaifer, A.E. Kaifer, *Chem. Commun.* **2004**, 1677; (c) M. Ballauff, C. N. Likos, *Angew. Chem. Int. Ed.* **2004**, *43*, 2998; (d) A.-M. Caminade, J.-P. Majoral, *Acc. Chem. Res.* **2004**, *37*, 341; (e) D. Astruc, F. Lu, J. R. Aranzaes, *Angew. Chem. Int. Ed.* **2005**, *44*, 7852; (f) P. Ceroni, G. Bergamini, F. Marchioni, V. Balzani, *Prog. Polym. Sci.* **2005**, *30*, 453.

[3] (a) *Metal Nanoparticles: Synthesis, Characterization, and applications* (Eds: D. L. Feldheim, C. A. J. Foss), Dekker, New York **2002**; (b) *Nanoparticles* (Ed: G. Schmid), Wiley-VCH, Weinheim **2004**.

[4] (a) G. Schmid, L. F. F. Chi, *Adv. Mat.* **1998**, *10*, 515; (b) A. C. Templeton, W. P. Wuelfing, R. W. Murray, *Acc. Chem. Res.* **2000**, *33*, 27; (c) E. Katz, I. Willner, *Angew. Chem. Int. Ed.* **2004**, *43*, 6042; (d) Y. Yadong, A. P. Alivisatos, *Nature* **2005**, *437*, 664. (e) D. Astruc, F. Lu, J. R. Aranzaes, *Angew. Chem. Int. Ed.* **2005**, *44*, 7852; (f) M. Brust, *Nature Mat.* **2005**, *4*, 364; (g) C. Burda, X. Chen, R. Narayanan, M. A. El-Sayed, *Chem. Rev*. **2005**, *105*, 1025; (h) A. B. Descalzo, R. Martínez-Máñez, F. Sancenón, K. Hoffmann, K. Rurack, *Angew. Chem. Int. Ed.* **2006**, *45*, 5924.

[5] (a) R. M. Crooks, B. I. Lemon III, L. Sun, L. K. Yeung, M. Zhao, *Top. Curr. Chem.* **2001**, *212*, 81; (b) M.-C. Daniel, D. Astruc, *Chem. Rev.* **2004**, *104*, 293;.(c) I. Willner, R. Baron, B. Willner, *Adv. Mater.* **2006**, *18*, 1109.

[6] (a) R. M. Crooks, M. Zhao, L. Sun, V. Chechik, L. K. Yeung, *Acc. Chem. Res.* **2001**, *34*, 181; (b) J. J. Michels, J. Huskens, D. N. Reinhoudt, *J. Chem. Soc., Perkin Trans. 2* **2002**, *1*, 102; (c) R. W. J. Scott, O. M. Wilson, R. M. Crooks, *J. Phys. Chem. B* **2005**, *109*, 609; (d) S. Dend, J. Locklin, D. Patton, A. Baba, R.C. Advincula, *J. Am. Chem. Soc.* **2005**, *127*, 1744; (e) G. Schmid, W. Meyer-Zaika, R. Pugin, T. Sawitowski, J.-P. Majoral, A.-M. Caminade, C.-O. Turrin, *Chem. Eur. J.* **2000**, *6*, 1693.

[7] (a) K. Esumi, A. Suzuki, N. Aihara, K. Usui, K. Torigoe, *Langmuir* **1998**, *14*, 3157; (b) M. E. Garcia, L. A. Baker, R. M. Crooks, *Anal. Chem.* **1999**, *71*, 256; (c) A. D'Aleo, R. M.

Williams, F. Osswald, P. Edamana, U. Hahn, J. van Heyst, F. D. Tichelaar, F. Vögtle, L. De Cola, *Adv. Funct. Mater.* **2004**, *14*, 1167.

[8] (a) M. Brust, M. Walker, D. Bethell. D. J. Schiffrin, R. Whyman, *J. Chem. Soc., Chem. Commun.* **1994**, 801. (b) M. R. Knecht, J. C. Garcia-Martinez, R. M. Crooks, *Langmuir* **2005**, *21*, 11981; (c) S. Wu, H. Zeng, Z. A. Schelly, *J. Phys. Chem. B* **2005**, *109*, 18715.

[9] (a) T. Ishii, H. Otsuka, K. Kataoka, Y. Nagasaky, *Langmuir* **2004**, *20*, 561; (b) T. Sakai, P. Alexandridis, *J. Phys. Chem. B* **2005**, *109*, 7766.

[10] S. Eustis, M. A. El-Sayed, *J. Phys. Chem. B* **2006**, *110*, 14014.

[11] M. F. Bertino, Z.-M. Sun, R. Zhang, L.-S. Wang, *J. Phys. Chem. B* **2006**, *110*, 21416.

[12] M. Gingras, J.-M. Raimundo, Y. M. Chabre, *Angew. Chem. Int. Ed*. **2006**, *45*, 1686.

[13] R. D. Johnson, A. Pinchart, I. H. A. Badr, M. Gingras, L. G. Bachas, *Electroanalysis* **2002**, *14*, 1419.

[14] E. Gachard, H. Remita, J. Khatouri, B. Keita, L. Nadjo, J. Belloni, *New J. Chem.* **1998**, 22, 1257.

[15] F. A. Cotton, G. Wilkinson, Advanced Inorganic Chemistry, John Wiley & Sons, New York **1980** (4^{th} ed.), 966.

[16] From the experimental molar absorption coefficient of $HAuCl_4$ in acetonitrile, the Au^{3+} concentration in the 2.2×10^{-3} M AuCl solution is estimated as 1/10.

[17] A. Moores, F. Goettmann, *New J. Chem.* **2006**, *30*, 1121.

[18] (a) S. Eustis, H.-Y. Hsu, M. A. El-Sayed, *J. Phys. Chem. B* **2005**, *109*, 4811; (b) C. H. Gammons, Y. Yu, *Geochim. Cosmochim. Acta* **1997**, *61*, 1971.

CHAPTER 11

Visualizing spatial and temporal heterogeneity of single molecule rotational diffusion in a glassy polimer by defocusing wide-field imaging

11.1 Introduction

Over the last 15 years, single molecule spectroscopy (SMS) has been established as a new tool in the ever expanding range of spectroscopic methods. SMS is especially useful to study inhomogeneous systems.[1] Biological systems are by their nature highly heterogeneous and as such perfect targets for SMS. From this it is clear that, next to biological samples, polymers form a study object of SMS as polymers are very often heterogeneous in their behavior. Many theories that describe polymer properties are based on a microscopic picture[2] that now can be evaluated experimentally by applying single molecule techniques. A variety of polymers and several SM techniques have been exploited for these studies. Some groups focused their attention on unraveling the complex photophysics of conjugated polymers and tried to establish a relationship between single polymer chain conformation, interaction with the surrounding inert matrix and the observed photophysics.[3] Other groups devoted effort in testing and validating, on a

microscopic level, the theories developed to describe the physical properties of polymers. Especially the behavior close to the glass transition temperature of the polymer under consideration has drawn a lot of attention. In order to validate theories describing this transition, probe molecules are embedded in the polymer. One approach consists of measuring changes in the radiative lifetime of a single molecule below or close to the glass transition temperature.[4] According to the free volume theory, the free volume that can be thought of as sub-nanometer holes caused by structural disorder in the polymer, fluctuates around the probe molecule both in time and in space. This in turn causes changes in the local density around the probe molecule and subsequent changes in the radiative life time. Alternatively, segmental relaxation above T_g can be probed by the rotational motion, of a probe molecule, induced by the relaxation process.[5] The rotation of single molecules is typically followed by measuring the degree and orientation of linear polarization of fluorescence, resulting from the projection of the emission dipole orientation on a two-dimensional plane. This usually leads to a loss of the out-of-plane information of the molecule under investigation.

However, several detection schemes were developed for measuring the 3D orientation of single molecules via the orientation of their transition dipole moment.[6] Scanning near field optical microscopy[6a] as well as confocal microscopy, eventually modified by using annular beams,[6c] have been used for this goal. Also, fluorescence wide-field microscopy has been applied to get information about the angular distribution of single molecule's fluorescence emission (and hence 3D

orientation) by defined image defocusing or by introducing aberrations. The latter approach was used by Dickson and co-workers in their study of polymer (poly(methyl methacrylate)) below T_g. Here we use defocused wide-field imaging in combination with an extremely robust perylendiimide dye (Figure 11.1) to study rotational motion of the dye in a polymer with a T_g close to room temperature.

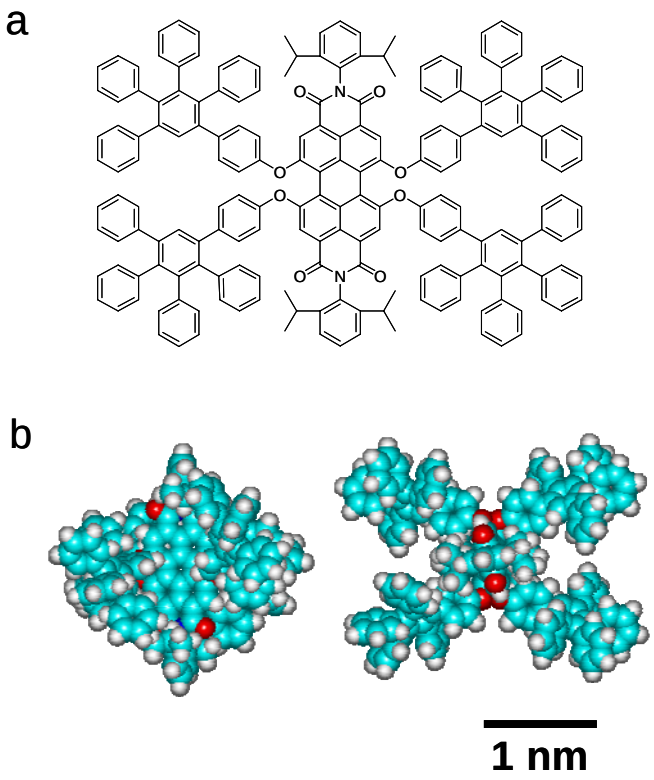

Figure 11.1. (a) The chemical structure of compound **1**. (b) 3D representation of **1** from different view points; along the vertical axis of the plane of the perylenediimide core (left) and along the long axis of the perylenediimide core (right).

Defocused imaging offers several advantages: it allows for highly parallel data collection by looking at many molecules in the field of view and it gives exact

information on the 3D orientation as mentioned before. Furthermore the photostability of the dye used allows imaging for an extended period of time (more than 30 minutes). In this way, spatial and temporal inhomogeneities of the rotational movement of the dyes could be demonstrated. The high quality of the images allows for a decomposition of the movement in the x-y plane and the z-plane. We could demonstrate both static and temporal heterogeneity in polymer relaxation, in good agreement with previous literature reports. Furthermore, the full 3-D rotational diffusion can be analyzed using a model for an isotropic rotor. The detailed analysis suggests the existence of different relaxation regimes for the polymer used.

11.2 Sample preparation

Thin polymer films (thickness of 50 - 100 nm) were prepared on cleaned glass cover slips by spincoating from 0.5 - 1.0 wt% solution of poly(methyl acrylate) (PMA, bulk T_g ~ 8 °C, M_n=11,340 g/mol, M_w/M_n = 3.65, purchased from Aldrich and used without further purifications) containing 1 – 10 nM of a perylene diimide substituted with polyphenylene groups in the bay positions (compound **1**, M_W=2601.25, see the structure in Figure 11.1) in toluene. The number-average molecular weight (M_w) and polydispersity index (M_w/M_n) was estimated using Size Exclusion Chromatography (SCL-10Avp, Shimazu Co.). The films were put in vacuum at room temperature for more than 2h in order to remove residual solvent. All samples were kept in vacuum before the experiment and measured within one

day after preparation. Note that the glass transition temperature of a thin film can be lower than the glass transition temperature measured in bulk.[7]

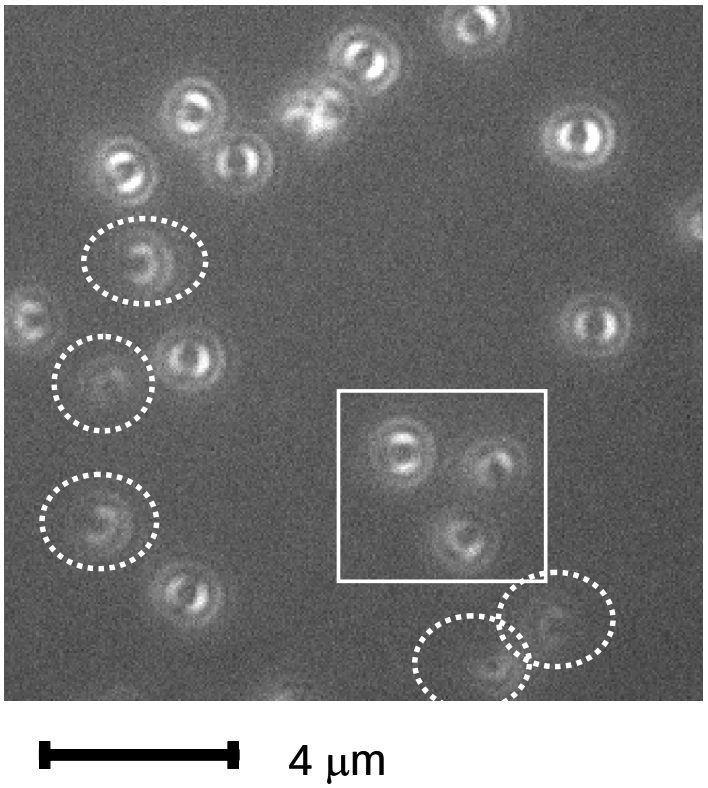

Figure 11.2. A typical defocused image of **1** embedded in a 50 nm film of PMA with 1 μm defocusing toward the sample. The white dashed circles indicate molecules which are substantially oriented out of plane. The white square are the molecules discussed in Figure 11.5-11.7.

11.3 Results and discussion

Figure 11.2 shows a typical defocused image of **1** embedded in a thin PMA film at an excitation power of 1 kW/cm^2 with 1 second integration. Although various emission patterns are observed, the majority of spots show a clear two-lobe pattern. As can be seen in the picture, 25 % of the molecules show a substantial out of

plane contribution (molecules indicated by the dashed white circles). The fluorescence intensity varies from molecule to molecule. Especially molecules oriented out of plane are not excited efficiently[8] and therefore show lower emission intensity. The center position of the defocused pattern corresponds to the spatial coordinate of the corresponding single molecule, and can be determined by the image analysis. No translational mobility could be observed. The center part of the defocused pattern (the bright two-lobe) is imaged with 22 x 22 pixels so that the pattern of a single molecule occupies an area of about 1 x 1 μm^2 on the image. Thus, molecules separated by this distance can be analyzed by our analytical method. For precise analysis of the out-of-plane orientation, the ideal separation between molecules is 1.5 μm, because the outer rim of the pattern is very helpful for the analysis (see below).

Figure 11.3 shows examples of calculated emission patterns for different out-of-plane orientations (θ) of the transition dipole moment of a single molecule (defocusing depth 1 micrometer, for details on the calculations see 6e). The in-plane orientation of the transition dipole moment was kept constant during the calculation. In order to demonstrate the changes in calculated patterns for different out of plane orientations, the patterns are calculated for changes in θ of 10 degrees. Clearly the bilaterally symmetric two-lobe pattern at 90 degree (completely in-plane orientation) changes into asymmetric ringed pattern as the out-of-plane angle

(θ) decreases. At 0 degree (complete out-of-plane), the pattern has a symmetric circular ring shape.

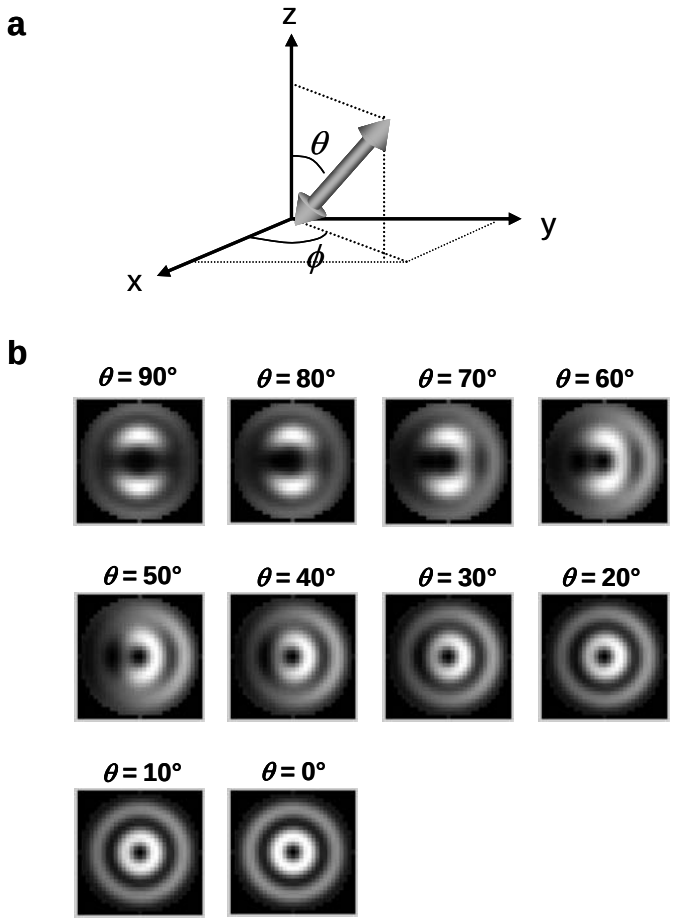

Figure 11.3. Calculated defocused patterns of a single molecule for 10 different out-of-plane orientations. These values of θ are the same as those used in pre-analysis using the pattern-matching.

The size of the inner lobe part and the symmetry of the outer rim are crucial in addition to the shape for the analysis. The size of lobe is very sensitive to the out-of-plane angle. The symmetry of the rim is often helpful to determine the in-plane

angle, especially for images with a low signal-to-noise ratio. Note that it becomes progressively harder to distinguish patterns with an out of plane angle of less than 50°.

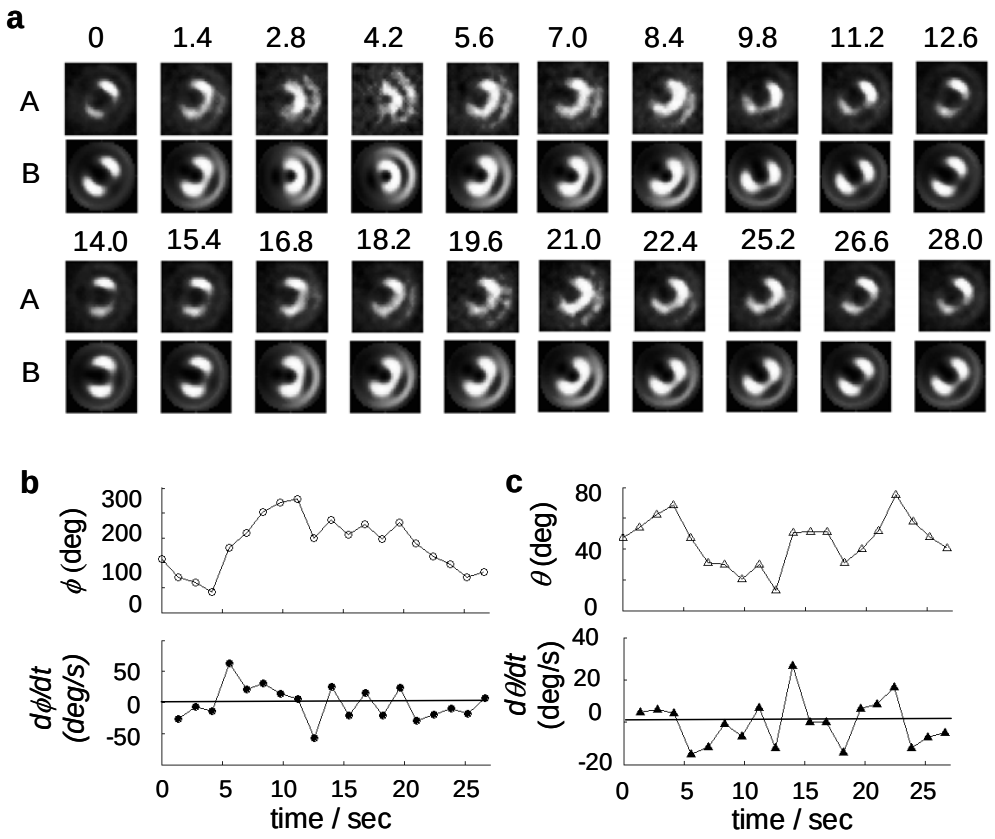

Figure 11.4. (a) Snapshots of experimentally observed emission patterns (sequence A) and corresponding computed patterns (sequence B) as a function of time. Transition dipole orientation trajectories and their first time derivatives are shown for the in plane (b) and out of plane component (c), respectively.

The sequence shown in Figure 11.4a consists of snapshots of an individual molecule showing rotational diffusion in a PMA film as function of time. An image is shown every 1.4 seconds (with 1 second integration and 0.4 second interval

time). The sequence **A** represents experimental data, the sequence B shows the corresponding calculated patterns. By fitting each emission pattern as function of time, transition dipole orientation trajectories are obtained (Figure 11.4b). The first derivative of such trajectory clearly shows that the rotational diffusion is not unidirectional but random instead. This is to be expected since the dynamics of the probe molecule are driven by polymer segmental motions and hence result from relaxations of the polymer chains which should be random.

Figure 11.5a shows 3 molecules that are relatively close to each other in space. Figure 11.5 b-d show the projection maps for molecules **1-3** shown in Figure 11.5a, respectively. The defocused images were obtained with 1 second integration and 0.4 second interval time. Two different types of behavior can be observed in the maps. Molecule **2** (Figure 11.5c) exhibits fast rotations with no preference for any orientation. On the other hand, molecules **1** and **3** are temporarily locked in one orientation and occasionally jumps to a completely different orientation occur. For example, molecule **1** is first oriented in the region indicated by the black line but undergoes a jump in orientation, indicated by the red line, after 970 second. Molecule **3** shows an even more complex behavior: though it is locked in three different orientations for 1760 seconds, it starts rotating in rather wide range of angles afterwards. From that point on, completely different rotational dynamics are observed. This clearly reflects temporal heterogeneity of polymer relaxations. Most interestingly, molecule **3** passes through the initial region on the projection map, observed between 0 and 190 seconds and indicated in black, when jumping from

the green region into the red region after 890 seconds. These results clearly indicate temporal heterogeneity and may point to a memory effect in polymer relaxation at the dimension of the probe molecule, meaning approximately 3 nm.

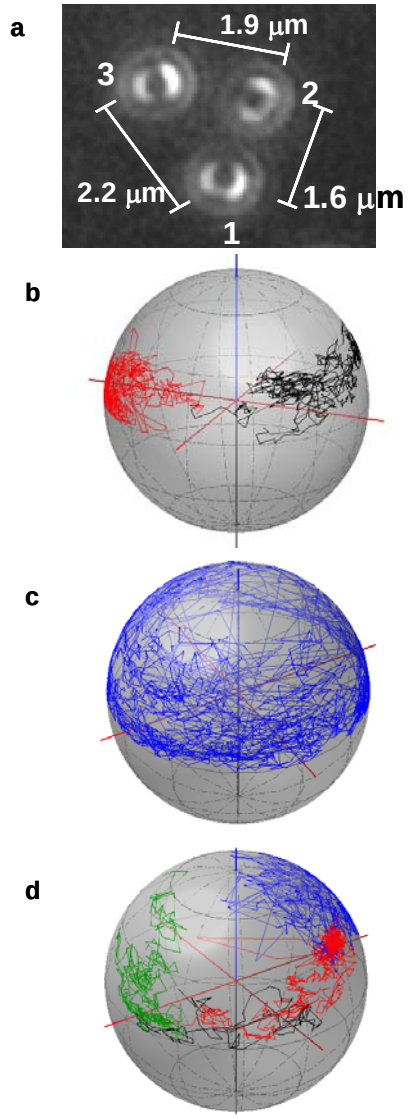

Figure 11.5. Spatial and temporal heterogeneity of dynamics at 295 K. (a) A zoom of the three molecules indicated by the white square in Figure 11.2. Molecules are separated by ~ 1.5 μm. (b) - (d) projection maps for molecule **1**-**3**, respectively. The red lines indicate the x-y image plane and blue line is the optical (z) axis: 0-960 s (black) and 960-2380s (red) in (b), 0-190s (black), 190-895s (green), 895-1763s (red), and 1763-2940 (blue) in (d).

A more quantitative evaluation of the phenomena seen in the projection maps can be obtained by constructing time trajectories of the dipole orientation and analyzing the observed fluctuations by correlation functions.

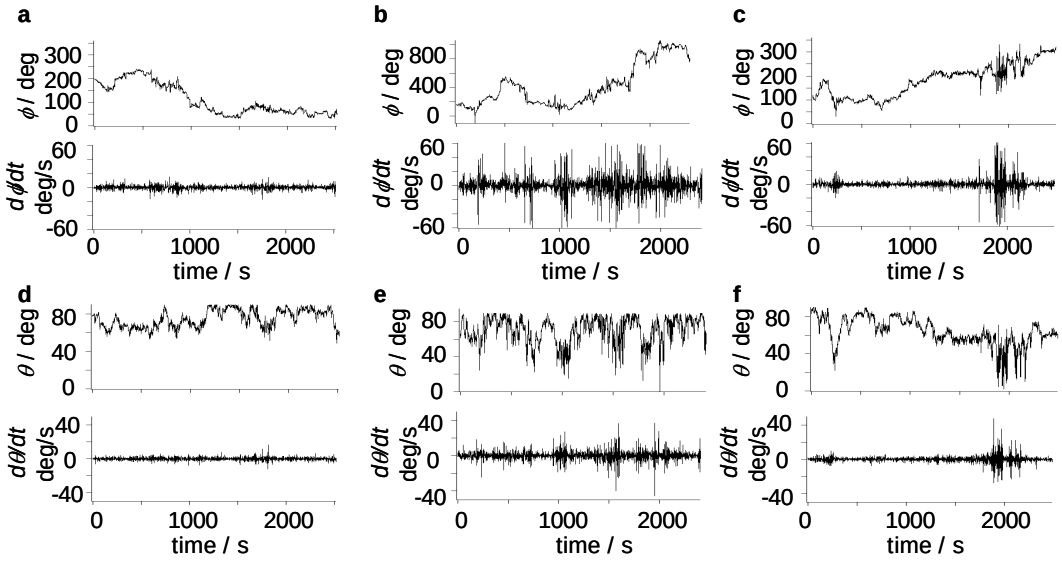

Figure 11.6. Transition dipole orientation trajectories in plane and out of plane and their time derivatives for molecule **1** (a) and (d), **2** (b) and (e), and **3** (c) and (f).

Figure 11.6 shows the time trajectories of the dipole orientation and their first derivatives for the three molecules in Figure 11.5a. Several important observations can be made for these molecules. First, the analysis of the rotational movement of these molecules clearly indicates spatial heterogeneity on a micrometer scale (see Figure 11.5a). Secondly, molecule **1** (Figure 11.6a) shows no large changes in rotation rate during the observation time of 2500 seconds. The behavior of molecule **2** (Figure 11.6b) is in striking contrast with the behavior of molecule **1**. Clear changes in the rotational rate can be observed, both for the in and the out of

plane part of the rotation. This difference between these molecules is also reflected in the correlation function of the rotational movement (vide infra). Molecule **3** (Figure 11.6c) shows a wide variety of behaviors. Changes of the rotation rate for both in and out of plane rotation components occur after 1800 seconds. These changes correspond to the wide angular distribution observed in the projection map in Figure 11.5 after 1800 seconds, indicated in blue. Note that for the kind of polymer matrix used, temporal heterogeneity is expected on a time scale of about 500 s at room temperature.

In order to evaluate our experimental technique and in order to compare the results obtained with data reported earlier in literature, we first estimate the in plane component of the rotational diffusion using a similar analysis as reported in. The autocorrelation function was calculated using

$$C(t) = \langle A(t')A(t'+t)\rangle / \langle A(t')A(t')\rangle \qquad (1)$$

where $A(t) = \cos(2\phi(t))$. The decay of *C(t)* is then fitted with Kohlrausch-Williams-Watt (KWW) stretched exponential function:

$$C(t) = \sum_i \exp\left[-\left(t/\tau_{i\,KWW}\right)^{\beta_{i\,KWW}}\right] \qquad (2)$$

The averaged time scale of rotational diffusion (τ_C) is estimated by $\tau_c = \int_0^\infty C(t)dt$.

The correlation functions and the fitting results of the three molecules in Figure 11.5a are illustrated in Figure 11.7. The individual molecules show significantly different behavior.

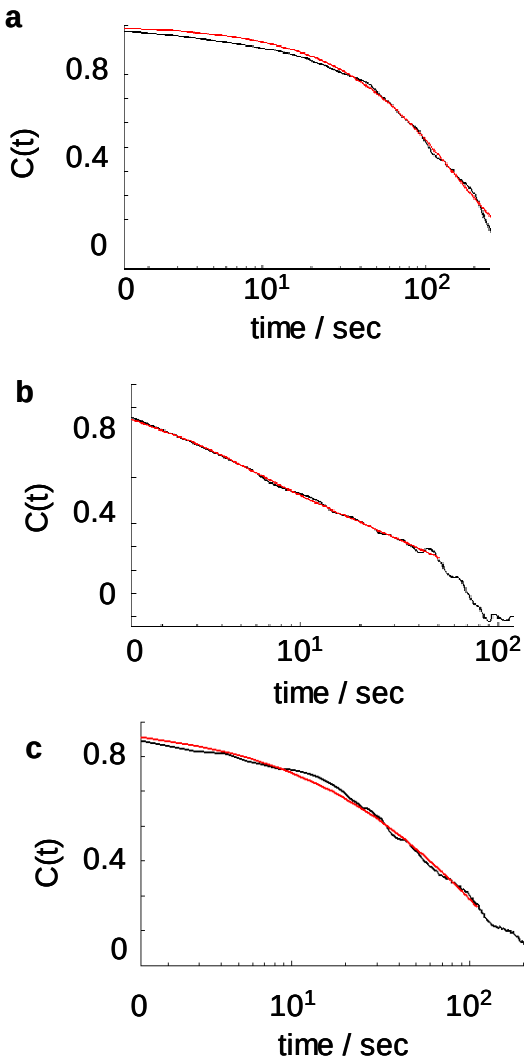

Figure 11.7. Correlation function of the in-plane transition dipole orientation of molecule **1** (a) (τ_c = 164 s, τ_{KBB} = 160 s, β_{KBB} = 0.95), **2** (b) (τ_C=47s, $\tau_{1\,KBB}$ = 4.2 s, $\beta_{1\,KBB}$ = 1.0 and $\tau_{2\,KBB}$ = 49 s, $\beta_{2\,KBB}$ = 0.65), and **3** (c) (τ_c = 231 s, τ_{KBB} = 169 s, β_{KBB} = 0.65),

The correlation function of molecule **1** and **3** can be fitted with a stretched exponential decay with a β_{KWW} close to one. The τ_C was estimated to be 164 and 230 seconds for molecule **1** and **3**, respectively. These values are more than twice

slower than the correlation times of rhodamine 6G and rubrene embedded in PMA in the earlier reports. This is not surprising since it is known that rotation of large probes is more hindered and can deviate from the collective relaxation of surrounding matrix, resulting in high β_{KWW} value and large τ_{KWW}.[9] On the other hand, molecule **2** shows a much faster average decay of τ_C=47 s actually consisting of two components, yielding $\tau_{1\,KBB}$ = 4.2 s ($\beta_{1\,KBB}$ = 1.0) and $\tau_{2\,KBB}$ = 44 s ($\beta_{2\,KBB}$ = 0.7). This smaller value of $\tau_{2\ KBB}$ can be related to spatially heterogeneous dynamics present in polymers, especially in the very poly-disperse PMA matrix used. However, interfacial effects at the air/polymer or polymer/glass interfaces where the probe molecule might exhibit different dynamics can not be excluded.. The $\tau_{1\,KBB}$ might represent a shorter second relaxation regime of the polymer. Note that the mismatch between the correlation function and the exponential at the initial part of molecule **1** might also indicate the presence of this faster polymer relaxation regime. However, it was recently argued that for the approach described above, e.g. analyzing a 3D rotation by only considering the in plane contribution by calculating the linear dichroism, even an isotropic rotational diffusion can lead to non-exponential correlation functions.[10] If so, the obtained stretched exponential behavior of the correlation functions might be the result of a complex mixture of an analysis artifact and polymer dynamics. Indeed, assume one is interested in the probability that the dipole orientation, within time *t*, changes its polar angle from θ_0 to θ_1, and its in-plane angle by ϕ, as shown in the Figure 11.8.

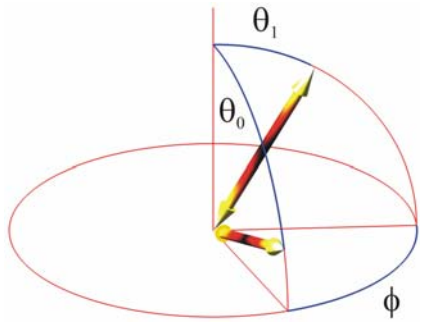

Figure 11.8. Schematic representation of the angular changes in a time interval t for a 3 D rotational diffusion of the transition dipole. The in plane projection of the transition dipole is also shown.

For an isotropic rotator, the associated probability distribution is given by:

$$P(\theta,\phi,t\,|\,\theta_0)=\sum_{n=0}^{\infty}\sum_{m=-n}^{n}\frac{2n+1}{4\pi}\frac{(n-|m|)!}{(n+|m|)!}P_n^m(\cos\theta)P_n^m(\cos\theta_0)\exp[i\phi-n(n+1)D_{rot}t] \qquad (3)$$

where P_n^m are associated Legendre polynomials. D_{rot} is the rotational diffusion constant. Knowing this distribution, one can compute the average of the $\cos 2\phi$ as

$$\begin{aligned}\langle\cos 2\phi\rangle &= \int_0^{\pi}d\theta\sin\theta\int_0^{\pi}d\theta_0\sin\theta_0\int_0^{2\pi}d\phi P(\theta,\phi,t\,|\,\theta_0)\cos 2\phi\\ &= \int_0^{\pi}d\theta\sin\theta\int_0^{\pi}d\theta_0\sin\theta_0\sum_{n=2}^{\infty}\frac{2n+1}{2}\frac{(n-2)!}{(n+2)!}P_n^2(\cos\theta)P_n^2(\cos\theta_0)\exp[-n(n+1)D_{rot}t] \qquad (4)\\ &= 8\sum_{n=1}^{\infty}(4n+1)\frac{(2n-2)!}{(2n+2)!}\exp[-2n(2n+1)D_{rot}t]\end{aligned}$$

which is a complicated infinite series of exponential decays. As stated above, it is difficult to interpret the physical meaning.

A very recent report claims, however, that the above mentioned effect is minimal when one uses high NA objective lenses.[11] The authors state that to best compare to ensemble measurements of reorientation dynamics it would be ideal to measure the

full three-dimensional orientation of the molecule. They also mention that single molecule techniques able of measuring the 3-D orientation require many photons to determine the orientation and thus limit the length of trajectories and impairing useful correlation analysis.. Here, we demonstrate measurements of long trajectories of the full 3D orientation with high signal-to-noise ratio that allow correlation analysis.

The 3D rotational diffusion equation for an isotropic rotational diffusion with diffusion constant D_{rot} on the other hand is simply is given by

$$\frac{\partial h(\Psi,t)}{\partial t} = D_{rot}\frac{1}{\sin\Psi}\frac{\partial}{\partial\Psi}\sin\Psi\frac{\partial h(\Psi,t)}{\partial\Psi} \qquad (5)$$

where *h(Ψ, t)* is the orientation distribution function. Ψ is angular change as defined by $\Psi = \arccos(\mathbf{n}_t \cdot \mathbf{n}_{t+\delta t})$, where $\mathbf{n}_t$ is the unit orientation vector of the molecular dipole moments at time *t*. The average of $\langle\cos(\Psi)\rangle$ over Ψ as function of time,

$$\langle\cos(\Psi)\rangle = \int_0^\pi d(\Psi)\sin(\Psi)h(\Psi,t)\cos(\Psi) = \exp(-2D_{rot}t) \qquad (6)$$

shows a single exponential decay. The relaxation time is given by $\tau = 1/2D_{rot}$.

We analyzed 54 of the molecules shown in Figure 11.9 using the mathematics for a 3D isotropic rotor as outlined above (equations 5 and 6). The images were taken with 200 ms integration time and no interval time between the different frames. Although in this contribution trajectories are analyzed with 1000 data points (200 ms integration time per image) to demonstrate the method, it is possible to obtain

trajectories with more than 10,000 data points if one uses integration times of 50 ms. Note that the image in Figure 11.9a sample film of more than 100 nm was used to rule out the earlier dicussed interfacial effects.

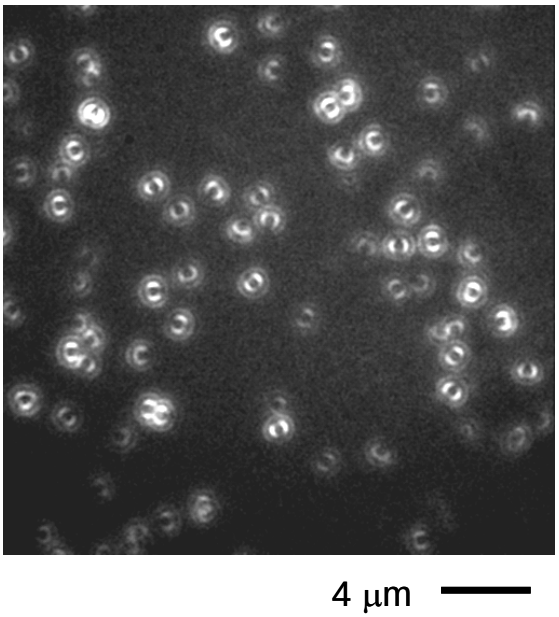

Figure 11.9. A defocused image used for the statistical analysis of 54 of the molecules in view. The images were taken with 200 ms integration and no interval time between frames.

Figure 11.10a shows typical decays and fitting results. Again, two different time scales were found in the correlation functions. The best fitting could be obtained by using bi-exponential decays. The obtained values of the diffusion coefficients for 40 of the 54 molecules, showing a clear bi-exponential decay, are shown in Figure 11.10b. Note that the difference between the fast and the slow rotational component is nearly two orders of magnitude. The fast component of most molecules is distributed between 0.1 second and 10 seconds and the slow decay between several hundreds to thousands of seconds. From a phenomenological point of view, it is

well know that fast local rearrangements of a polymer (referred as Johari-Goldstein β process, or secondary relaxation) are followed by the main slower relaxation, commonly termed as α process.

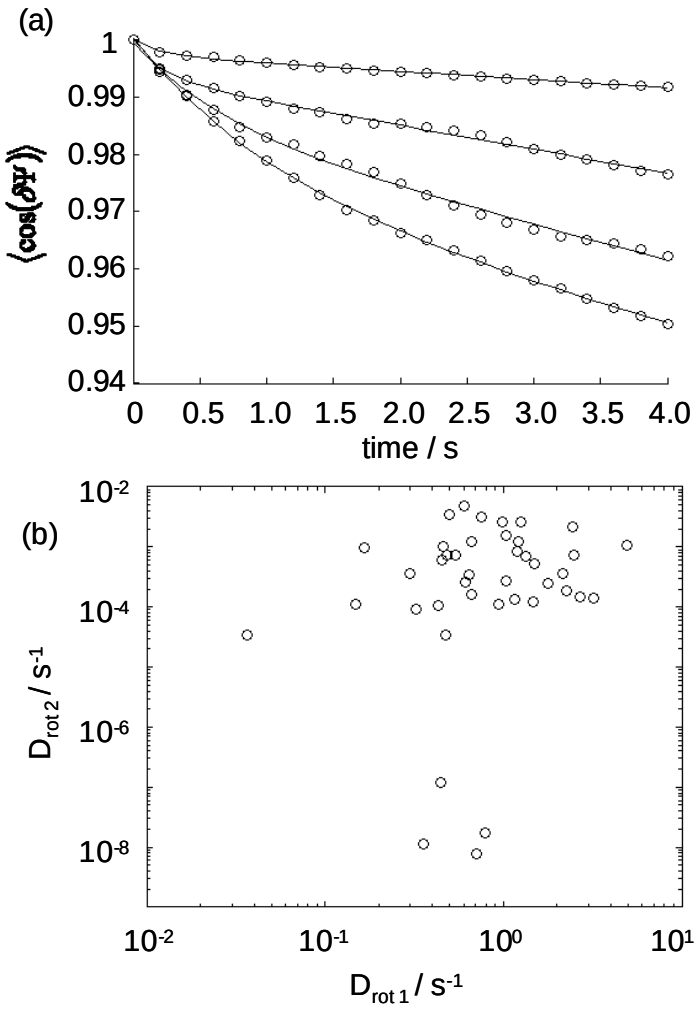

Figure 11.10. (a) Typical autocorrelation functions (o) and bi-exponential fits (solid line) for 4 molecules from Figure 11.9. (b) The distribution of diffusion coefficients for 40 of the molecules in Figure 11.9.

This process involves cooperative molecular motions. The observed relaxation time scale may reflect different relaxation regimes of polymer relaxation dynamics. Namely, the observed fast relaxation of molecular rotation might reflect the β-process polymer relaxation and the slower rotational diffusion could reflect the collective polymer motion. The tentative assignment made here to different relaxation regimes will be further investigated in detail by using a variety of fluorescent probes with different sizes and aspect ratios in well-defined mono-disperse polymer matrixes.

11.4 Conclusions

We demonstrated the potential of defocused wide-field fluorescence microscopy to monitor molecular rotational diffusion in a glassy polymer. Due to the good signal-to-noise ratio of the fluorescence images, 3D reorientation of molecular dipole moment could be followed. Using the full 3D rotation avoids the introduction of analysis artifacts. The data clearly evidence non-directional molecular rotation, resulting from random polymer relaxation. We showed that the autocorrelation function for the rotation of different probe molecules can vary greatly, resulting in large differences in rotational correlation times. This is due to the highly poly-disperse PMA matrix used. The advantage of wide-field imaging (parallel data collection of many molecules) allows us to prove spatially heterogeneous dynamics on the sub-1 μm scale, which is a promising result for investigating local environmental changes in phase separation processes or for investigating changes

in viscosity during polymerization reactions. The 3-D rotational correlation function could only be fitted bi-exponential. This might relate to different relaxation regimes predicted by polymer theories. In order to evaluate this hypothesis, experiments in better-defined, mono-disperse polymers will be conducted.

References

[1] (a) W. P. Ambrose, P. M. Goodwin, J.H. Jett, A. Van Orden, J. H. Werner, R. A. Keller**,** *Chem. Rev.* **1999**, *99*, 2929; (b) W. E. Moerner, D. P. Fromm, *Rev. Sci. Instru.* **2003**, *78*, 3597; (c) F. Kulzer, M. Orrit, *Annu. Rev. Phys. Chem.* **2004**, *55*, 585; (d) J. Enderlein, M. Böhmer, *ChemPhysChem* **2003**, *4*, 792; (e) D. E. Smith, T. T. Perkins, S. Chu, *Phys. Rev. Lett.* **1995**, *75*, 4146; (f) S. Chu, *Phil. Trans. R. Soc. Lond. A* **2003**, *361*, 689; (g) D. E. Smith, H. P. Babcock, S. Chu, *Science* **1999**, *283*, 1724.

[2] (a) R. Schilling, in *Collective Dynamics of Nonlinear and Disordered Systems*, G. Randons, W. Just, P. Haeussler, Eds.; Springer, **2003**, and references therein; (b) W. J. Götze *Phys.* **1999**, *11*, A1-A45, and references therein.

[3] (a) P. F. Barbara, A. J. Gesquiere, S.J. Park, J. L. Young, *Acc. Chem. Res.* **2005**, *38*, 602; (b) S. S. Sartori, S. De Feyter, J. Hofkens, M. Van der Auweraer, F. C. De Schryver, K. Brunner, J. W. Hofstraat, *Macromolecules* **2003**, *36*, 500; (c) B. Schartel, V. Wachtendorf, M. Grell, D. D. C. Bradley, M. Hennecke, *Phys. Rev. B* **1999**, *60*, 277; (d) T. Huser, M. Yan, L. J. Rothberg, *Proc. Natl. Acad. Sci. USA* **2000**, *97*, 11187.

[4] (a) R. A. L. Vallee, N. Tomczak, L. Kuipers, G. J. Vancso, N. F. van Hulst, *Phys. Rev. Lett.* **2003**, *91*(3), 38301. (b) R. A. L. Vallee, P. Marsal, E. Braeken, S. Habuchi, F. C. De Schryver, M. Van der Auweraer, D. Beljonne, J. Hofkens, *J. Am. Chem. Soc.* **2005**, *127*, 12011; (c) R. A. L. Vallee, M. Cotlet, J. Hofkens, F. C. De Schryver, K. Müllen, *Macromolecules* **2003**, *36*, 7752; (d) V. P. Biju, J. Y. Ye, M. J. Ishikawa, *Phys. Chem. B.* **2003**, *107*, 10729.

[5] (a) T. Ha, T. A. Laurence, D. S. Chemla, S. Weiss, *J. Phys. Chem. B* **1999**, *103*, 6839; (b) N. Tomczak, R. A. L. Vallée, E. M. H. P. van Dijk, M. García-Parajó, L. Kuipers, N. F. van Hulst, G. J. Vancso, *Euro Polym J* 2004, 40, 1001; (c) Q. Zhou, *J. Kor. Phys. Soc.* **2005**, *47*, S190.

[6] (a) J. A. Veerman, M. F. Garcia-Parajo, L. Kuipers, N. F. van Hulst, *J. Microsc.* **1999**, *194*, 477; (b) R. J. Moerland, N. F. van Hulst, *Opt. Express* **2005**, *13*, 1604; (c) B. Sick, B. Hecht, L. Novotny, *Phys. Rev. Lett.* **2000**, *85*, 4482; (d) L. Novoty, M. R. Beversluis, K. S. Youngworth, T. G. Brown, *Phys. Rev. Lett.* **2001**, *86*, 5251; (e) M. Böhmer, J. J. Enderlein, *Opt. Soc. Am. B* **2003**, *20*, 554; (f) D. Patra, I. Gregor, J. J. Enderlein, *J. Phys. Chem. A* **2004**, *108*, 6836; (g) A. P. Bartko, K. Xu, R. M. Dickson, *Phys. Rev. Lett.* **2002**, *89*, 026101.

[7] C. B. Roth, J. R. Dutcher, *J. Electroanal. Chem.* **2005**, *584*, 13.

[8] H. Piwonski, C. Stupperich, A. Hartschuh, J. Sepiol, A. Meixner, J. Waluk, *J Am Chem Soc* **2005**, *127*, 5302.

[9] T. Inoue, M. T. Cicerone, M. D. Ediger, *Macromolecules* **1995**, *28*, 3425.

[10] G. Hinze, G. Diezemann, T. Basche, *Phys Rev. Lett.* **2004**, *23*(20), 203001.

[11] C. Y. J. Wei, Y. H. Kim, R. K. Darst, P. J. Rossky, D. A. Vanden Bout, *Phys. Rev. Lett.* **2005**, *95*(17), 173001.

List of publications

G. Bergamini, P. Ceroni, V. Balzani, F. Vögtle, S.-K. Lee, "*Designing Systems for a Multiple Use of Light Signals*", *ChemPhisChem*, **2004**, *5*, 100-105.

G. Bergamini, P.Ceroni, M. Maestri, V. Balzani, S.-K. Lee, F. Vögtle, "*Forward (singlet-singlet) and backward (triplet-triplet) energy transfer in a dendrimer with peripheral naphthalene units and a benzophenone core*", *Photochem. Photobiol. Sci.*, **2004**, *3*, 898-905.

G. Bergamini, C. Saudan, P. Ceroni, M. Maestri, V. Balzani, M. Gorka, S.-K. Lee, J. Van Heyst, F. Vögtle, "*Proton-driven self-assembled system based on cyclam-cored dendrimers and* $[Ru(bpy)(CN)_4]^{2-}$", *J. Am. Chem. Soc.*, **2004**, *126*, 16466-16471.

P. Ceroni, G. Bergamini, F. Marchioni, V. Balzani, "*Luminescence as tool to investigate dendrimer properties*", *Prog. Polym. Sci.*, **2005**, *30*, 453-473.

G. Bergamini, P. Ceroni, V. Balzani, L. Cornelissen, J. Van Heyst, S.-K. Lee, F. Vögtle, "*Dendrimers based on a bis-cyclam core as fluorescence sensors for metal ions*", *J. Mater. Chem.*, **2005**, *15*, 2959-2964.

P. Ceroni, G. Bergamini, N. Aubert, V. Troiani, N. Solladié, "*A pentaporphyrin as a switching device activated by proton and redox stimuli*", *ChemPhisChem*, **2005**, *6*, 2120-2128.

H. Uji-i, S. M. Melnikov, A. Deres, G. Bergamini, F. De Schryver , A. Herrmann, K. Müllen, J. Enderlein, J. Hofkens, "*Visualizing spatial and temporal heterogeneity of single molecule rotational diffusion in a glassy polymer by defocused wide-field imaging*", *Polymer*, **2006**, *47*, 2511-2518.

V. Balzani, G. Bergamini, F. Marchioni, P. Ceroni, "*Ru(II)-bipyridine complexes in supramolecular systems, devices and machines*", *Coord. Chem. Rev.*, **2006**, *250*, 1254-1266.

G. Bergamini, P. Ceroni, V. Balzani, M.D.M. Villavieja, Ramchandra Kandre, I. Zhun, O. Lukin, "*A Photophysical Study of Terphenyl Core Oligosulfonimide Dendrimers Exhibiting High Steady-State Anisotropy*", *ChemPhysChem,* **2006**, *7*, 1980-1984.

G. M. L. Consoli, C. Geraci, P. Neri, G. Bergamini, V. Balzani, "*Azobenzene-bridged calix[8]arenes*", *Tetrah. Lett.*, **2006**, *47*, 7809-7813.

B. Branchi, P. Ceroni, G. Bergamini, V. Balzani, M. Maestri, J. van Heyst, S.-K. Lee, F. Luppertz, F. Vögtle, "*A Cyclam Core Dendrimer Containing Dansyl and Oligoethylene Glicol Chains in the Branches: Protonation and Metal Coordination*", *Chem. Eur. J.*, **2006**, *12*, 8926-8934.

N. Armaroli, G. Accorsi, G. Bergamini, P. Ceroni, M. Holler, O. Moudam, C. Duhayon, B. Delavaux-Nicot, J.-F. Nierengarten, "*Heteroleptic Cu(I) complexes containing phenanthroline-type and 1,1'-bis(diphenylphosphino)ferrocene ligands: Structure and electronic properties*", *Inorg. Chim. Acta*, **2007**, *360*, 1032-1042.

G. Bergamini, P. Ceroni, M. Maestri, S.-K. Lee, J. van Heyst, F. Vögtle, "*Cyclam cored luminescent dendrimers as ligands for Co(II), Ni(II) and Cu(II) ions*", *Inorg. Chim. Acta*, **2007**, *360*, 1043-1051.

V. Balzani, G. Bergamini, P. Ceroni, F. Vögtle, "*Electronic spectroscopy of metal complexes with dendritic ligands*", *Coord. Chem. Rev.*, **2007**, *251*, 325-335.

V. Vicinelli, G. Bergamini, P. Ceroni, V. Balzani, F. Vögtle, O. Lukin, "*Mechanisms for fluorescence depolarization in dendrimers*", *J. Phys. Chem. B*, in press.

P. Passaniti, M. Maestri, P. Ceroni, G. Bergamini, F. Vögtle, H. Fakhrnabavi, O. Lukin, "*First generation TREN dendrimers functionalized with naphthyl and/or dansyl units. Ground and excited state electronic interactions and protonation effects*", *Photochem. Photobiol. Sci.*, in press.

V. Balzani, G. Bergamini, S. Campagna, F. Puntoriero, "*Photochemistry and Photophysics of Coordination Compounds: Overview and General Concepts*", *Top. Curr. Chem.*, in press.

V. Balzani, G. Bergamini, S. Campagna, F. Nastasi, F. Puntoriero, "*Ruthenium*", *Top. Curr. Chem.*, in press.